

**Gas Retention and Release
Behavior in Hanford
Single-Shell Waste Tanks**

C. W. Stewart
M. E. Brewster
P. A. Gauglitz
L. A. Mahoney

P. A. Meyer
K. P. Recknagle
H. C. Reid

December 1996

MASTER

Prepared for the U.S. Department of Energy
under Contract DE-AC06-76RLO 1830

Pacific Northwest National Laboratory
Richland, Washington 99352

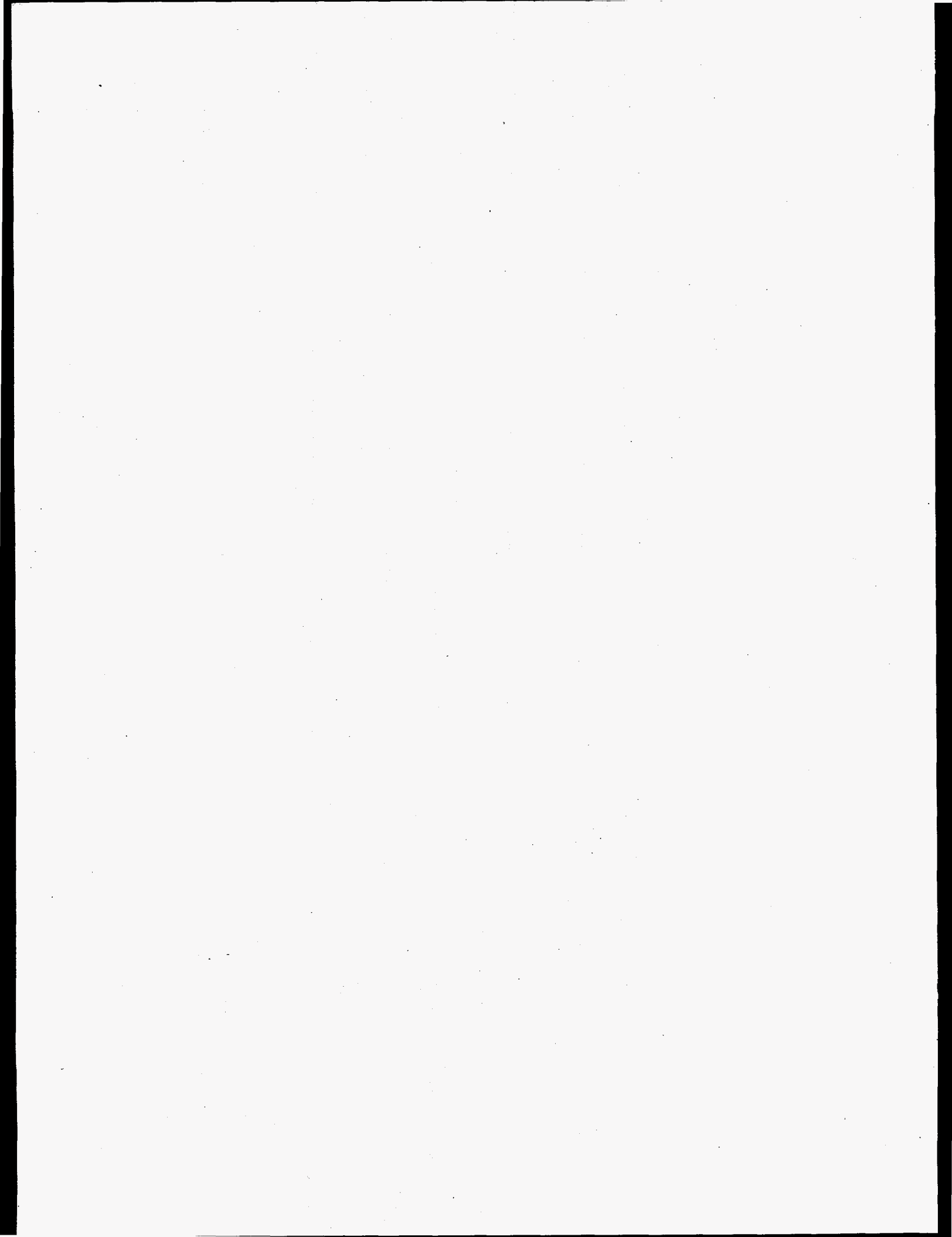
DISTRIBUTION OF THIS DOCUMENT IS UNLIMITED

DISCLAIMER

**Portions of this document may be illegible
in electronic image products. Images are
produced from the best available original
document.**

Abstract

This report describes the current understanding of flammable gas retention and release in Hanford single-shell waste tanks based on theory, experimental results, and observations of tank behavior. The single-shell tanks likely to pose a flammable gas hazard are listed and described, and photographs of core extrusions and the waste surface are included. The credible mechanisms for significant flammable gas releases are described, and release volumes and rates are quantified as much as possible. The only mechanism demonstrably capable of producing large ($\sim 100 \text{ m}^3$) spontaneous gas releases is the buoyant displacement, which occurs only in tanks with a relatively deep layer of supernatant liquid. Only the double-shell tanks currently satisfy this condition. All release mechanisms believed plausible in single-shell tanks have been investigated, and none have the potential for large spontaneous gas releases. Only small spontaneous gas releases of several cubic meters are likely by these mechanisms. The reasons several other postulated gas release mechanisms are implausible or incredible are also given.



Executive Summary

This report presents analyses, experimental results, and observations of tank behavior to describe and assess the potential for spontaneous and induced releases of free (as opposed to dissolved) gas in Hanford single-shell tanks (SSTs). Gas releases by all plausible "natural" mechanisms, earthquakes, salt-well pumping, and local disruptions, are discussed. Potential gas releases during retrieval operations are mentioned but not analyzed. Gas retention mechanisms are described in relation to their associated release processes.

The flammability hazard in Hanford waste tanks was first recognized in the large periodic gas releases that occurred in the double-shell Tank 241-SY-101 (SY-101). The hazard in SY-101 was mitigated in late 1993 by installing a mixer pump that prevents the buildup of retained gas. But the experience with SY-101 created anxiety that other tanks might be having similar large gas releases or the potential to do so, thus associating a perception of imminent danger with all 177 waste tanks. We know now that this perception was not correct, especially for the SSTs.

The historic gas releases in SY-101 were buoyancy-induced displacement events (also termed "rollovers," as in Allemann et al. [1994]). Before a buoyant displacement occurs, a portion of the settled solids layer accumulates gas until it becomes sufficiently buoyant to overcome the weight and strength of material restraining it. At that point, it suddenly breaks away and rises through the liquid. The stored gas expands as it rises, failing the retaining matrix and allowing a portion of the gas to escape into the head space.

In order for a large gas release to occur by buoyant displacement, there must be a settled solids layer that traps gas, and sufficient potential energy must be released to free the trapped gas from the rising waste. The potential energy available for release depends on the depth of supernatant liquid above the gas-bearing solids layer. Experiments, thermodynamics, and tank experience all show that a relatively deep layer of supernatant is required to provide sufficient energy for a significant gas release.

Only the double-shell tanks (DSTs) currently have a waste configuration with enough potential energy to release a significant amount of gas in a buoyant displacement. None of the SSTs have a supernatant liquid layer deep enough to be subject to this gas release mechanism. All release mechanisms believed plausible in SSTs have been investigated, and none have the potential for large spontaneous gas releases—only small spontaneous gas releases of several cubic meters are likely by these mechanisms. There is no evidence for large gas releases from SSTs in the recent waste level history or tank head space gas monitoring data.

Besides these small spontaneous releases, only severe earthquakes have the potential to induce a large release in SSTs. However, sufficiently severe seismic events are rare; only those with estimated return frequencies of 1000 years are expected to release a large fraction of stored gas in SSTs, while a 100-year event might do so in DSTs.

Free gas can accumulate only in submerged solids (i.e., beneath the free liquid level that would be observed inside a well); gas is not retained in unsubmerged solids because it escapes by diffusion. The configuration, limiting size, and maximum volume fraction of gas bubbles can now be predicted as a function of surface tension, particle size, yield stress, and waste depth (Gauglitz et al. 1996).

The size of individual bubbles (both round and dendritic) is quite limited. Pore-filling, litho-dendritic bubbles have a maximum vertical extent of about 1 m; particle displacing, hydrostatic or hydro-dendritic bubbles are limited to about 20 cm. We estimate the horizontal extent of

these bubbles to be no more than about three times their height. Very large (~1 m in diameter) individual bubbles are not believed possible. Because bubble size is so limited, local waste disruptions cannot suddenly trigger releases of large volumes of gas; gas is released only from the volume of waste actually disturbed.

An example of a more general disruption is salt-well pumping, in which liquid removal is expected to release a relatively large volume of gas but slowly, as a series of small releases over many months. No large gas releases have been observed in the limited gas monitoring data available from recent pumping campaigns (Caley et al. 1996) although preliminary analysis indicates relatively large ammonia releases are possible (Peurrung et al. 1996). In tanks with waste sufficiently permeable to allow most of the liquid to be removed by salt-well pumping, the combination of decreased volume of wet solids available to store gas, reduction in hydrostatic head on the gas remaining, and the increase in tank head space is believed to effectively eliminate the flammable gas hazard.

Other proposed gas release mechanisms have been shown to be extremely unlikely or not hazardous: penetration of a few very large bubbles, venting through a fracture, uncovering of a gas reservoir by dryout, collapse of a postulated 'cavern' created by subsidence following salt-well pumping, and a 'weak sludge' cascade release that has been observed in the laboratory under very specific conditions.

The large number of tanks and the uncertainties in waste properties make it difficult or impossible to study them individually in detail. A prioritized list of SSTs was developed by choosing those that are likely to present a flammable gas hazard. Since data are lacking on many specific tanks, tank groupings or clusters were chosen to represent the general characteristics of important tanks. Knowledge of the waste configuration in one tank thus can clarify our understanding of several related flammable gas tanks, even if the tank itself does not present a hazard.

The main objective of this report is to provide a sound technical foundation for estimating gas release rates and volumes in SSTs based on credible mechanisms. Though actual models to predict release behavior are as yet incomplete and not fully validated, we believe all the potential pathways for large gas releases have been defined.

References

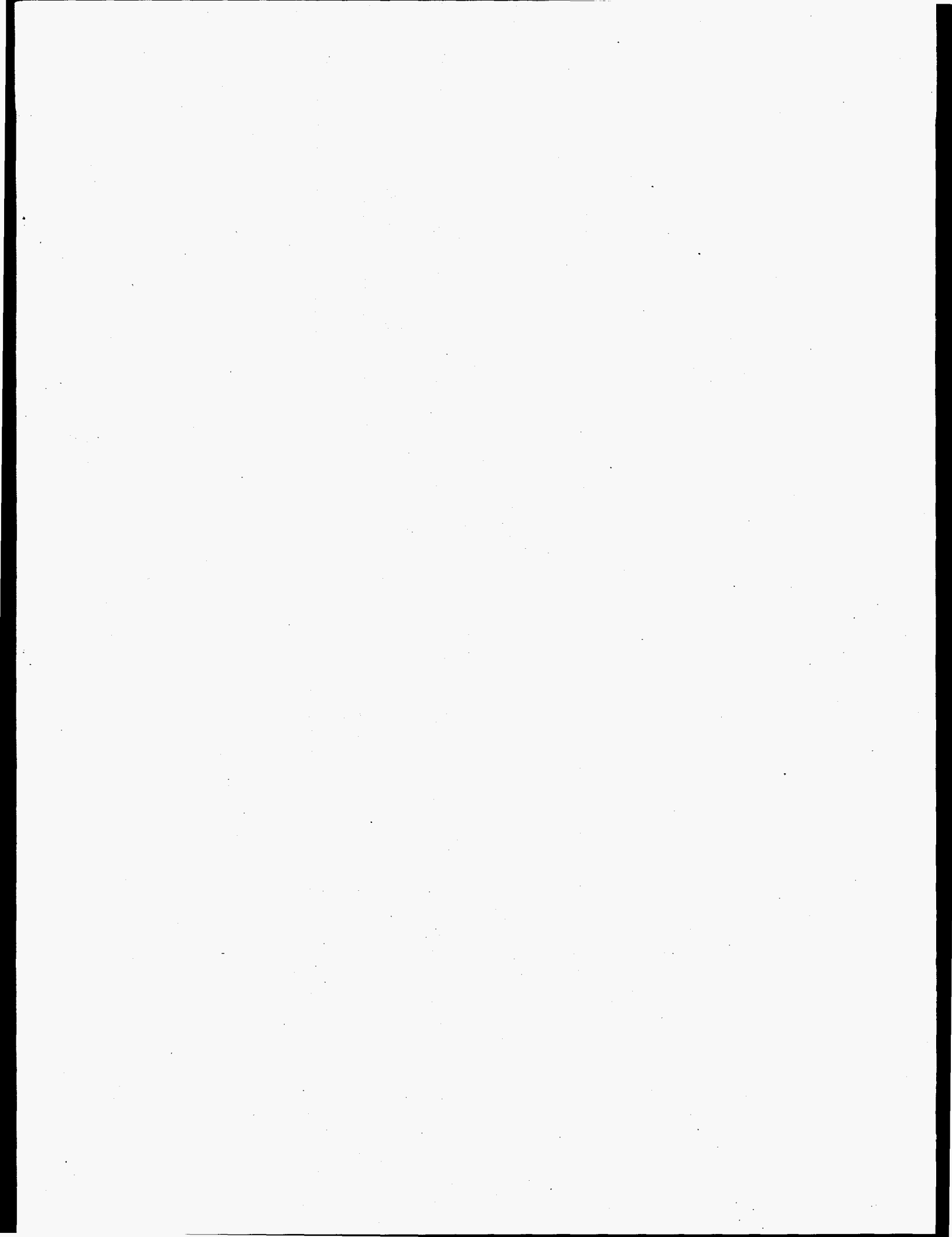
- Allemann RT, ZI Antoniak, WD Chavala, LE Efferding, JG Fadeff, JR Friley, WB Gregory, JD Hudson, JJ Irwin, NW Kirch, TE Michener, FE Panisko, CW Stewart, and BM Wise. 1994. *Mitigation of Tank 241-SY-101 by Pump Mixing: Results of Testing Phases A and B*. PNL-9423, Pacific Northwest Laboratory, Richland, Washington.
- Caley SM, LA Mahoney, and PA Gauglitz. 1996. *Summary of Tank Information Relating Salt Well Pumping to Flammable Gas Safety Issues*. PNNL-11335, Pacific Northwest National Laboratory, Richland, Washington.
- Gauglitz PA, SD Rassat, PR Bredt, JH Konynenbelt, SM Tingey, and DP Mendoza. 1996. *Mechanisms of Gas Bubble Retention and Release: Results for Hanford Waste Tanks 241-S-102 and 241-SY-103 and Single-Shell Tank Simulants*. PNNL-11298, Pacific Northwest National Laboratory, Richland, Washington.
- Peurrung LM, SM Caley, EY Bian, and PA Gauglitz. 1996. *Gas Release During Salt-Well Pumping: Model Predictions and Comparisons to Laboratory Experiments*. PNNL-11310, Pacific Northwest National Laboratory, Richland, Washington.

Acknowledgments

This report owes a large debt to Rudy Allemann, who tackled gas retention and release theory head-on and developed some of the premises that form the basis for this work. Yasuo Onishi, Steve Simmons, and John Hudson also made valuable contributions to our initial understandings.

We greatly appreciated the suggestions and encouragement of Blaine Barton, Dave Hopkins, Kent Hodgson, and Steve Barker, who are on the front lines actually reducing theory to practice in evaluating and categorizing the tanks. Thanks also to Jerry Johnson for patience and guidance along the way and for several opportunities to expose the developing gas release theories to critical review. We also appreciate the continuing support of John Gray, Craig Groendyke, and Gary Rosenwald of DOE-RL.

Finally a great big thanks to Sheila Bennett who edited this report and saw it through to final publication with her usual skill and thoroughness, and to Kathy Rightmire, who prepared the final color photo reproductions.



Contents

Abstract	iii
Summary.....	v
Acknowledgments	vii
1.0 Introduction.....	1.1
1.1 Single-Shell Tanks on the Flammable Gas Watch List	1.2
1.2 Historical Review of Single-Shell Tanks.....	1.4
1.3 Earlier Single-Shell Tank Gas Release Studies	1.6
2.0 Waste Configuration	2.1
2.1 Prioritization of Single-Shell Tanks for Waste Configuration Study.....	2.1
2.1.1 Definition of Waste Configurations.....	2.5
2.1.1.1 Waste Configuration 1.....	2.5
2.1.1.2 Waste Configuration 2.....	2.5
2.1.1.3 Waste Configuration 3.....	2.6
2.1.1.4 Waste Configuration 4.....	2.6
2.1.2 Prioritization Of Waste Configurations.....	2.6
2.2 Analysis of Visual Data.....	2.7
2.2.1 Waste Physical Configuration Profiles.....	2.8
2.2.1.1 Waste Configuration 1 Profile.....	2.8
2.2.1.2 Waste Configuration 2 Profile.....	2.9
2.2.1.3 Waste Configuration 3 Profile.....	2.9
2.2.2 Waste Surface Appearance.....	2.9
3.0 Gas Retention.....	3.1
3.1 Gas Retention Mechanisms	3.1
3.1.1 Particle-Displacing Bubbles	3.2
3.1.2 Nonconvective Layer Subject to Buoyant Displacement.....	3.4

3.1.3	Pore-Filling Bubbles in Submerged Saltcake.....	3.5
3.1.4	Gas in Unsaturated Saltcake.....	3.5
3.2	Retained Gas Volume Estimates.....	3.6
3.2.1	Barometric Pressure Effect Method	3.6
3.2.2	Surface Level Rise Method	3.10
3.2.3	Direct Void Fraction Measurement.....	3.11
3.3	Conclusion on Gas Retention.....	3.12
4.0	Single-Shell Tank Gas Release Mechanisms.....	4.1
4.1	Buoyant Displacement	4.3
4.1.1	Experimental Observation of Buoyant Displacements.....	4.4
4.1.1.1	Results for 67-Pa Bentonite Simulant.....	4.6
4.1.1.2	Results for 14-Pa Bentonite Simulant.....	4.6
4.1.1.3	Results for Thin Layer, 14-Pa Simulant.....	4.6
4.1.2	An Energy Criterion for Buoyant Displacement Gas Release	4.12
4.1.3	Conclusions on Buoyant Displacement	4.17
4.2	Gas Percolation from Connected Dendritic Regions.....	4.18
4.2.1	Configuration of the Connected Litho-Dendritic Bubble Region.....	4.18
4.2.2	Dynamics of Litho-Dendritic Percolation	4.21
4.2.3	Particle-Displacing, Hydrostatic Bubbles.....	4.24
4.2.4	Dynamics of Hydrostatic Bubble Release.....	4.26
4.2.5	Particle-Displacing, Hydro-Dendritic Bubbles	4.28
4.2.6	Dynamics of Hydro-Dendritic Bubble Percolation.....	4.29
4.2.7	Conclusions on Percolation Release.....	4.35
4.3	Earthquake-Induced Gas Release.....	4.36
4.3.1	Stress Modeling of Waste for a Design Basis Earthquake	4.37
4.3.2	Energy Developed in Waste for a Design Basis Earthquake.....	4.43
4.3.3	Conclusion on Earthquakes.....	4.46

4.4 Salt-Well Pumping	4.47
4.4.1 Salt-Well Pumping Process.....	4.48
4.4.3 Experimental Results	4.52
4.4.4 Gas Release from Caverns Formed after Salt-Well Pumping	4.53
4.4.5 Conclusions	4.55
4.5 Gas Release During Local Disruption.....	4.55
4.5.1 Summary of Field Observations	4.56
4.5.2 Experimental Results	4.57
4.5.3 Analysis and Conclusions on Disruption	4.60
5.0 Conclusions and Recommendations	5.1
5.1 Conclusions.....	5.1
5.2 Recommendations.....	5.2
6.0 References.....	6.1
Appendix A: Single-Shell Tank Prioritization Data	A.1
Appendix B: Core Descriptions	B.1

Figures

2.1	Waste Surface in U-109.....	2.10
2.2	Waste Surface in A-101.....	2.10
2.3	Waste Surface in S-106.....	2.12
2.4	Waste Surface in T-101.....	2.12
2.5	Large Vent or Fumarole in SY-101.....	2.13
2.6	Crater Formed by Water Dripping from Riser in BY-108.....	2.14
2.7	Jellyfish in S-103.....	2.14
2.8	Pock Marks in T-104.....	2.15
3.1	Bubble Morphology Map.....	3.3
3.2	Measured and Predicted Level Responses to Pressure Variations in S-106.....	3.9
4.1	Basic Waste Configurations.....	4.2
4.1.1	Schematic of Apparatus for Observing Buoyant Displacements.....	4.4
4.1.2	Top View of Test 1a.....	4.7
4.1.3	Side View of Test 1a.....	4.7
4.1.4	Top View of Test 2a.....	4.8
4.1.5	Side View of Test 2a.....	4.8
4.1.6	Top View of Test 2a.....	4.9
4.1.7	Later Top View of Test 2a.....	4.9
4.1.8	Side View of Test 2a.....	4.10
4.1.9	Top View of Test 2b.....	4.10
4.1.10	Side View of Test 2b.....	4.11
4.1.11	Top View of Test 3.....	4.11
4.1.12	Geometry and Nomenclature for Displacement Model.....	4.12
4.1.13	Stress-Strain Data for Bentonite Clay Simulant.....	4.14
4.2.1	Schematic of an Equilibrated Bubble.....	4.19

4.2.2	Limitations on Litho-Dendritic Bubbles.....	4.21
4.2.3	Maximum and Minimum Gas Fractions.....	4.22
4.2.4	Litho-Dendritic Bubble Release Time and Volume	4.23
4.2.5	Particle-Displacing Bubble Behavior Map.....	4.26
4.2.6	Round Bubble Cascade Gas Release Volume Versus Bubble Diameter.....	4.28
4.2.7	Cumulative Distribution of Hydro-Dendritic Release Fraction	4.33
4.2.8	Effect of Discharge Fraction on Hydro-Dendritic Release	4.33
4.2.9	Effect of Waste Depth on Hydro-Dendritic Release	4.34
4.2.10	Effect of Bubble Height on Hydro-Dendritic Release.....	4.34
4.3.1	Design-Basis Earthquake Spectrum for Hanford	4.36
4.3.2	Excitation Modes for Tank Seismic Analysis.....	4.37
4.3.3	Natural Frequency Versus Overall Waste Height - Vertical.....	4.39
4.3.4	Natural Frequency Versus Overall Waste Height - Horizontal	4.39
4.3.5	Peak Stresses at Mid-Depth - Vertical Excitation, 1000-Year DBE.....	4.40
4.3.6	Peak Stresses at Mid-Depth - Horizontal Excitation, 1000-Year DBE	4.40
4.3.7	Peak Stresses at Mid-Depth - Vertical Excitation, 100-Year DBE	4.41
4.3.8	Peak Stresses at Mid-Depth - Horizontal Excitation, 1000-Year DBE	4.41
4.3.9	Average Waste Stresses with Damping Coefficient.....	4.42
4.3.10	Strain Induced with Cyclic Vibration.....	4.43
4.3.11	Average Absorbed Energy - Vertical Excitation.....	4.44
4.3.12	Average Absorbed Energy - Horizontal Excitation	4.45
4.3.13	Yield Energy Limit, 640-cm Height - Horizontal	4.46
4.3.14	Possible Gas Release Fraction Versus Earthquake Severity.....	4.47
4.4.1	Salt-Well Pumping Data for Tank S-108: April–August 1996.....	4.49
4.4.2	Salt-Well Pumping Data for Tank S-108: May–June 1996.....	4.49
4.4.3	Salt-Well Pumping Data for Tank T-104: April–August 1996.....	4.50
4.4.4	Salt-Well Pumping Data for Tank S-108: June–July 1996.....	4.50

4.5.1	Schematic of Disruption Apparatus.....	4.57
4.5.2	Percent of Gas Released as a Result of Disruption	4.59

Tables

1.1	List of Flammable Gas Tanks	1.4
2.1	Short List of High-Priority Tanks for Gas Retention and Release Studies	2.3
2.2	Tanks Ranked by Cluster	2.4
3.1	Void Fraction Estimates.....	3.8
3.2	BPE and BPE2 dL/dP and Waste Properties	3.10
4.1	Test Conditions for Buoyant Displacement Experiments	4.5
4.2	Energy Model Applied to Tank SY-101.....	4.16
4.3	Energy Model Applied to Scaled Buoyant Displacement Experiments	4.16
4.4	Energy Model Applied to Tank A-101	4.17
4.5	Clay Simulant Composition and Shear Strength for Each Disruption Experiment.....	4.59

1.0 Introduction

Since 1943, large underground concrete storage tanks have been used at Hanford to store the byproducts of uranium and plutonium production. There are 146 single-shell tanks (SSTs) and 26 double-shell tanks (DSTs), each up to 75 feet (23 m) in diameter and 32 feet (10 m) high and capable of holding up to one million gallons (3,800 m³) of waste. The SSTs have a single steel liner on the bottom and sides; they are up to 50 years old, and some are known to leak. The DSTs were constructed during the late 1970s and have a full steel inner liner and a second steel shell around the bottom and sides, with ventilation and leak detection systems in the annulus between the two. The chemically complex waste in these tanks ranges from mostly liquid to thick, sticky sludge to a crystalline saltcake. The sludge typically has the consistency of stiff clay to soft mud, and the saltcake ranges in consistency from fine, wet slush to rock-like crystalline salt.

Essentially all radioactive waste slowly generates flammable gases by radiolysis of water and complex chemical reactions. In most waste tanks, this gas is released to the tank head space at about the same rate as it is generated. The generation rate is so low compared with passive or active ventilation flow rates that the flammable gas is diluted far below the concentration necessary for ignition. However, certain tanks show evidence that they might retain significant volumes of flammable gas (mainly hydrogen with smaller amounts of ammonia, methane, and other hydrocarbons) in the waste.

The flammability hazard associated with these tanks depends on the peak concentration and volume of flammable gases that might occur in the tank head space following a sudden release of retained gas. If the peak concentration remains everywhere below the lower flammability limit (LFL), the gas cannot be ignited, and there is no flammability hazard. If the concentration locally exceeds the LFL, and a source of ignition is present, the mixture could burn. If a sufficiently large fuel volume is burned in the dome space, the resulting pressure increase might be large enough to fail the exhaust filters and even the dome structure, potentially releasing radioactive material to the environment.

Evaluating the flammable gas hazard in a particular tank requires an estimate of the volume of gas retained and knowledge about what fraction of the retained gas can be released and how rapidly it might enter the tank head space in relation to the ventilation rate. The retained gas volume can be estimated from the correlation of waste level measurements with barometric pressure fluctuations, from accumulated surface level rise, or from the local void fraction as determined by the void fraction instrument (VFI) and retained gas sampler (RGS). The potential gas release fraction and rate rely mainly on historical observations and continuous monitoring data in tanks that exhibit spontaneous gas release events (GREs). Gas release predictions in tanks that do not show evidence of GREs must rely on theory-analytical models, experimental data, and indirect observations. Theory must also account for potential gas releases resulting from external disturbances such as a major seismic event, core sampling, or removal of liquid by salt-well pumping.

Most of the Hanford DSTs that are suspected of retaining significant gas volumes also exhibit significant GREs, as evidenced by sudden waste level drops and increases in head space hydrogen concentration. DST gas retention and release mechanisms are fairly well characterized after being studied intensively since about 1990 in the effort to understand the behavior of SY-101 (Gauglitz et al. 1996; Stewart et al. 1996). However, none of the SSTs show clear evidence of large, sudden gas releases, and the mechanisms by which they retain and release gas are not well understood.

This report presents analyses, experimental results, and observations of tank behavior to describe and assess the potential for spontaneous and induced releases of free (as opposed to

dissolved) gas in Hanford SSTs. Gas releases by all plausible "natural" mechanisms, earthquakes, salt-well pumping, and local disruptions, are discussed. Potential gas releases during retrieval operations are mentioned but not analyzed. Gas retention mechanisms are described in relation to their associated release processes. Section 2 lays out a priority list to focus the study effort on tanks that truly represent the flammable gas hazard. Four waste configurations are defined, and the physical attributes of the waste column in each are shown. Section 3 summarizes the current understanding of gas retention mechanisms and techniques for measuring the amount of gas stored. These two sections introduce and provide background for Section 4, which describes each of the plausible gas release mechanisms. Release volumes and rates are quantified if possible. The overall summary and conclusions are given in Section 5, and references are listed in Section 6. Supporting documentation can be found in the appendixes.

1.1 Single-Shell Tanks on the Flammable Gas Watch List

The potential for a flammable gas mixture in the dome space and ventilation system of certain Hanford waste tanks was first proposed in DST 241-SY-101 (SY-101). The waste level in this tank began rising and suddenly dropping periodically shortly after it was filled in 1980, but the amount of gas release was not well quantified. In January 1990 it was hypothesized that a burn above, within, or even under the crust layer was possible because the waste generated both fuel (hydrogen) and oxidizer (nitrous oxide) (Babad et al. 1992). Some of the releases in SY-101 in fact caused the dome space mixture to exceed the LFL.

In April 1990, additional DSTs and SSTs were identified as potentially having behavior similar to SY-101. This was the genesis of the flammable gas watch list (FGWL). Because the process was not well understood and the hydrogen and nitrous oxide releases were not covered by existing safety analyses, this was declared to be an unreviewed safety question (USQ) in May 1990. Twenty-three tanks were included in the USQ based on evaluations of waste level growth, changes in waste level, high total organic carbon (TOC) content, presence of a floating crust layer, and waste received from B-plant.

In January 1991, these same 23 tanks were formally identified on the FGWL in response to Public Law 101-510, Section 3133 (the Wyden Amendment), as having a "serious potential for release of high level waste due to uncontrolled increases in temperature or pressure" from a flammable gas burn. Two more DSTs were added to the FGWL in 1992 and 1993 for a total of 25 tanks, six DSTs and 19 SSTs. Separate watch lists were established for other safety issues that could lead to uncontrolled increases in pressure and temperature, including organics, ferrocyanide, criticality, and high heat. Some FGWL tanks are also on one or two of these other watch lists.

After 1990, experiences of relatively high hydrogen concentrations in core sampling equipment, observation of large void spaces in core radiographs, and hydrogen and nitrous oxide measured in the dome space of various tanks all indicated that a number of additional tanks were retaining flammable gas in the waste. If gas was retained, the question was also raised whether the tank presented a "serious potential for release" and should be added to the FGWL. Accordingly, a goal was set to screen all 177 tanks for flammable gas risk.

Conservative criteria were developed for placing tanks on the FGWL (Hopkins 1994), based on four scenarios that could lead to a release of radioactive material:

- A steady background release of flammable gas, causing the dome space to exceed 25% of the LFL
- A large episodic GRE causing the dome space to exceed 25% of the LFL

- A localized episodic gas release exceeding 25% of the gas volume sufficient to cause serious release if ignited (plume burn scenario)
- An episodic GRE resulting in a pressure pulse exceeding 25% of that required to force material out of system openings, even if no burn occurs.

A review of tank level data by PNNL in 1994 uncovered a relationship between level change and barometric pressure fluctuations that indicated the presence of stored gas. That is, the presence of gas makes the waste 'compressible,' such that the waste level decreases when barometric pressure increases and vice versa. The stored gas volume can be estimated directly from the waste compressibility. By early 1995, PNNL completed a screening of all 177 tanks using this method (Whitney 1995). The results indicated that 58 tanks retained detectable volumes of gas. Twenty-one of these tanks were already on the FGWL; the Hanford Plant Review Committee issued standing orders to place flammable gas work controls on the remaining 37 suspect tanks.

A more detailed, formal methodology was developed to evaluate tanks for inclusion on the FGWL in late 1995 (Hopkins 1995); it used the barometric pressure response method along with surface level rise to calculate the volume of gas trapped in the waste. All 177 tanks were evaluated in accordance with this methodology by early 1996 (Hodgson et al. 1996). Fifty-three tanks failed the evaluation criteria, and 21 of these were already on the FGWL. Four of the original 25 tanks passed the evaluation and are therefore suggested as potential candidates for removal from the FGWL. In November 1995, flammability controls (ignition sources, ventilation requirements, and monitoring for flammable gases) were established in all 177 tanks.

Twenty five of the remaining 32 tanks (only three of which are DSTs) were placed under the flammable gas USQ in February 1996 and recommended for the FGWL. These tanks plus the 25 original FGWL tanks are listed in Table 1.1. The recommendation was withdrawn in July 1996 after the Chemical Reactions SubPanel and DOE-HQ raised questions about the assumptions used in the methodology and the quality of the data on which the evaluation was based (Johnson 1996). A major finding of the review team was that the methodology was not sufficiently definitive for recommending the addition or removal of tanks from the FGWL. However, all of the additional tanks remained under the USQ. The remaining seven tanks were added to the USQ in July 1996.

WHC updated the original USQ and consolidated previous determinations into one overall USQ determination that was adopted by DOE-RL on November 1, 1996. This expanded the USQ in flammable gas composition; applicability to additional structures; methods of gas generation, retention, and release; location of hazard; and energetics and characteristics of burns. The USQ now applies to 176 tanks. It is noteworthy that SY-101, the tank that initiated the entire process, was dropped from the USQ as having an adequate authorization basis.

One of the main issues with the evaluation methodology is the implicit assumption that any tank will spontaneously and rapidly release up to 25% of its stored gas. While gas releases of this magnitude by energetic buoyant displacement can be found in the history of several DSTs, none have been observed in SSTs. These tanks are not subject to buoyant displacement, and theory and analysis indicate that there is no other mechanism that can create such spontaneous GREs. The only possible source of a large sudden gas release in an SST is an abrupt external disturbance of most of the waste such as might occur in a severe seismic event. These issues are discussed in detail in Section 4.

Table 1.1. List of Flammable Gas Tanks

Tank	Type	Tank	Type
A-101 ^(a)	SST-4	SX-101 ^(a)	SST-4
A-103	SST-4	SX-102 ^(a)	SST-4
AN-103 ^(a)	DST	SX-103 ^(a)	SST-4
AN-104 ^(a)	DST	SX-104 ^(a, b)	SST-4
AN-105 ^(a)	DST	SX-105 ^(a)	SST-4
AN-107	DST	SX-106 ^(a)	SST-4
AW-101 ^(a)	DST	SX-109 ^(a, c)	SST-4
AW-104	DST	SY-101 ^(a)	DST
AX-101 ^(a, b)	SST-4	SY-103 ^(a)	DST
AX-103 ^(a, b)	SST-4	T-110 ^(a)	SST-2
AY-101	DST	T-201	SST-1
B-201	SST-1	T-202	SST-1
B-202	SST-1	T-204	SST-1
BX-107 ^(d)	SST-2	TX-102 ^(d)	SST-3
BY-101 ^(d)	SST-3	TX-111 ^(d)	SST-3
BY-102 ^(d)	SST-3	TX-112 ^(d)	SST-3
BY-103	SST-3	TX-113 ^(d)	SST-3
BY-105	SST-3	TX-115 ^(d)	SST-3
BY-106	SST-3	U-102	SST-2
BY-109	SST-3	U-103 ^(a)	SST-2
C-104	SST-2	U-105 ^(a)	SST-2
C-107 ^(d)	SST-2	U-106	SST-2
S-101	SST-3	U-107 ^(a)	SST-2
S-102 ^(a)	SST-3	U-108 ^(a)	SST-2
S-103	SST-3	U-109 ^(a)	SST-2
S-105 ^(d)	SST-3	U-111	SST-2
S-106	SST-3	Tank Capacities	
S-107	SST-3	SST - 55,000 gal.	SST-1
S-109	SST-3	SST - 530,000 gal.	SST-2
S-111 ^(a)	SST-3	SST - 758,000 gal.	SST-3
S-112 ^(a)	SST-3	SST - 1,000,000 gal.	SST-4
		DST - 1,160,000 gal.	DST

(a) Original FGWL (25 tanks).
 (b) FGWL tanks that passed the latest evaluation.
 (c) Placed on the FGWL because five other FGWL tanks vent into it.
 (d) Tanks whose free liquid was removed by recent salt-well pumping.

1.2 Historical Review of Single-Shell Tanks

There are several designs of SSTs that differ mainly in size. The smaller tanks are generally the oldest. The B, C, T, and U tank farms were constructed in 1943-44 and contain four of the small type 1 tanks that are 20 ft in diameter with a 17 ft operating depth (giving a 55,000 gal. capacity) and 12 of the larger, type 2 tanks (75 ft diameter, 15 ft operating depth, 530,000 gal. capacity). The BX farm was constructed next, in 1946, with 12 tanks of type 2 design. The TX, BY, S, and TY farms, constructed in 1948, 1949, 1951, and 1952, respectively, used type 3 design with the operating depth increased to 23 ft, creating a 758,000 gal. capacity. The operating depth increased to 31 ft with a 1,000,000 gal. capacity in the type 4 tanks of the SX and A farms in

1954–55. The A farm tanks had a flat rather than a dished bottom. The last SSTs constructed in the AX farm in 1964 were of the flat-bottom, type 4 design but included a grid of drain slots under the steel bottom liner for leak detection and drainage (Anderson 1990).

The flammable gas SSTs listed in Table 1.1 include all four designs. Ignoring those that have been salt-well pumped or passed the FGWL evaluation, eight of the 12 SST farms are represented; there are two tanks from the A farm, two from B, four from BY, one from C, eight from S, five from SX, three from T, and eight from U farm. Of these, tanks in the S, SX, and U farms generally retain the largest gas volumes and heavily populate the original FGWL (Hodgson et al. 1996). The BY tanks also contain gas and are a major contributor to the USQ list. The rest of this sketch will feature these four farms.

The four farms had very different histories. Furthermore, the sequence of waste transfers into and out of these tanks is extremely complicated, and transactions were sometimes incompletely or inaccurately documented. It is not worthwhile here to recount the details. Models are available that attempt to estimate current tank contents from the historical records (e.g., Agnew et al. 1995); however, regardless of which process produced the initial fill, the current tank content and configuration represent a broad blend of many waste streams and were essentially established, with a few exceptions, during the concentration campaigns (i.e., 242-A and 242-S evaporators and in-tank solidification system) in the 1970s (De Lorenzo et al. 1994).

The U farm tanks U-101 through 109 were filled in 1947–49 with metal waste from the original bismuth phosphate process in T-plant. They were sluiced out to the U-plant in 1952–56 for uranium recovery, and cesium in the return waste was scavenged to allow disposal of the liquid to trenches or cribs. During this time, the 242-T evaporator was used to concentrate nonboiling liquids remaining in these first nine tanks. In the late 1950s, U-101 through U-109 were again pumped empty and refilled with waste from the REDOX process. After this second fill, there was little activity in these tanks until the 242-S evaporator campaigns began in the 1970s. Tanks U-110, -111, and -112 were initially filled from the first-cycle B-plant decontamination process in 1946–1948 which self-concentrated, allowing addition of REDOX waste in 1954–57. The U tanks were removed from service in 1978–1980.

The S farm tanks were initially filled with REDOX waste in 1952–53. In 1952 the waste in some tanks began to boil spontaneously, and surface condensers were installed in the first six tanks to self-concentrate the waste. No significant transfers occurred for about 20 years, until the 242-S evaporator campaigns of the mid-1970s. At that time the liquid was pumped out to the evaporator feed tanks and replaced with the evaporator bottoms, which eventually solidified. The tanks were removed from service, and supernatant liquid was pumped out in 1976–78. S-102 remained in operation as an evaporator feed tank until 1980.

The SX tanks were designed to accommodate self-boiling waste up to 250°F for five years. Tanks SX-101 through -106 were initially filled in 1954–55 with REDOX waste. After this waste had self-concentrated for several years, these six tanks supported the 242-S evaporator campaign as bottoms and receiver tanks and were very active throughout their operational history, essentially being emptied and refilled many times. The remaining SX tanks received boiling high-level REDOX waste. Condensate was fluxed back to the tanks to maintain cooling, and airlift circulators were needed to mix the waste and prevent steam bumping. The waste in all SX tanks, which were removed from service in 1980, remains hot, with temperatures approaching 200°F in some.

The BY farm was constructed in 1948–49, and Tanks BY-101 through 106 were filled with metal waste in 1950–51, in cascade from the BX farm after it was filled. They were sluiced out in the mid-1950s and refilled with uranium recovery and cesium scavenging waste. BY-107 through 110 received B-plant first-cycle decontamination waste in 1951–52 and uranium recovery waste in 1952–53. In-tank solidification (ITS) systems were operated in the BY farm from 1967–

1967–1977 to concentrate nonboiling supernatant directly in designated tanks. Tanks BY-102 and BY-112 were used as evaporators. The concentrate was cascaded through a series of receiver tanks, and the final supernatant was recycled for further concentration. This process effectively homogenized the waste in the entire BY farm, and it has its own classification as “BY saltcake.” The BY tanks were removed from service in 1977–79, and many have been salt-well pumped.

The end result of all these processes is a waste in the BY, S, SX, and U tanks that consists mainly of wet saltcake (soluble salts) with relatively little sludge (insoluble metal oxides). The physical consistency of the saltcake can range from quite coarse ‘rock salt’ to very fine crystals that appear almost clay-like, similar to actual sludge. Though the wastes are generally similar in these tanks, there are some subtle differences in waste configuration and amount.

- U-tanks: The waste is generally 3–5 m of fine-grained salt slurry with 0–30 cm of supernatant liquid. The tanks contain 5–10% sludge, although U-107 has 24% sludge, and relatively high TOC.
- S-tanks: Waste is 3–5 m of saltcake (coarser than salt slurry) with a liquid level 0–200 cm below the waste surface. Tanks with the most gas have a higher liquid level. They contain less than 10% sludge, except S-111, which has 24% sludge.
- SX-tanks: The waste is 5–6 m of saltcake with 0–10 cm of supernatant liquid. The tanks hold 10–15% sludge, except SX-106, which contains no sludge. Temperatures approach 200°F.
- BY-tanks: Contain 3–6 m of saltcake with a liquid level 20–90 cm below the waste surface. They are 9–15% sludge, although BY-105 has 33% sludge, and BY-105 and 106 have relatively high TOC.

Certain tanks in other farms also retain significant gas volumes, specifically, A-101 and A-103. However, these tanks were emptied and refilled in the 242-A evaporator campaign and are quite similar to the U tanks. In fact, the waste configuration in these and other tanks can be related by formal grouping studies. These relationships are described in detail in Section 2.1. Color photographs of core samples and the waste surface representing the various tank groupings are shown in Section 2.2.

1.3 Earlier Single-Shell Tank Gas Release Studies

Several mechanistic models were proposed originally to explain the gas releases in SY-101 (Allemann et al. 1991) and can apply to releases from SSTs today. Two models were proposed that assume a large volume of gas collected under the crust layer; the gas would be released either by fracturing the crust or tilting it. Structural calculations showed that the one-meter crust layer in SY-101 could not hold down sufficient gas volume to account for known GRE behavior.

A large bubble model was also proposed in which a large volume of gas was held under a sealing membrane until its yield strength was exceeded. A jet of gas then issued from the nonconvective layer, bringing entrained liquid and solids to the surface in a sort of grand geyser. Again, structural calculations showed that only relatively small bubbles could be retained in the waste given the known or estimated yield strength. Eventually, a partial buoyant displacement model (the ‘gob’ theory) was settled upon as the dominant mechanism for gas release in SY-101 and other DSTs (Allemann et al. 1993).

LANL has investigated extensively the potential for gas release from SSTs while developing formal safety assessments for rotary mode core sampling (WHC 1996a) and salt-well

pumping (WHC 1996b). The conclusion of this work is that "...large and prompt releases are not likely in single-shell tanks." The 19 SSTs on the FGWL were separated into four gas release categories:

1. Tanks that experience neither episodic behavior or long-term level growth
2. Tanks with insufficient data to evaluate their behavior
3. Tanks that potentially exhibit episodic behavior
4. Tanks that show level growth only.

Only Tank A-101 was listed in category 3 with potentially episodic behavior; however, the tank was placed there before it was discovered that the gas-bearing solids were floating on the free liquid. There were six tanks in category 1 with no evidence of GREs, five tanks without sufficient data in category 2, and seven tanks with level growth only in category 4.

A complete summary of GRE evidence from the tanks' operational history is given in the rotary core sampling safety assessment (WHC 1996a). During 49 intrusive sampling events, only one possible GRE was observed—in Tank A-103 between March 24 and 31, 1986, where the waste level dropped 2.4 inches over one week, bracketing the time lower segment samples were being removed. During 38 liquid observation well (LOW) installations in SSTs, only one, in SX-104 on May 24, 1984, showed a 2.1-inch level drop, but this occurred 1–8 days *before* LOW installation. During none of these activities was there a significant elevation of flammable gas concentrations in the head space, sudden changes in waste temperature profile, or detection of ammonia outside the tank that would be evidence of a GRE.

A discussion of available models for GRE behavior concluded that the classic buoyant displacement mechanism was not supported by the waste conditions typically found in SSTs. Nor was any other specific mechanism found that could result in a large prompt release. A probabilistic model for gas release is developed based on expert opinion and available evidence that predicts an expected gas release of 100 ft³ at a rate of one ft³/min. Release volumes over 2,500 ft³ and release rates over 100 ft³/min. are considered "very unlikely."

The salt-well pumping safety assessment (WHC 1996b) discusses several specific gas release mechanisms. The possibility of increased ammonia releases is discussed as an operational issue. Cavern formation is not considered a hazard because of rapid dilution by diffusion through the 'dry' saltcake. However, the existence of a cavern in a liquid-saturated region is postulated but not analyzed. Dryout rate is estimated but not considered a gas release mechanism. Some analysis of very large bubbles is included to argue that they cannot be present. Intrusion of dendritic and round bubble regions is discussed with the conclusion that no large release would occur.

A buoyant displacement mechanism without supernatant liquid is postulated in which gas is stored in a dendritic bubble region below a sealing round bubble region. A 44% release fraction is also postulated for this mechanism, although energy considerations are believed to make such a release "slow." Finally, a porous media flow model is given for gas releases during salt-well pumping due to gas bubble uncover and pressure reduction.

Aside from the analyses above and the work presented in this report, gas releases from SSTs are typically treated conservatively by assuming a large fraction of the stored gas volume is released by an unspecified mechanism (e.g., 25% in Hodgson et al. [1996]). The basis for this treatment is that the actual release mechanisms are not understood, and large, prompt releases cannot be ruled out. We hope the analyses and experimental results presented in this report will begin to provide a sound technical foundation for gas release estimates based on credible mechanisms.

2.0 Waste Configuration

One of the most important facets of flammable gas retention and release in SSTs is understanding the physical characteristics of the waste the gas is stored in. Relating gas retention and release behavior to specific particle size, liquid content, layering, or some other property of the waste that we can observe or measure will greatly increase our understanding of the flammable gas hazard and increase the accuracy of our predictions.

2.1 Prioritization of Single-Shell Tanks for Waste Configuration Study

The large number of tanks and the uncertainties regarding properties of the waste they contain make it difficult or impossible to study them all in detail. Accordingly, a prioritized list was developed of the SSTs most likely to present a flammable gas hazard to help select viable candidates for detailed study. This list includes most of the SSTs on the current FGWL and those tanks known or potentially likely to store significant flammable gas volumes. At least one of the following criteria placed a tank on the list:

1. The tank must be on the flammable gas or organic salt watch list, according to WHC (1995b), as having one or more characteristics that suggest safety concerns.
2. The tank must have been flagged by the screening calculation in Whitney (1995) with an estimated response greater than 0.2 cm/kPa.^(a) These tanks show evidence of sufficient retained gas volumes to potentially produce flammable mixtures if it were all released into the tank head space.
3. The tank must be observed to contain high head-space concentrations of hydrogen (>200 ppm) or ammonia (>400 ppm).^(b) This would suggest a significant gas generation rate, though the gas is not necessarily retained.

To narrow the field, tanks were eliminated because of evidence that they stored relatively little flammable gas based on one or more of the following factors:

1. Insufficient waste depth (<2.5 m).
2. Interim-stabilized and head-space concentrations of hydrogen and ammonia low (hydrogen <100 ppm and ammonia <200 ppm) or unavailable.
3. Flagged by Whitney's screening calculation but had a level response of magnitude less than 0.2 cm/kPa. In this case, the screening calculation confirms a relatively small retained gas volume. This tank is thus of less concern for gas retention and episodic release, even though it might have watch list status and/or show high head space concentrations of hydrogen or ammonia.

^(a) Personal communication with PD Whitney, Pacific Northwest National Laboratory.

^(b) Head space data from the Tank Waste Information System (TWINS) database as of 12/14/95 were used to evaluate this criterion.

4. Passive ventilation and low observed head-space concentrations (hydrogen <100 ppm and ammonia <200 ppm), indicating that gas generation rates are low.

Elimination was somewhat more subjective; some tanks with lower or borderline depths were retained on the list because of other factors such as a large level response to barometric pressure or high head-space concentrations of some gases. Unusual features of the level history were also considered, such as large rises, declines, or oscillations.

This procedure selected 25 tanks for a high-priority "short list," which is given in Table 2.1. The table gives the watch list (WL) status of each tank; those with official WL status are in capital letters, the rest are those proposed (Johnson 1996). The 50th percentile value of the level response (dL/dP) in cm/kPa from Hodgson et al. (1996) is given if measured by the Food Instrument Corporation (FIC) or Enraf devices.^(a) The depth of the waste is given in meters. Hydrogen (H₂) and ammonia (NH₃) concentrations measured in the headspace are given in ppm. The priority rating of these tanks was verified with Brown et al. (1995); all but four ranked above the median on this priority score.

A major concern in any study or survey of SSTs is the quality and reliability of the data on which it is based, and data are lacking on many of the tanks on the short list. Most of the information available on the concentration of analytes in the SSTs comes from the historical tank content estimates (HTCEs), which are based on the tank layering model (Agnew et al. 1995), the historical record for waste transfers (Brevick 1995), and the Hanford-defined wastes (HDW) (Agnew 1995). Currently, the most uncertain part of the estimates is the HDW, which defines the composition of the waste streams that go into the tanks.

Several important pieces of information are still needed for evaluating the tanks for flammable gas generation, retention, and release. Better data are desirable on the constituents in the tank, both to check the accuracy of the HTCE estimates and to evaluate the tanks for gas generation. Physical property measurements appear to be almost nonexistent and are important in determining gas retention mechanisms and waste transport and disposal issues. Important physical properties include waste rheology, yield strength, porosity, and particle size distribution.

To stretch the limited amount of data available, tanks were grouped into related clusters. Knowledge of the waste configuration for a related tank, even if it does not present a hazard itself, will clarify our understanding of the high-priority flammable gas tanks. Tank groupings or clusters were chosen according to the analysis of Remund et al. (1995) to represent the general characteristics of important tanks. All tanks in a cluster are presumed to be similar, so data for one tank may provide insights into the behavior of waste in the other tanks in the cluster.

The tanks on the short list represented nine of the 36 SST clusters found by Remund et al. (1995) in their grouping study. The list of tanks was expanded by including all tanks in the clusters. The final list, containing all tanks in all nine clusters, consisted of 54 SSTs. As much information as possible about these SSTs was then obtained and assembled into a spreadsheet, which was used to evaluate the different tank clusters for potential flammable gas release. The master spreadsheet is given in Appendix A; an abbreviated list is shown in Table 2.2. Forty-three of these tanks scored above the median value (33) in the priority rating determined by Brown et al. (1995). Further, the 11 top-priority tanks according to Brown are included on our list. Some of the tanks not on our short list, such as TX-118, had high-priority ratings according to Brown et al. (1995). In all such cases, the high-priority rating is due to a factor such as ferrocyanide or discrepancies in historical information that are unrelated to safety issues associated with flammable gas retention and release.

^(a) According to Johnson (1996), neutron ILL and manual tape are not considered appropriate for determining waste compressibility.

Table 2.1. Short List of High-Priority Tanks for Gas Retention and Release Studies

Tank	Watch List	dL/dP	Depth	H ₂	NH ₃	Rationale for Selection
C-102	ORG		3.78	165	192	WL, some H ₂ , NH ₃
SX-104	FG		5.59			WL, level oscillations
S-102	FG/ORG	-0.51	5.18	670	418	WL, large dL/dP, slurry growth, high H ₂ , NH ₃
S-103	fg	-0.34	2.70			WL, dL/dP, erratic slurry growth, borderline depth
U-103	FG/ORG	-0.27	4.20	557	761	WL, dL/dP, slurry growth, high H ₂ , NH ₃
U-105	FG/ORG	-0.23	3.80			WL, dL/dP, slurry growth
U-107	FG/ORG	-0.18	3.70	505	474	WL, slurry growth
U-108	FG/org		4.20			WL, slurry growth
U-109	FG/org	-0.20	4.20			WL, dL/dP, slurry growth
U-111	ORG		3.00	250	682	WL, slurry growth, high H ₂ , NH ₃
BY-109	fg		3.30			WL, slurry growth between pumpings, head space conc. N/A
T-110	FG		3.70			WL, annual oscillation, slight growth
SX-102	FG	-0.35	5.00			WL, dL/dP
SX-105	FG		6.20			WL, head space conc. N/A, large linear level decline
SX-103	FG/ORG	-0.57	6.10	<23	80	WL, large dL/dP, linear level decline
SX-106	FG/ORG	-0.23	5.10	<98	188	WL, dL/dP, slurry growth
S-106	fg	-0.94	4.52			WL, large dL/dP, slurry growth
S-111	FG/ORG	-0.40	5.20	392		WL, dL/dP, slight slurry growth, high H ₂
S-112	FG		5.00			WL, surface decline, liquid rise, head space conc. not available
BY-104	FC/org		3.30	312		WL, high H ₂
BY-107	FC/org		2.60	698	963	WL, high H ₂ , NH ₃
BY-110	FC/org		2.50	<160	426	WL, high NH ₃
A-101	FG/ORG	-0.15	8.76	786	800	WL, large long-term oscillation, high H ₂ , NH ₃
AX-101	FG		7.00			WL, large short-term oscillations
BY-108	FC/ORG		2.20	647	1140	WL, high H ₂ , NH ₃

The spreadsheet confirms the idea that all tanks in the cluster have similar characteristics. This is particularly true for the larger tank clusters where it is possible to generalize about the overall behavior of each of the properties. For example, the tanks in cluster 13 all have about 0.1% TOC, relatively high amounts of total radiation, moderate temperatures (80–100°F), high nitrite concentrations, and equal liquid and surface levels, indicating the presence of significant amounts of liquid. Almost all the tanks in cluster 13 are also on the flammable gas and organic WLs. Most of the other tank clusters exhibit similar levels of agreement for the tank properties.

Table 2.2. Tanks Ranked by Cluster

Tank	Watch List	dL/dP	Depth	H ₂	NH ₃	Cluster	SL
S-102	FG/ORG	-0.51	5.1	670	418	13	*
S-103	fg	-0.34	2.1			13	*
SX-106	FG/ORG	-0.23	4.4	<98	188	13	*
U-103	FG/ORG	-0.27	4.2	557	761	13	*
U-105	FG/ORG	-0.23	3.5	<49	354	13	*
U-107	FG/ORG	-0.18	3.5	505	474	13	*
U-108	FG/org		4.1			13	*
U-109	FG/org	-0.20	4.1			13	*
U-111	ORG		3.0	250	682	13	*
A-101	FG/ORG	-0.15	8.8	786	800	22	*
A-102	org		0.3			22	
A-103	fg	-0.19	3.4			22	
AX-101	FG		6.9	103	44	22	*
S-105		-0.30		21	36	20	
S-106	fg	-0.94	4.4			20	*
S-108			5.6			20	
S-109			5.2			20	
S-111	FG/ORG	-0.40	5.4	392	124	20	*
S-112	FG		4.8			20	*
SX-102	FG	-0.35	5.0			20	*
SX-103	FG/ORG	-0.57	6.0	<23	80	20	*
SX-105	FG		6.3			20	*
U-106	fg/ORG	-0.06	1.9	214	1013	20	
BX-111			1.9			15	
BY-101			3.6			15	
BY-102	fg/org		3.1			15	
BY-103	fg/FC/org		3.7	22	30	15	
BY-106	fg/FC/org		5.9	104	78	15	
BY-109	fg	0.001	3.9			15	*
BY-111	FC		4.2	<160	61	15	
BY-112	FC		2.7	<94	71	15	
BY-104	FC/org		3.7	312	255	21	*
BY-105	fg/FC/org		4.7	87	44	21	*
BY-107	FC/org		2.5	698	978	21	*
BY-110	FC/org		3.7	<160	426	21	*
S-101	fg	-0.15	3.8			11	
S-110			3.6			11	
SX-104	FG	0.001	5.7			11	*
BY-108	FC/ORG		2.1	647	1140	33	*
C-102	ORG		3.9	165	192	6	*
C-105			1.4	24	3	6	
T-101			0.9			6	
T-102			0.2			6	
T-103			0.2			6	
B-110			2.3			19	
B-111			2.2			19	
T-105			0.9			19	
T-110	FG		3.5			19	*

* Tanks on original FGWL short list (SL).

2.1.1 Definition of Waste Configurations

The clusters were categorized by the waste configuration defined by the relative amounts of sludge, saltcake, and salt slurry. Four distinct configurations were found among the nine tank clusters: 1) tanks containing saltcake and salt slurry—clusters 13 and 22; 2) tanks containing primarily saltcake—clusters 15 and 20; 3) tanks containing sludge and saltcake—clusters 11, 21, and 33; and 4) all sludge tanks—clusters 6 and 19. The four waste configurations under consideration here are described below. Most of the 149 SSTs with a significant waste depth can be placed in one of these four primary categories.

2.1.1.1 Waste Configuration 1

Most tanks of waste configuration 1 (WC1) have some saltcake (0–75%) under salt slurry (25–75%) with possibly a thin layer of sludge (0–25%). Subcategory 1A (cluster 13) is distinguished from subcategory 1B (cluster 22) by the source of saltcake and salt slurry (A or S evaporator campaigns, respectively). There are indications (Agnew 1995; Remund et al. 1995) that these waste types are very similar. Thus the distinction between these two categories may be artificial. Tank A-103 is listed in this category because of its classification by Remund et al. (1995) in cluster 22, although it has no slurry and thus appears to match waste configuration 2 better.

Cluster 13 (WC1A): The nine tanks in this cluster exhibit substantial dL/dP and relatively high H₂, N₂O, and NH₃ concentrations in the dome space (when values are available). Most of the tanks exhibit large level rises. Eight of the tanks in this cluster are on the short list, and all tanks are either on the flammable gas or organic watch lists. With the exception of Tank U-107, which is about one-fourth sludge, the tanks in this cluster are all a combination of saltcake and salt slurry. The tanks all have fairly high levels of total radioactivity and temperatures in the region 80–100°F. All tanks have high concentrations of nitrite ion and about 0.1% TOC.

Cluster 22 (WC1B): Only two of the four tanks in this cluster report reliable values of dL/dP, and these indicate a low to moderate level response. None of the tanks show any level rise. The tanks contain mostly saltcake and salt slurry and generally have high TOC and nitrite ion concentrations. The total radioactivity is variable, but the tanks are generally on the warm side, with median temperatures in the range 90–150°F, and most of the tanks are on the FGWL.

2.1.1.2 Waste Configuration 2

Tanks with waste configuration 2 (WC2) are primarily saltcake (75–100%) with possibly thin layers of sludge (0–25%) and salt slurry (0–25%). Subcategory 2A (cluster 20) is distinguished from subcategory 2B (cluster 15) by the source of saltcake (S or BY farms, respectively, which differ significantly in their concentrations of nitrite).

Cluster 20 (WC2A): Many of the ten tanks in this cluster have substantial and reliable values for dL/dP. However, only one tank shows a large level rise, and most tanks show a level decrease. The waste is primarily saltcake, with some sludge. The TOC is low, in the range of 0.03–0.05%, and the concentrations of nitrite ion are modest, in the range 0.1–0.16 M. The tanks all contain high levels of radioactivity, but temperatures in the tanks vary over a wide range, from 70 to 170°F.

Cluster 15 (WC2B): This cluster contains eight tanks, only one of which has a reliable dL/dP that is near zero. The waste is mostly saltcake, with some sludge. They generally have low TOC (0.05%) and nitrite concentrations around 0.25 M. The tanks all have moderate to high total

radioactivity levels and temperatures in the range of 65–120°F. Several of these tanks appear to be quite dry, with liquid levels, as given by neutron data, substantially lower than the surface level.

2.1.1.3 Waste Configuration 3

Tanks with waste configuration 3 (WC3) consist of sludge (25–75%) and saltcake (25–75%) with possibly small amounts of salt slurry (0–25%). Subcategories 3A, 3B, and 3C correspond to clusters 21, 11 and 33. Sludge may be REDOX type (3B) or ferrocyanide type (3A, 3C). Saltcake may have originated in the S (3B) or BY farms (3A, 3C). Subcategories 3A and 3C differ mainly in the predominance of saltcake (3A) versus sludge (3C).

Cluster 21 (WC3A): None of the four tanks in this cluster has a reliable value of dL/dP. The waste in the tanks is primarily sludge and saltcake, but a comparison of liquid and surface levels indicates the waste may be on the dry side. TOC is high, about 0.15–0.26%, and the tanks have modest nitrite ion concentrations, 0.15–0.18%. They contain moderate radioactivity and, with the exception of Tank BY-107, temperatures over 100°F. All the tanks are on the ferrocyanide and organic watch lists. Dome space sampling for several of the tanks indicates the presence of significant H₂ and NH₃ concentrations.

Cluster 11 (WC3B): The value of dL/dP is low for SX-104, but S-101 has a moderate value of -0.15 cm/kPa. S-110 does not report a reliable value. SX-104 and S-101 show a level decrease. These tanks are mostly sludge and saltcake, although S-101 has a fair amount of salt slurry as well. All tanks in the cluster have substantial radioactivity but low TOC and modest nitrite ion concentrations. The tanks in this cluster are all at reasonably high temperature; the coolest tank has a median temperature of 117°F, the warmest, 158°F.

Cluster 33 (WC3C): This cluster has only one tank. No reliable value of dL/dP is reported. The tank is mostly sludge, with some saltcake. It shows high TOC but low nitrite ion concentrations, the total radioactivity is moderate, and the median tank temperature is 84°F. Dome space sampling indicates high concentrations of H₂ and NH₃.

2.1.1.4 Waste Configuration 4

Tanks with predominantly sludge (>75%) are classified here as waste configuration 4 (WC4). Category 4A has cladding waste, while category 4B has BiPO₄ waste.

Cluster 6 (WC4A): This cluster has five tanks, none with a reliable value of dL/dP. The waste is entirely sludge in all the tanks. The total radioactivity in the tanks is fairly low (the highest is 63,000 Ci in Tank T-101), but all tanks have a fairly high nitrite ion concentration. The temperatures range from 60–120°F; most contain only small amounts of waste, and all show low TOC (0.03% or less).

Cluster 19 (WC4B): None of the four tanks in this cluster has a reliable value of dL/dP. The tanks are entirely sludge and have negligible TOC and no appreciable nitrite ion concentration. The pH for most of these tanks is relatively low, about 8–10, with one tank at pH 12.7. The total radioactivity for these tanks varies widely, from 200–1,300,000 Ci.

2.1.2 Prioritization of Waste Configurations

Each waste configuration was examined to determine its priority for further study according to the following criteria:

- 1) The liquid level, as measured by neutron scattering, is comparable to the surface level. This indicates a significant amount of liquid in the waste, which is important for radiolysis, leading to the production of hydrogen gas, and for the more likely gas-retention mechanisms.
- 2) Moderate or high temperatures for the waste. The higher temperatures promote the reactions leading to gas production.
- 3) Relatively high TOC. The presence of hydrocarbons leads to higher hydrogen production. If chelates are present (EDTA and HEDTA) they may also promote ammonia production.
- 4) Relatively high nitrite ion concentration. The presence of nitrite ion may promote production of ammonia and nitrous oxide.
- 5) High radiation from cesium and strontium. High radiation levels promote flammable gas production from radiolysis and by warming the tank.
- 6) pH greater than 13. Concentrations of OH^- greater than 1 M combined with high concentrations of aluminate appear to point to elevated gas production rates. A pH in the range 7-13 is associated with low gas production rates. Most tanks show an elevated pH, but a few clusters exhibit what appeared to be relatively low average pH. From the information available, the concentration of aluminate cannot currently be determined.

Using these criteria, waste configuration 1 (cluster 13, saltcake and slurry) was the most interesting and has the highest priority. Several tanks in WC1 have exhibited elevated levels of hydrogen, nitrous oxide, and ammonia in head space samples, and most are at high pH. All tanks exhibit level rise and most show substantial dL/dP . Six of the nine tanks are rated among the ten top-priority tanks, according to Brown et al. (1995).

Waste configuration 3A (cluster 21, sludge and saltcake) is also of potential interest. This configuration has high TOC (about 0.2%), reasonably high radioactivity, and temperatures around 100°F. It also has nitrite concentrations of about 0.15 M and high pH. The tanks in the cluster all exhibit modest level rises and are on the ferrocyanide watch list.

Waste configuration 2A (cluster 20, saltcake) is also chosen as a possible candidate for further study, primarily for its high temperature, high radioactivity, and reasonably high nitrite concentrations. No tanks in this cluster exhibit slurry growth, although many have a high dL/dP , and S-106 has the highest of all tanks on the list.

2.2 Analysis of Visual Data

Core sample extrusion and waste surface photos were studied in an attempt to correlate the physical appearance of the waste with tendency for gas retention in the absence of measured physical properties. While no formal correlation was possible, some key features were found that may be useful indicators of gas retention subject to confirmation from in situ measurement such as with the RGS.

Tanks with the most retained gas appear to have two characteristics in common: abundant liquid and fine-grained, clay-like waste. The SSTs in waste configuration 1A, which are of highest priority with respect to gas retention, have a substantial layer of fine, clay-like solids that appear wet or damp but release little drainable liquid on the sample tray. The waste surface has a floating

yellow crust or foam with areas of dark-colored liquid visible. The tanks in lower-priority groups generally contain coarser-grain saltcake material whose moisture content increases with depth and, in some cases, a bottom layer of dark brown, damp, fine-grain sludge. The upper waste regions in these tanks generally appear dryer than WC1A. The waste surface of these tanks appears to be a dry yellowish or gray-white saltcake. Little or no liquid is visible.

In-tank photographs show no surface features indicative of episodic gas releases; no large vents, mudpots, or fumaroles were obvious. However, such indications are clearly seen on the surface of SY-101, where regular gas releases are known to have occurred.

2.2.1 Waste Physical Configuration Profiles

We studied written core sample extrusion descriptions, several core extrusion videos, and still photographs of extruded cores to develop a composite description of the physical character of the waste as a function of height for the various waste configurations defined in Section 2.1.

The first step was to standardize the core extrusion descriptions. The extruded segments were described by waste type, color, moisture content, grain size, and extrusion surface trait. Composite descriptions of entire cores, arranged by segment, are included in tabular form in Appendix B along with photos illustrating the descriptions. Once standard segment-by-segment descriptions were developed for available core samples from tanks representing each waste configuration, the core descriptions were superposed to characterize the appearance of the entire waste configuration.

Core extrusion photos or videos were not available for all of the waste configurations. We were able to characterize only WC1A (three tanks), WC2B (one tank), WC3A (three tanks), and WC3C (one tank). We did not inspect cores from WC4.

2.2.1.1 Waste Configuration 1 Profile

Only core samples from waste configuration 1A were available. Extrusions from S-102, U-105, U-107, and U-109 were studied. This configuration consists mainly of saltcake and salt slurry with some sludge. In general, the waste is a damp brown or gray material in which the colors darken, moisture content increases, and the grain size decreases with depth. Very little free liquid drains from the core on the extrusion tray. Beyond these similarities, a composite description of WC1A is difficult to construct.

S-102 was a damp, gray, coarse-grained saltcake for most of its depth, with roughly one meter of black, fine-grained, smooth sludge near the tank bottom. About the last half-meter nearest the tank bottom was a damp, gray, fine-grained saltcake.

The upper meter of U-105 was a thick, wet, dark-brown sludge, and the lower three meters was a damp, coarse-grained, dark-brown saltcake-sludge mixture described as having white, coarse-grained solids throughout.

U-107 was difficult to describe because the two cores differ markedly. Only three segments (out of a possible eight) were taken in the first core, which contained a very wet, coarse saltcake from which over 400 mL of drainable liquid was recovered. In contrast, the top meter of the other core (five segments totaling about 2 meters) was dry, gray-white saltcake, followed by about half a meter of dark-brown or black, damp sludge over more gray saltcake. Only 70 mL of liquid came out of this core.

Cores from U-109 contained a gray saltcake/salt slurry mixture. The color darkened, moisture increased, grain size decreased, and surface texture became smoother with depth. The bottom two meters was described as "putty-like."

2.2.1.2 Waste Configuration 2 Profile

BY-106 is the only tank in WC2B for which sampling has been completed; SX-103 is being sampled currently. No cores are available from WC2A, although S-106 might be sampled in FY 1997.

The BY-106 extrusion video showed saltcake for the entire waste depth of about 5.8 m that released little drainable liquid. The waste near the surface was a dry, off-white, coarse saltcake. The mid-region to the bottom contained a light gray, coarse-grained material with sufficient moisture and adhesion to be extruded in 5- to 8-cm subsegments. There was no sludge layer.

2.2.1.3 Waste Configuration 3 Profile

Waste configuration 3 consists of sludge and saltcake, but these tanks do not necessarily have a distinct sludge layer. In general, the waste is a brown, damp, coarse-grained material in which the color darkens and the moisture content increases with depth. WC3A was represented by cores from BY-104, BY-105, and BY-110. None was available from WC3B. Extrusion video from the WC3C tank, BY-108, was also available.

BY-104 was a brown, dry to wet, coarse-grain saltcake down to about two meters, followed by about a meter of brown, fine-grained, slushy saltcake. The bottom meter was a dark brown, smooth sludge. Cores yielded very little drainable liquid.

The upper 2.4 meters of BY-105 contained a wet, brown, coarse-grained, slushy saltcake whose color darkened with depth. No video was available below 2.4 meters. Very little drainable liquid was found. The waste appeared similar to that of BY-104.

The top 1.5 meters of BY-110 was dry, light-brown saltcake followed by one meter of wet (one segment described as "soupy"), brown, coarse, crumbly saltcake that extruded in 2-cm subsegments. The bottom segment was dark brown, damp, fine-grained, smooth sludge.

BY-108, the only tank in WC3C, contained a brown, damp, coarse-grained saltcake throughout the roughly 2.2 meters of waste. The waste appeared similar to that in the upper region of BY-104.

2.2.2 Waste Surface Appearance

Tanks within the same waste configuration have similar surface appearances. In-tank surface photos and video footage taken in the tanks are, in general, similar. Each tank in waste configuration 1A (cluster 13), with the possible exception of U-111, has a dark liquid supernatant and floating yellowish-gray crust or foam. Figure 2.1 is an in-tank photograph of U-109 that is representative of WC1A tanks. Tanks of waste configuration 1B (cluster 22) have dry, yellowish or grayish saltcake surfaces with no liquid visible. Figure 2.2 is an in-tank photograph of A-101 and is representative of waste configuration 1B.

Waste configuration 2A and 2B tanks, which are of clusters 20 and 15, have mostly dry, yellowish saltcake surfaces. There are small patches of waste of various colors and some liquid

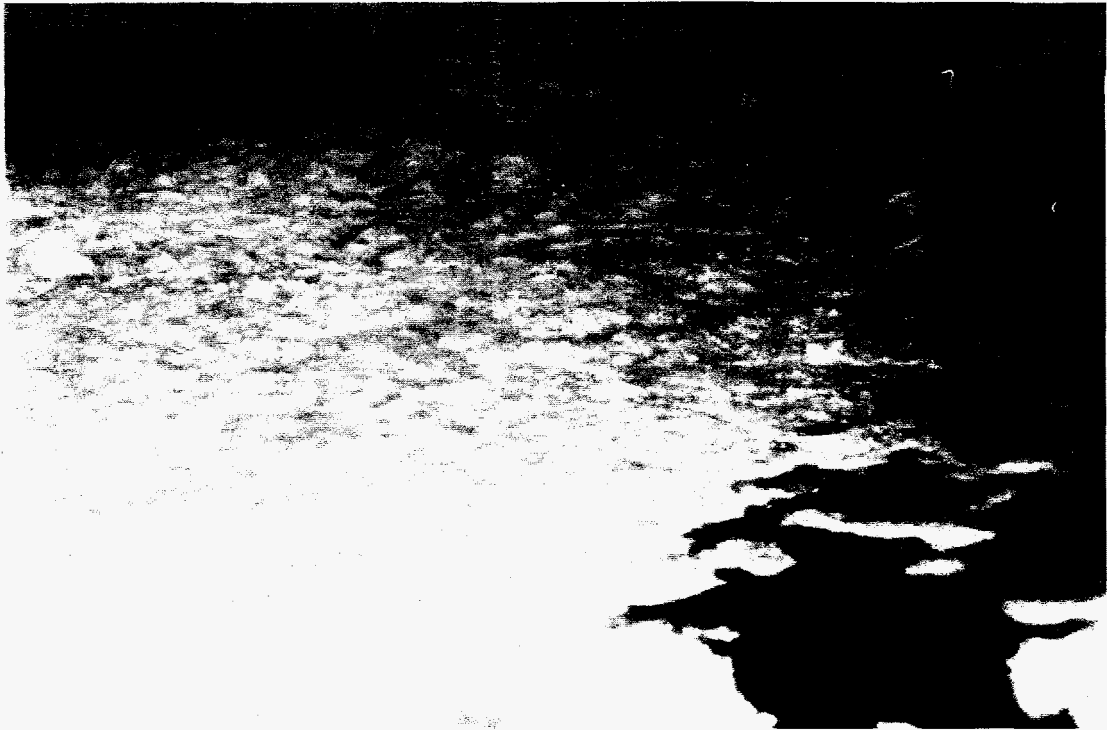


Figure 2.1. Waste Surface in U-109 (Waste Configuration 1A)

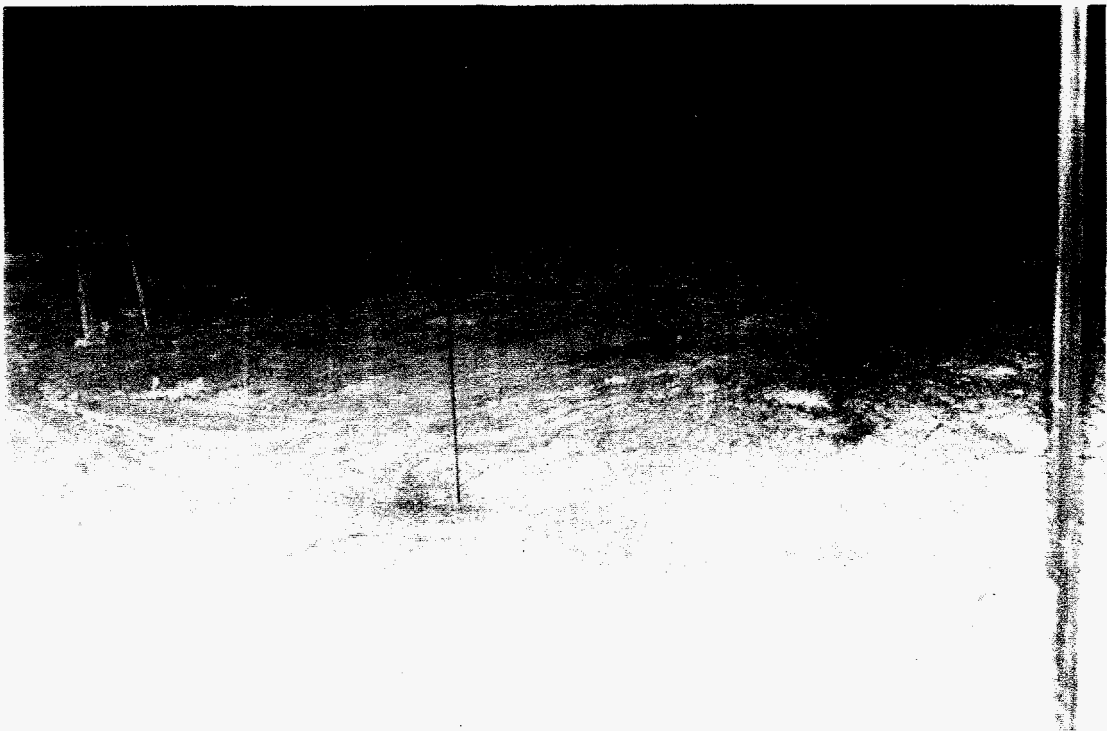


Figure 2.2. Waste Surface in A-101 (Waste Configuration 1B)

pools, but they all appear roughly alike. Figure 2.3 is an in-tank photo of S-106, representative of tanks with waste configuration 2. There is a great deal of similarity in the appearance of the surfaces of waste configurations 2 and 3; in fact, Figure 2.3 is a good representation of the configuration 3 tank waste surfaces as well. Tanks with waste configuration 3 are members of clusters 21 and 11; these tanks have saltcake buildup from the tank walls and mostly dry saltcake surfaces that might vary by as much as a meter in height from one location to another. Waste configuration 4 has a brown, damp, cracked surface similar to a drying mud hole, as shown in Figure 2.4.

Large gas releases can create distinct surface features as evidence. During the months of November and December 1993, the mixer pump in SY-101 produced a series of significant gas releases (Allemann et al. 1994) that did not disrupt the crust layer but filtered through it. Figure 2.5 shows two video frames of the surface of SY-101 displaying two large, volcano-like deposits resulting from these releases (the frames are time-stamped December 1994, but video from December 1993 shows the same formations).

No features of this kind can be found in the SSTs listed in Section 2.1. However, some surface features such as craters below risers, formed by water dripping from above, may be confused with gas release locations. One such crater pattern from BY-108 is seen in Figure 2.6.

A few other features were found that might be identifiable with a small, local, gas releases. Figure 2.7 is the surface in S-103 and shows a "jellyfish" of gray waste material that may have been transported to the surface by escaping gas or thermal convection. Figure 2.8 is the surface in T-104 showing "pock marks" where small pockets of gas may have escaped or local subsidence may have created depressions.

One of the violent release events in SY-101 generated sufficient force to bend a thermocouple tube. Because of this, bent or broken hardware that can be seen in several SSTs is sometimes attributed to prior large GREs. However, tanks in which such damage is found have usually been stabilized and contain hard, dry-looking waste with large hills and valleys (see photos in Caley et al. 1996). Therefore, the apparent damage is much more likely the result of subsidence following liquid removal.

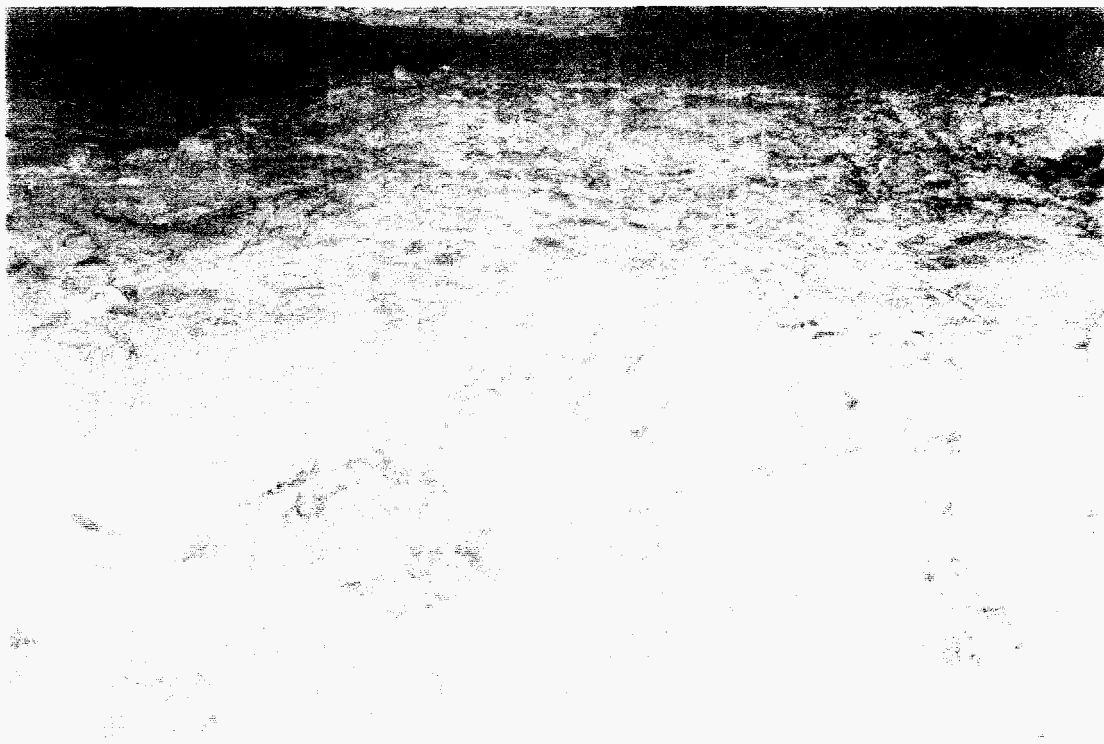


Figure 2.3. Waste Surface in S-106 (Waste Configurations 2 and 3)



Figure 2.4. Waste Surface in T-101 (Waste Configuration 4)

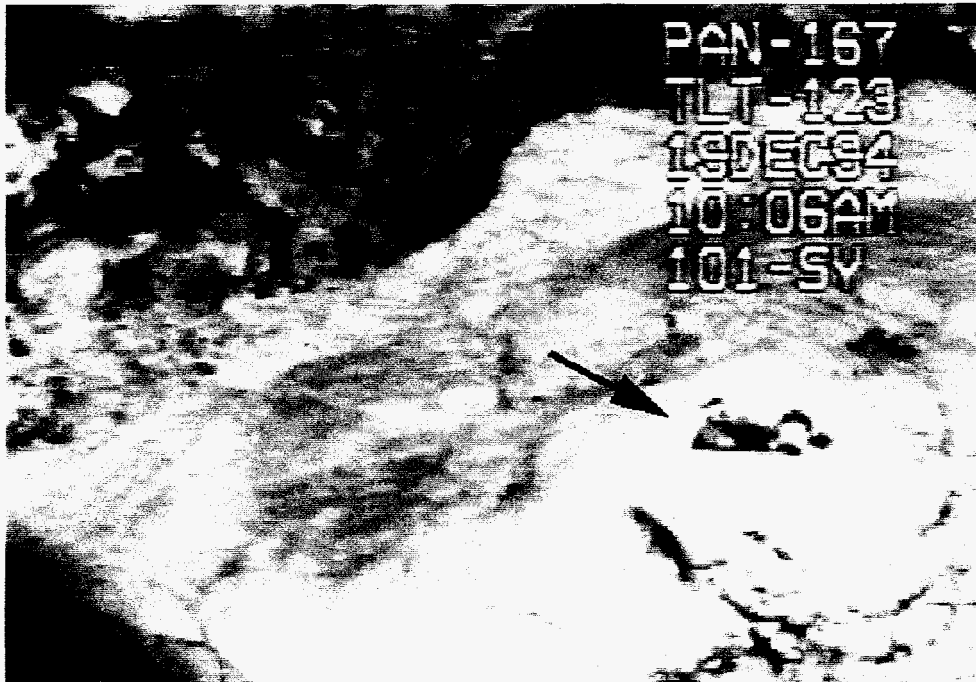


Figure 2.5a. Large Vent or Fumarole (arrow) in SY-101

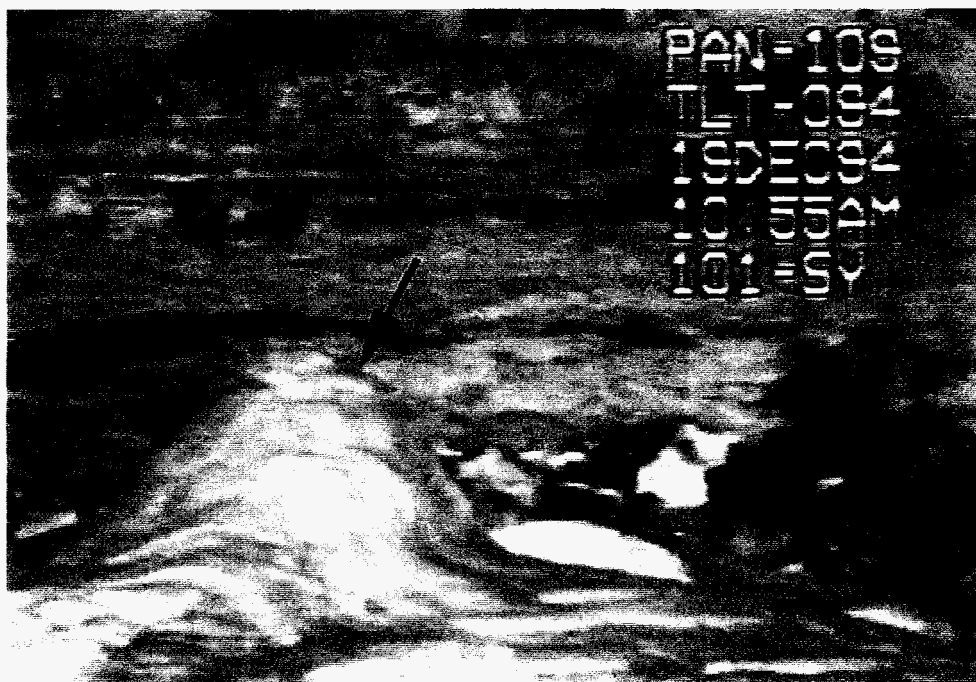


Figure 2.5b. Large Vent or Fumarole (arrow) in SY-101



Figure 2.6. "Crater" Formed by Water Dripping from a Riser in BY-108

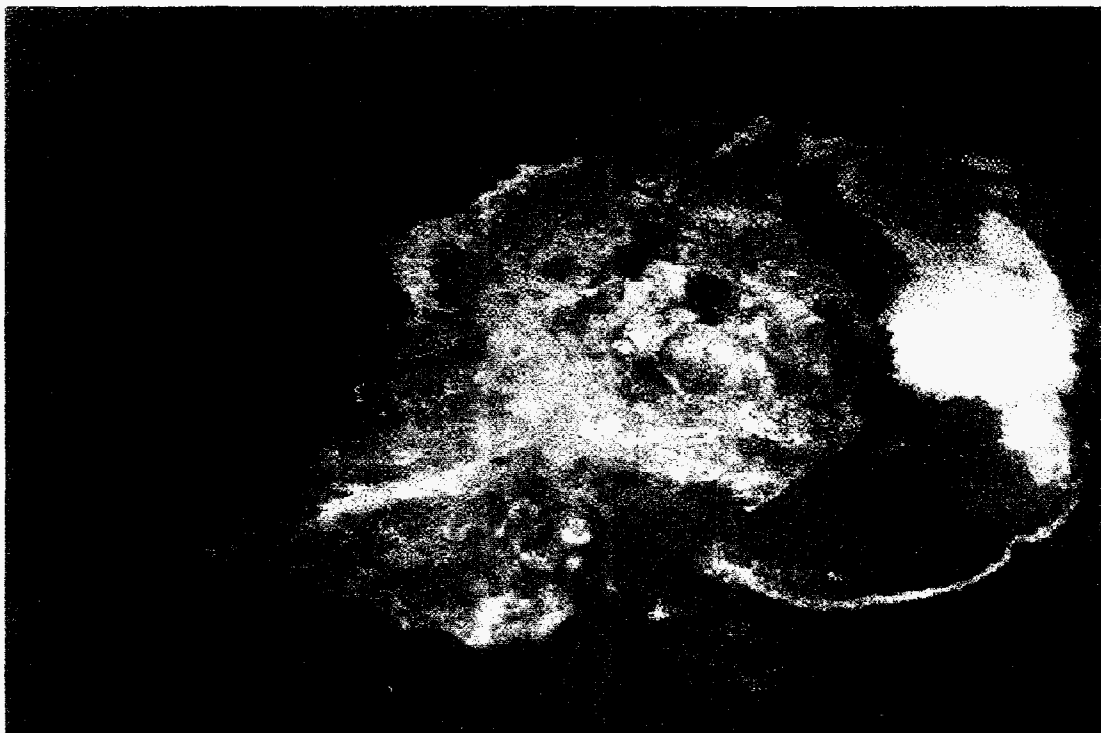
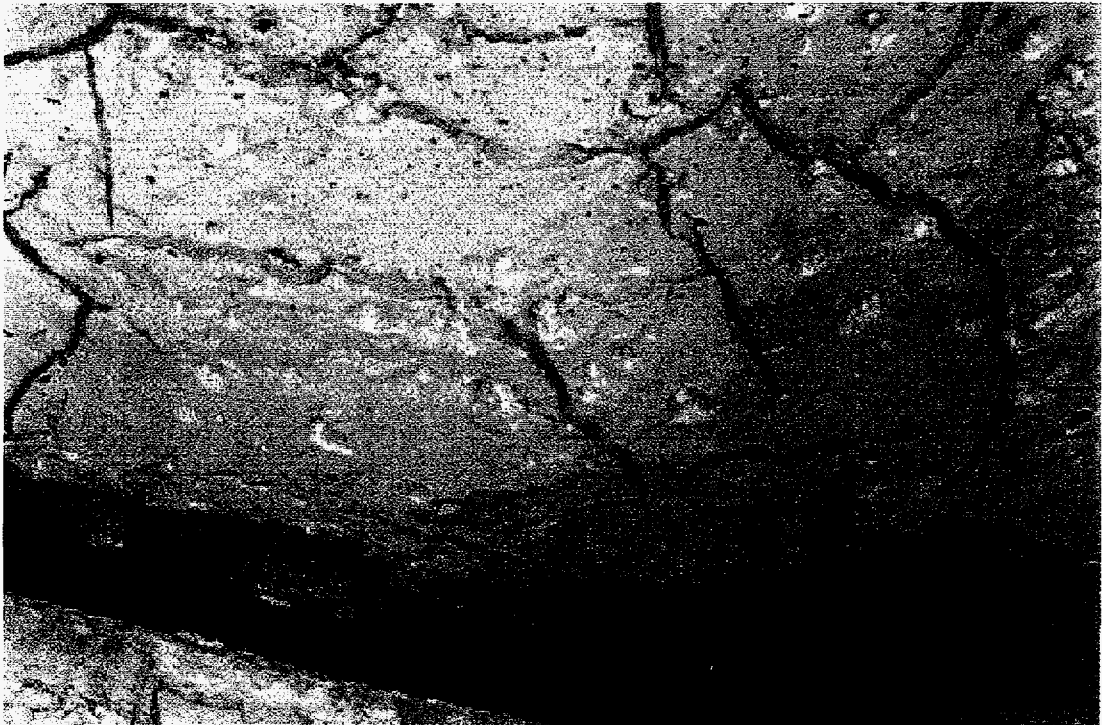
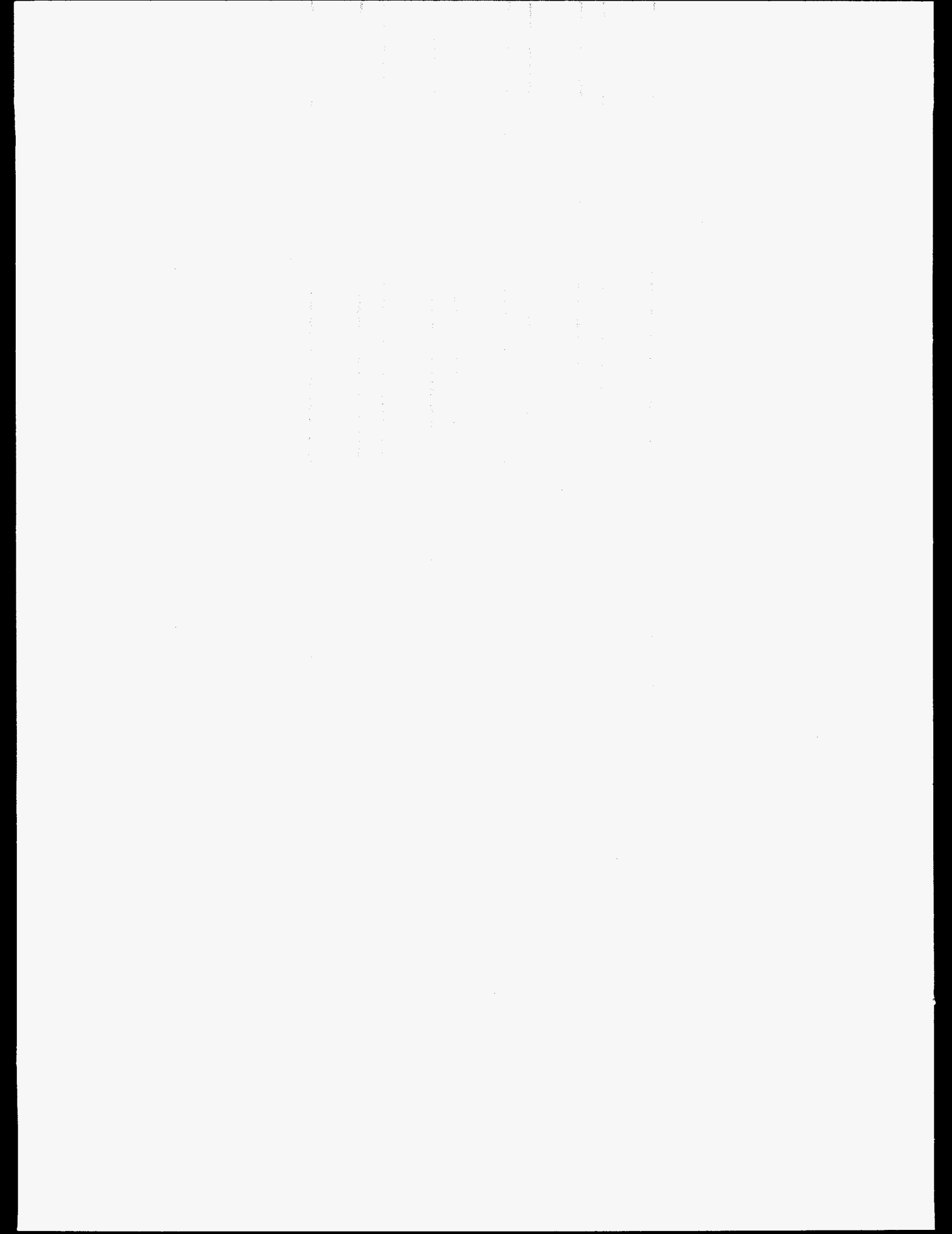


Figure 2.7. "Jelly-Fish" in S-103

Figure 2.8. "Pock Marks" in T-104





3.0 Gas Retention

The potential for gas release from a tank depends on the gas volume that is present and how it is retained. The amount of gas that can be retained and the mechanics of the gas release process depend on the form in which gas bubbles are stored. Undissolved gas may be present in waste as pore-filling bubbles or particle-displacing bubbles; the latter may be discrete "round" bubbles or connected dendritic regions. Section 3.1 describes the currently understood gas retention mechanisms, the type of waste in which they occur, and the maximum void fraction each can attain. Section 3.2 discusses the methods available to measure retained gas volume and some of the results obtained to date. Section 3.3 summarizes the discussion.

3.1 Gas Retention Mechanisms

Particle-displacing bubbles occur most often in waste layers that are under little hydrostatic pressure or have low yield strength and small pore size. The particle-displacing bubbles are called hydrostatic if they have not merged into networks, hydro-dendritic if they have. On the other hand, bubbles that are confined to the pore volume often appear in deep layers of waste or in waste that has large pores and high yield strength. These bubbles, which displace only the interstitial liquid, exist as pore-filling networks and may be referred to as litho-dendritic bubbles. The maximum gas retention due to pore-filling bubbles is limited by the waste porosity; the upper limit on gas retention by particle-displacing bubbles is higher, because porosity is not relevant for this bubble type.

In pore-filling bubbles, gas is retained primarily by surface tension forces on the bubble-liquid interface rather than by the yield strength of the material itself, as with particle-displacing bubbles. The transition from particle-displacing to pore-filling bubbles occurs when the litho-static load and material strength holding the particles together exceeds the surface tension force tending to push them apart. This force balance can be expressed as a dimensionless group similar to the Bond number (Gauglitz et al. 1995). The Bond number criterion for existence of litho-dendritic bubbles is given by

$$N_{Bo} = \frac{\Delta\rho gh D_p}{4\sigma} + \frac{\tau_s D_p}{4\sigma} \left(\frac{A_2}{A_1} \right) > 1 \quad (3.1.1)$$

- where N_{bo} = the Bond number (1 at transition)
 h = the depth of the bubble, in meters
 D_p = the mean pore diameter through which a bubble must pass to escape retention, in meters. Pore diameter is essentially equal to the particle diameter in an irregular, crystalline material.
 $\Delta\rho$ = the difference between solid and liquid density; if the solids density is 1800 kg/m³ and the liquid density is 1400 kg/m³ then $\Delta\rho = 400$ kg/m³
 σ = the surface tension, 0.08 N/m
 τ_s = the yield stress; 500 Pa is used
 A = A_2/A_1 is a ratio related to how the yield stress resists bubble expansion; it was estimated at 2.8 by Gauglitz et al. (1995).

For a particle diameter of 30 microns (3×10^{-5} m), expected for typical SST saltcake,^(a) pore-filling bubbles can be present at depths below 2.5 m. All but four of the tanks on the SST "short list" (see Table A.1) significantly exceed this waste depth. However, tanks in waste configurations 1, 3, and 4 contain fine-grained salt, slurry, or sludge in the lower layers (see Section 2.2 and Appendix B). With a particle diameter under 10 microns, these tanks will probably retain gas entirely in particle-displacing form. Some tanks have very coarse saltcake near the surface whose pore diameter might be on the order of 100 microns. If submerged, litho-dendritic bubbles could exist below a depth of about half a meter in this material.

Gauglitz et al. (1996) showed that bubble morphology could be described by lithostatic and yield stress components of the Bond number, as shown in Figure 3.1. The transition between pore-filling and particle-displacing bubbles is determined by the balance of lithostatic load against the force of capillary force (the plot's horizontal axis) and by the ratio of the yield strength of the porous medium to the capillary force (the right axis). At the transition values of the pore-based Bond numbers, the capillary force equals that required to expand the bubble against the pressure and the material strength. High yield strength, high lithostatic load, and/or large pores will cause bubbles to be litho-dendritic or pore-filling rather than particle-displacing.

The shape of a particle-displacing bubble is described by the balance between the bubble excess pressure due to surface tension and the material yield stress (left axis of Figure 3.1). Bubbles tend to remain roughly spherical (round), hydrostatic, until material strength becomes the dominant force resisting expansion. Then the bubbles grow into the weakest point on their surface and evolve into a slit shape. The higher the yield stress, the smaller the bubble that can retain a spherical shape and the lower the void fraction at which bubbles interconnect into a hydro-dendritic network. This phenomenon also precludes the existence of individual discrete bubbles of more than about a centimeter in diameter.

The remainder of this section is concerned with the maximum volumetric gas fraction (void fraction) that can be retained in each of several waste configurations: particle-displacing bubbles in solids that are not subject to buoyant displacement, solids subject to buoyant displacement (either particle-displacing or pore-filling bubbles), pore-filling bubbles, and unsaturated (drained) saltcake.

3.1.1 Particle-Displacing Bubbles

Without a supernatant liquid layer, a buoyant solids layer cannot rise and release its accumulated gas. In this case gas is retained until the bubbles become large enough to rise or until connected, dendritic bubble regions break through to the surface. Several different gas retention mechanisms have been observed that depend largely on the waste strength.

Gauglitz et al. (1996) have performed gas retention experiments using bentonite clay to simulate the fine clay-like sludge found in waste configurations 1, 3, and 4. Bubbles were generated by decomposing hydrogen peroxide. The tests were performed in vessels with diameters ranging from 2.5 to 30 cm and initial layer heights ranging from 15 to 90 cm. The results showed that the strength of the simulant affected the shape of the retained bubbles, the void fraction at maximum retention, and the gas release mechanisms. In all cases the bubbles in the sludge simulant were particle-displacing, either hydrostatic (round) or hydro-dendritic.

^(a) Lenhard RJ. January 20, 1995. *Assessment of Average Salt-Cake Pore Sizes in Tank 241-BY-107 at Hanford and Determination of a Particle-Size Distribution for a Salt Cake Surrogate*. White paper prepared for RM Bean, Pacific Northwest Laboratory, Richland, Washington.

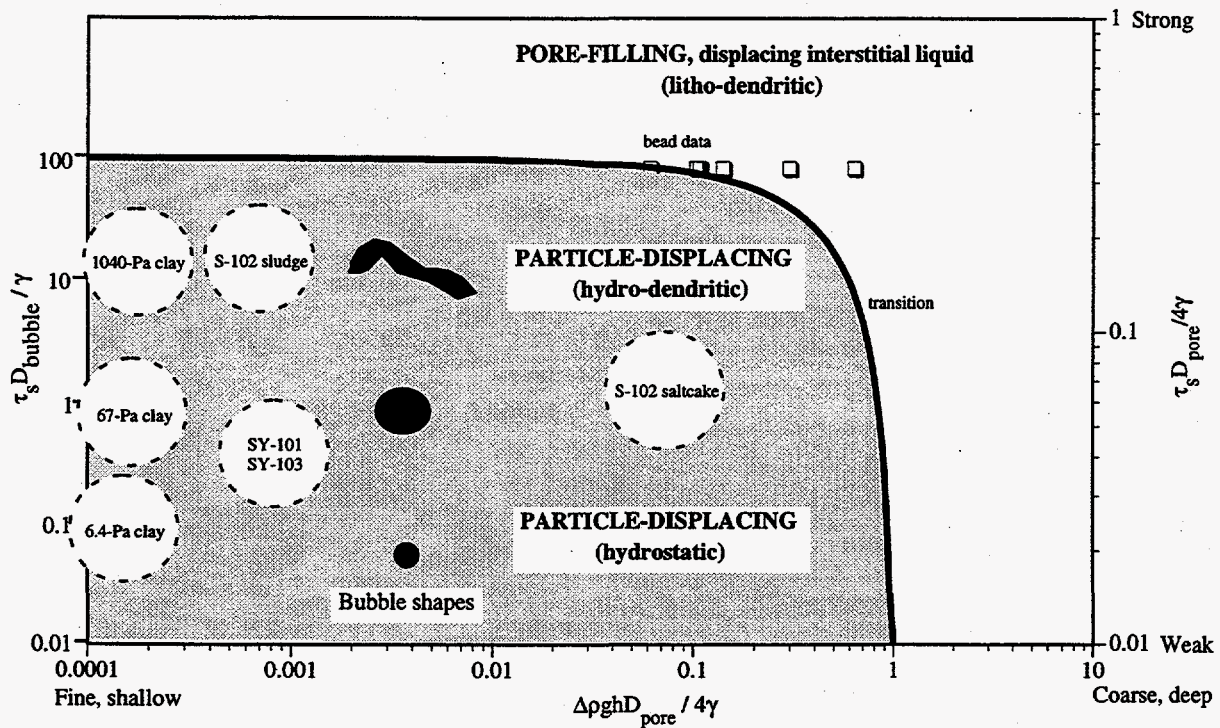


Figure 3.1. Bubble Morphology Map

In strong simulants (shear strength of about 1000 Pa), bubbles immediately assumed a slit-shaped, hydro-dendritic form, and maximum void fractions were about 30% (based on level rise). No large, rapid gas releases were seen in these strong simulants (in the absence of a liquid layer); instead, the gas bubbles connected and formed a flow path that released gas continuously as it was generated.

For bentonite clays with moderate strengths (shear strength of 50–200 Pa), bubbles smaller than 0.5-mm diameter were spherical, while bubbles larger than 1-mm diameter were always distorted. In 200-Pa clay, the bubbles eventually connected into a hydro-dendritic network, exhibiting either a continual, steady gas release or cycles of retention followed by small periodic releases.

In 67-Pa clay the bubbles eventually coalesced to span the 2.54-cm vessel, and releases occurred when these aggregates partially collapsed. The same behavior was observed in a 10.2-cm vessel. However, in the vessels 15.2 and 30.5 cm in diameter, individual hydrostatic bubbles grew until their buoyant force exceeded the material strength, and they began to rise. This disturbance yielded nearby material, which released neighboring bubbles. These in turn spread the disturbance in a general cascade that suddenly released a large fraction of the vessel's retained gas. This bubble cascade release phenomenon was also observed in the small, 2.54-cm vessel with weak, 6-Pa clay, but it was never observed in 200-Pa simulants, even in test vessels up to 90 cm in diameter.

The maximum retention for these moderate-strength, sludge-like simulants was about a 40% void fraction for an initial depth of 30 cm, including tests in which the bubble cascade occurred. This intermediate range of strength (roughly 100 Pa) gave the largest gas retention of all the simulants tested. Additionally, the maximum retention increased with increasing initial

simulant height, and a void fraction of 50% was observed in the experiment with the largest initial height (90 cm). However, this was due to presence of more vessel-spanning bubbles that would not exist in a large tank.

For weak bentonite clays (shear strength in the range of about 6 Pa), the retained bubbles were always round or nearly round. In even the smallest-diameter vessels, before the bubbles could connect and allow continual release of gas, the clay lost its ability to retain the bubbles, and essentially all of the retained gas was released in the bubble cascade described above. The maximum void fraction attained was 30%.

For extremely weak clays (less than about 3 Pa shear strength), round bubbles grew only to a small size (1 mm or less) before yielding the surrounding material and rising individually without producing a general bubble cascade release. Typically, the void fraction of retained bubbles was small (less than 10%), and the release of these bubbles was continuous.

Some tank waste of sludge-like consistency was also studied using similar methods (Gauglitz et al. 1996). The results qualitatively confirmed those obtained for clays. A stiff sludge sample from S-102 (waste configuration 1A) retained about 20% void fraction at maximum growth, whereas a softer and apparently lower-strength sample from the same tank retained about 33%. Also, as for the clays, the stiffest waste (stiff S-102 sludge) released gas continuously, while the softer sludge exhibited periodic releases.

In summary, the amount of retained gas showed a clear maximum with increasing material strength. The maximum was about 40% void for clays in a range of about 100-Pa yield strength. Clays of less than 10 Pa were pourable, and their maximum gas retention, in the range of 5–20% void, was governed by the tendency of bubbles to escape by rising individually, giving a continuous gas release. At 200 Pa and higher yield strengths, retention reached about 30–35% void; the slit-shaped bubbles interconnected and continuously released gas at a lower void fraction than would have been necessary for rounded bubbles. Thus bubble rise limits gas retention for weak material, while gas percolation (which is affected by bubble shape) limits retention for strong materials.

The fraction of the retained gas that was released in any one event was also dependent on yield strength, as shown in the same experiments. The weakest, 3-Pa shear-strength clay released gas continuously by individual bubble rise. Ten-Pa and weaker clays released 70–100% of the retained gas by a general bubble cascade. At about 60 Pa, maximum periodic releases of 70% of the retained gas were observed, both from the cascade in larger vessels and from the cyclic release in smaller vessels. At 200 Pa and above, continuous percolation release occurred.

Based on the laboratory evidence above, the upper bound of gas retention for particle-displacing hydro-dendritic bubbles is about 40% void. This value occurs in moderate-strength material (~100 Pa). Stiffer, sludge-like waste with yield stress above about 1000 Pa stores a maximum 30% void. However, the in situ gas fractions measured in actual tank waste are typically less than 20%, and the highest value (the only one above 20%) is 33% gas (see Section 3.2). Taking the in situ as well as the laboratory data into account, we suggest a maximum gas fraction of 30%.

3.1.2 Nonconvective Layer Subject to Buoyant Displacement

The neutral buoyancy void fraction sets the upper bound of the void fraction for tanks with enough supernatant liquid to allow buoyant displacements, regardless of whether the gas is stored in a particle-displacing or pore-filling mode. The void fraction at neutral buoyancy, α_{NB} , can be estimated from the densities of the supernatant and ungasged nonconvective material by

$$\alpha_{NB} = 1 - \frac{\rho_{LIQ}}{\rho_{NC}} \quad (3.1.2)$$

Typical neutral buoyancy void fractions range from about 15% in AN-103 to about 6% in SY-103 (Stewart et al. 1996).

Recent experiments by Gauglitz et al. (1996), which are discussed in Section 4.1, have shown that (in laboratory vessels) buoyant displacements can occur when the thickness of the supernatant layer is 25% or more than that of the nonconvective layer. A clay simulant with a 14-Pa yield stress under a deep supernatant liquid layer rolled over violently at about 15% void. With a shallow liquid layer the solids and liquid gently traded places at 20% void without releasing any gas. Neutral buoyancy would have occurred at about 7% void. The void fraction was significantly higher than neutral buoyancy because of the restraining effect of the strength of the clay in the relatively small vessel. A stronger, 67-Pa clay did not displace spontaneously regardless of liquid depth. When buoyant displacement was manually initiated at 25% void, the tests repeated the behavior of the 14-Pa clay tests except that less gas was released in the deeper supernatant.

Actual DST waste samples showed the same behavior. A sample of the nonconvective layer from SY-103 rolled over at 9.2% void as determined by level growth. When the supernatant liquid layer thickness was less than 10% of the nonconvective sample thickness, gas release occurred not by buoyant displacement but by erosion, in which the liquid infiltrated the bubbly waste and provided a path for gas flow. In these cases, the retained gas fractions were greater than the neutral buoyancy values and were roughly as high as for tests in which no supernatant was present.

3.1.3 Pore-Filling Bubbles in Submerged Saltcake

The void fraction in a region of pore-filling bubbles can approach the porosity of the material less a fraction to account for liquid trapped along with the gas. That is, if the porosity is 40%, the maximum void might be around 30%. This agrees with the volume of gas that is required to float the crust layer in SY-101, where voids of 25–35% are calculated (Brewster et al. 1995).

Gauglitz' experiments with sand and sugar water, in which CO₂ bubbles were generated by yeast (Gauglitz et al. 1994), and with glass beads and ammonia, in which bubbles were generated by depressurizing ammonia (Rassat and Gauglitz 1995), provided an estimate of gas retention in a coarser-particle material typical of saltcake. In both experiments, the total gas retention for all three regions (hydrostatic, fracture, and litho-dendritic bubbles) did not exceed 25% void. In these relatively monodisperse simulants the porosity was about 35%, so the maximum retained gas volume was about 70% of the pore space.

No gas fractions higher than about 30% have been observed in situ. Taking all these very approximate items of evidence into account, we set the upper bound for gas retention at 30% in wet saltcake, regardless of its relation to the liquid level. It is not clear how much of this gas might be present as pore-filling bubbles and how much as particle-displacing bubbles.

3.1.4 Gas in Unsaturated Saltcake

Saltcake above the liquid level can hold gas only in regions where there is enough liquid to bridge across particles and trap individual bubbles. If the interstices (pores) are not blocked by a liquid, the gas present is not pressurized or contained (not retained) and communicates with the tank head space by diffusion, which is extremely rapid in gases. Experiments by Gauglitz et al.

(1996) have demonstrated that no gas retention occurs in saltcake that is higher than the free liquid level in the tanks. Thus if the liquid level is reduced relatively quickly, gas that had been blocked by liquid becomes free to diffuse out as liquid drains away. Salt-well pumping is one operation that has this result.

3.2 Retained Gas Volume Estimates

Three methods have been employed to estimate the gas content (void fraction) of waste. The first two approaches infer the overall tank-average void fraction from changes in the waste level. The other method measures the void fraction directly by sampling at several point locations in the tank; the overall gas content is estimated from the local data. These methodologies depend on the bubble morphology to different extents.

In the first inferential method, the amount of gas in the tank is derived from the short-term response of the waste level to variations in barometric pressure, under the assumption that the level changes result from isothermal compression and expansion of the retained gas in a uniform material. In the second, the long-term rise in waste level is taken to be the result of increased gas content, like rising bread dough. Both of these methods depend crucially on whether gas is present as pore-filling or particle-displacing bubbles. Pore-filling bubbles only displace liquid as their volume increases or decreases, so they affect the interstitial liquid level but not the surface level of the solid waste (unless it is floating on the liquid). Particle-displacing bubbles affect both the solid and liquid surface levels.

Two devices are available to make a direct measurement of the void fraction: the VFI and the RGS. The VFI can be operated only in DSTs and has made measurements in all six of the WL DSTs. The RGS can be used wherever push-mode core sampling is possible. To date it has been used in two DSTs (AW-101 and AN-105) and one SST (A-101). These do not depend on the bubble morphology, because the gas in a sample is measured equally well no matter which type of bubble was originally present.

3.2.1 Barometric Pressure Effect Method

Retained gas can be detected by correlating the waste surface level with changes in the atmospheric (barometric) pressure. This type of gas assessment is called the Barometric Pressure Effect (BPE) method. The barometric response of the level is referred to as "dL/dP" and is calculated as the slope of the correlation of waste surface level, or interstitial liquid level, with atmospheric pressure. Because increased pressure decreases the gas volume and height, gas is determined to be present (or not) depending on the frequency of negative slopes. The more negative the slope, the higher the void fraction. Positive dL/dP values have no physical significance. The relationship between dL/dP and the average in situ void fraction, α , based on the ideal-gas law, is

$$\alpha = P/L (-dL/dP) \quad (3.2.1)$$

where P is the effective pressure at which the gas is stored, and L is the total depth of the wetted waste. The total in situ gas volume is obtained by multiplying Eq. (3.2.1) by the total waste volume

$$V_{GAS} = AP (-dL/dP) \quad (3.2.2)$$

where A is the tank cross-sectional area.

The details of the statistical techniques for deriving the distribution of dL/dP from the waste level and barometric pressure data are described by Whitney (1995). A dL/dP value is obtained for the waste level and corresponding atmospheric pressure measurements for each 60-day period.

The inherent statistical uncertainty in dL/dP depends on the uncertainty and sensitivity of level measurement (see Johnson [1996] for a thorough discussion of waste level measurement as it pertains to gas volume estimates). The FIC contact probe and the Enraf buoyancy gauge both give acceptably low uncertainties; the latter is better if readings are automated. The manual tape (MT) is simply not sufficiently sensitive, and its uncertainty is too high to provide useful estimates of void fraction. The neutron interstitial liquid level (N-ILL) level measurements cannot be used to estimate trapped gas because the waste configuration in which it operates violates the basic assumptions of uniformity in Eq. (3.2.1). Unphysical void fractions greater than 100% can result from N-ILL data.

In addition, the frequency with which tank level measurements are made affects the accuracy of the BPE method; some tanks have hourly level measurements, others daily, monthly, or quarterly. Some readings are made and recorded automatically, but most are manual. In the latter, the level may be recorded several hours after the actual measurement was taken.

The single dL/dP value that is used to estimate the average void fraction in a tank is the 50th or 75th percentile value of the set of 60-day dL/dPs calculated for that tank. Half the calculated dL/dP values are higher, half lower than the 50th percentile dL/dP . For the 75th percentile, only 25% of the set of dL/dPs are higher. The 75th percentile is considered bounding. Table 3.1 shows BPE void fraction estimates made using 50th and 75th percentile dP/dL values. The dL/dP values and the methodology used to calculate the void are consistent with Hopkins (1995) and Hodgson et al. (1996). The table includes the tanks on the FGWL and the 25 tanks recommended for the FGWL. (Table 3.1 also includes void fractions estimated using the level rise method, which is the subject of Section 3.2.2.)

In Table 3.1, many tanks have a void fraction listed as undefined (UNDEF). In these cases, values less than 0 or higher than 30% were calculated. It is believed that 30% is the maximum void fraction possible in a tank (Hopkins 1995). For most of the tanks for which BPE void fractions greater than 30% were estimated, N-ILL or MT measurements were the source of the dL/dP values used. Therefore, the values of void fraction derived from these sources are not shown.

The BPE method, as just described, depends on the assumption that atmospheric pressure changes are immediately felt everywhere in the stored gas and that the level change is due only to the resulting isothermal thermodynamic expansion or compression. This assumption is not fully consistent with recent automatic, hourly Enraf level data, which show distinct hysteresis loops or parallelograms in the correlation between level and barometric pressure for the SSTs in which these fine-resolution measurements are available.

It is possible that expansion and compression of gas bubbles in the waste is hindered by the strength of the waste. The bubbles may freely expand and contract only when the pressure changes are large enough to cause the waste around the bubbles to yield. A model of waste elasticity has been included in a new version of the BPE method, called BPE2 for simplicity (Whitney et al. 1996). In this model, gas is assumed to exist as small spherical bubbles that do not interact with each other. When the atmospheric pressure changes are large enough to cause bubble-wall tangential stresses that exceed the waste's yield strength, the material fails. The waste is assumed to have simple linear elasticity: the stress increases linearly with strain until it equals the yield strength, after which the stress is constant (plastic region). Figure 3.2 shows the observed and

Table 3.1. Void Fraction Estimates

Tank	Category	Void Fraction (percent) based on			
		50th %ile dL/dP	75th %ile dL/dP	Level rise (with evap.)	Level rise (no evap.)
A-101	FGWL	^(a)	^(a)	---	---
A-103	rec.	5	15	---	---
AX-101	FGWL	---	---	---	---
AX-103	FGWL	---	15	4	UNDEF
BX-107	rec.	6	10	0.5	0.5
BY-101	rec.	UNDEF ^(a)	UNDEF ^(a)	15	15
BY-102	rec.	^(a)	^(a)	---	---
BY-103	rec.	^(a)	^(a)	---	---
BY-105	rec.	^(a)	^(a)	2	2
BY-106	rec.	---	---	11	11
BY-109	rec.	0	7	---	---
C-104	rec.	3	9	---	---
C-107	rec.	1	2	---	---
S-101	rec.	6	8	19	0.2
S-102	FGWL	21	25	20	20
S-103	rec.	20	26	20	8
S-105	rec.	^(a)	UNDEF ^(a)	8	8
S-106	rec.	UNDEF	UNDEF	25	15
S-107	rec.	4	7	30	18
S-109	rec.	^(a)	UNDEF ^(a)	3	3
S-111	FGWL	14	17	7	7
S-112	FGWL	---	---	6	6
SX-101	FGWL	2	6	---	---
SX-102	FGWL	13	15	7	5
SX-103	FGWL	18	23	6	0.2
SX-104	FGWL	0	1	0.7	0.6
SX-105	FGWL	---	---	8	4
SX-106	FGWL	10	13	23	7
SX-109	FGWL	---	---	7	UNDEF
T-110	FGWL	---	---	3	3
TX-102	rec.	UNDEF ^(a)	UNDEF ^(a)	1	1
TX-111	rec.	UNDEF ^(a)	UNDEF ^(a)	12	12
TX-112	rec.	UNDEF ^(a)	UNDEF ^(a)	10	10
TX-113	rec.	UNDEF ^(a)	UNDEF ^(a)	8	8
TX-115	rec.	UNDEF ^(a)	UNDEF ^(a)	14	14
U-102	rec.	^(a)	UNDEF ^(a)	11	2
U-103	FGWL	11	13	6	4
U-105	FGWL	9	14	UNDEF	13
U-106	rec.	4	7	12	10
U-107	FGWL	8	11	5	5
U-108	FGWL	---	---	15	6
U-109	FGWL	8	10	7	5

(a) BPE was based on MT or N-ILL data; therefore, no numerical values are included.

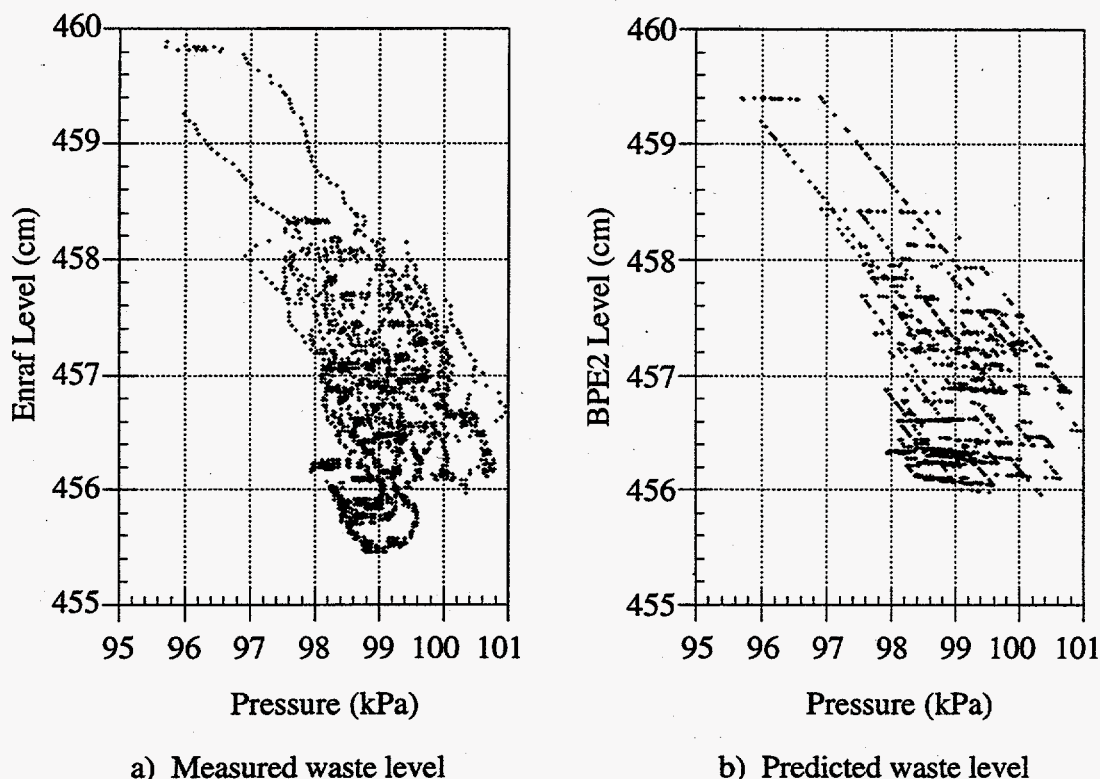


Figure 3.2. Measured and Predicted Level Responses to Pressure Variations for Tank 241-S-106

predicted tank levels versus atmospheric pressure for Tank S-106 during the last quarter of 1995, as an example of the behavior of the hysteresis effect. In general, the BPE2 predictions show a strong qualitative agreement with observations and capture the hysteresis scatter as the original BPE method could not. The BPE2 model is described below.

The stresses and strains at the boundary of a gas-filled bubble were derived analytically via classic linear elasticity theory. The gas pressure in the bubble was considered to vary with expansion or contraction according to the ideal gas law. It was found that, for yield to occur,

$$|\Delta P_a| > 2\tau \quad (3.2.3)$$

where ΔP_a = the change in the atmospheric (barometric) pressure
 τ = the waste yield stress.

The pressure change, ΔP_a , is measured relative to the last pressure inflection point (the last local maximum or minimum in pressure). The material around the bubble is assumed to be reset to its initial elastic state whenever the rate of pressure change reverses sign. The yield strength is half the pressure difference across the base of the hysteresis parallelogram. When a pressure change exceeds the yield criterion, the level response is as in the original BPE model. The average void fraction is determined from Eq. (3.2.1). When a pressure change is less than the yield criterion, the level response is that of an elastic material:

$$\frac{dL}{dP} = -\frac{9(1-\nu)\alpha L_0}{2E} \quad (3.2.4)$$

where ν = Poisson's ratio for the waste (assumed 0.4)
 α = the mean void fraction of retained gas
 L_0 = the waste depth before the pressure change
 E = elastic modulus of the waste.

The elastic modulus is actually derived from Eq. (3.2.4), where the void fraction is derived from Eq. (3.2.1) when the pressure exceeds the yield stress, and dL/dP is the slope of the base of the parallelogram across which the yield stress was measured.

The tanks that showed the largest hysteresis effect over the evaluation period (the last quarter of 1995) were S-106, S-107, S-111, U-103, and U-107. The Enraf level and pressure data for these high-hysteresis tanks were analyzed using BPE2. Table 3.2 compares the dL/dP slopes estimated by the BPE2 model with those from the unmodified BPE and gives the properties estimated from the hysteresis. Note that the BPE2 model can only be applied to tanks whose waste level is recorded with an automated Enraf gauge.

In general, the slope and therefore also the gas volume given by the improved model is 15–56% higher than the original BPE model. The range of values for E is consistent with the range of E measured for moist limestone agglomerates (Schubert et al. 1975). The yield stress values are one-fourth or less of the shear strengths measured for glass bead simulants of noncohesive wastes at low gas content (Gauglitz et al. 1995).

3.2.2 Surface Level Rise Method

Long-term trends in waste level can also be used to detect retained gas. In this surface-level-rise (SLR) method the cumulative surface level rise is estimated, generally setting a reference level at a time after tank transfers were complete. An increasing amount of gas in the tank is assumed to increase the total waste volume and the waste level by exactly the growth in gas volume.

The SLR method requires knowledge of the historical events or processes other than gas accumulation that might cause waste volume changes, including leakage, in-leakage, evaporation, waste compaction, and other phenomena. Another prerequisite for this method is a knowledge of the amount of gas retained in the waste at the reference level, that is, the level at the point in time from which level rise is calculated. Thus, much of the level rise and void fraction estimation depends on historical data (which may be impossible to confirm). For many tanks, half or more of the value of the SLR gas volume estimate comes from the evaporation term, which is grossly

Table 3.2. BPE and BPE2 dL/dP and Waste Properties

Tank	BPE dL/dP (cm/kPa)	BPE2 dL/dP (cm/kPa)	τ (kPa)	E (MPa)
S-107	-0.07	-0.15	0.50	1.6
S-111	-0.32	-0.52	0.40	8.1
S-106	-0.34	-0.69	0.55	13
U-103	-0.21	-0.40	0.40	> 20
U-107	-0.18	-0.21	0.20	> 20

over-conservative. This introduces so much uncertainty that the SLR method was not considered appropriate for quantitative gas volume estimation in a critical review of flammable gas evaluation methods (Johnson 1996).

Table 3.1, as already noted, contains the SLR void fraction estimates for the tanks already on the FGWL and those whose inclusion on the list has been recommended. Void fractions calculated both with and without evaporation are included.

3.2.3 Direct Void Fraction Measurement

The VFI directly measures the void fraction (undissolved gas fraction) at specific point locations in a tank, rather than inferring the average void fraction throughout the tank as the BPE and SLR methods do. The RGS is another point measurement device that operates on a different principle than the VFI.

The VFI does not measure gas composition, and its response is very nearly independent of gas composition. It measures void fraction by compressing the waste captured in a leak-tight sample chamber with nitrogen gas. The void fraction is calculated from the initial and final pressures and temperatures and known system volumes. Non-ideal gas effects (significant at the compression pressure of about 35 atm) were included in VFI data interpretation. The VFI cannot be operated in the typical DST crust layer or any relatively strong material, making it difficult or impossible to use in most SSTs.

The tank gas volume is computed from the average void fraction. The average void is computed in several vertical layers chosen consistent with the overall waste configuration. The entire convective layer is treated as a single layer extending from the estimated base of the crust to the approximate top of the nonconvective layer. The nonconvective layer is split into two or three sublayers with boundaries determined by a visual interpretation of the variation in void fraction to yield a fairly uniform vertical void distribution. The gas volume stored in the crust layer is estimated from the crust thickness and the void fraction required to make it float. Waste temperatures and densities are also required to calculate the gas volume from the void fraction.

In the six DSTs that have been studied with the VFI (SY-101, SY-103, AW-101, AN-101, AN-104, AN-105), the peak void fraction in the nonconvective layer occurs at about the same location as the peak temperatures. In some tanks there is considerable scatter in the measurements. Convective layer void fractions are effectively zero (zero to less than 1%). AN-103 showed the highest void fraction (11–15%) with the least scatter in void measurements.

The other direct in situ void fraction instrument is the RGS, which measures gas composition as well as void fraction.^(a) The RGS is a modified version of the universal core sampler (Cannon and Knight 1995) and is designed to be absolutely leak-tight. RGSs are loaded into the drill string during a normal push-mode core sampling event. After capturing a waste sample and recovering it from the drill string, the sampler is X-rayed to determine whether a full sample was captured; the X-ray images are also used to measure the line-of-sight density of the sample. In the 222-S laboratory, the sample is extruded into an extraction vessel, where the waste gas is removed for analysis by a combination of stirring, vacuum pumping, and heating. Samples of the gas are taken at each stage of the extraction process and sent to PNNL for mass spectrometry.

^(a) Shekarriz A, DR Rector, MA Chieda, M White, and JM Bates. 1996. *Retained Gas Sampler Measurement Results for Hanford Waste Tank 241-AW-101*. Letter report TWS-MIT-071996, Pacific Northwest National Laboratory, Richland, Washington.

The percentage of the in situ sample volume occupied by the insoluble and undissolved soluble gases (the void fraction) is calculated from the total measured quantities of these gases in each RGS segment using the ideal gas law. Henry's Law constants for soluble gases are calculated at each sample segment. The results are also corrected for entrained drill-string gases, making the assumption that all the oxygen and argon in the sample are from entrained rather than in situ gases. The local in-tank pressure is assumed to be the local hydrostatic pressure found from the density of the waste. The uncertainty in the resulting void fraction value is 10% in most samples and 20% in the supernatant liquid layer.

To date, Tank A-101 is the only SST in which in situ void fractions have been measured by the RGS.^(a) The most significant finding was that the excess liquid, which had been assumed to be supernatant, was actually on the bottom of the tank, with the gas-bearing saltcake on top. Thus A-101 might have more in common with the floating crust layer in a DST than with the typical SST configuration. The void fraction was also higher than expected. In the upper saltcake, void fraction appears to increase slightly with depth; it is 13% at 276 inches elevation, 15% at 200 inches. The void fraction in the lower liquid layer is essentially zero at 0.4–0.7%. It was estimated that 72% of the gas in the void volume was hydrogen, less than 6% nitrous oxide, and less than 1% ammonia.

In the two tanks (AW-101 and AN-105) where both VFI and RGS measurements have been made so far, both are entirely consistent with one another and with the BPE method.

3.3 Conclusion on Gas Retention

Gas retention mechanisms are becoming relatively well understood. It is now possible to predict the bubble shape and size given the basic material properties. Theory and experiment predict the maximum gas retention to be 30–40% void for particle-displacing bubbles in fine-grained sludges or waste near the surface, 25–30% void for pore-filling bubbles in coarse grained saltcake or waste near the tank bottom, and 15–20% where gas retention is limited by neutral buoyancy in nonconvective layers subject to buoyant displacement. Unsaturated waste that is above the free liquid level cannot retain flammable gas at high concentrations because the pore space is diluted with the head-space atmosphere.

The void fractions measured with the VFI in DSTs, the only tanks subject to buoyant displacement, are consistent with the neutral buoyancy limit. Though the peak void (7–15%) exceeds neutral buoyancy in some cases, the average void (4–12%) remains below it (Stewart et al. 1996). However, the average void in SST waste is significantly below the maximum retention values of 25–40%, where the gas volume can be measured accurately. Table 3.1 shows typical void fractions of 10% or less. Only four tanks (BY-101, S-102, S-103, and SX-103) register 20% void or higher.

The reasons for this difference are not yet fully understood. The accelerated gas generation rates necessarily employed in the experiments may artificially increase gas retention compared with the very low rates estimated for the actual waste. A long-term experiment is planned for FY 1997 to resolve this issue. The small vessels used in the experiments may also contribute to a higher void fraction, though the most recent work has largely discounted this effect.

^(a) Shekarriz A, DR Rector, MA Chieda, and JM Bates. 1996. *Preliminary Retained Gas Sampler Measurement Results for Hanford Waste Tank 241-A-101*. Letter report TWS-MIT-093096, Pacific Northwest National Laboratory, Richland, Washington.

There is evidence, however, that more gas is present in the waste than the measurements indicate. Gas is probably not stored uniformly but favors specific layers. If all the gas were stored in one-third of the tank at 30% void, the tank-wide average void would be 10%, consistent with a typical tank in Table 3.1. The true void may be up to twice the estimates in the table due to the hysteresis effect discussed in Section 3.2. Better retained gas estimates using the BPE2 method with automated Enraf level data might make the table more consistent with the maximum retention values.

The distribution of retained gas, the maximum void fraction, and the correlation of gas retention to waste properties will be revealed as more tanks are sampled with the retained gas sampler.

4.0 Single-Shell Tank Gas Release Mechanisms

Gas retention and release behaviors depend on the configuration of the waste; most importantly, the amount and location of free liquid with respect to the solids. Figure 4.1 shows some of the typical waste configurations. Figure 4.1(a) represents the waste in a typical DST. It consists of a nonconvective solids layer on the tank bottom, in which most of the gas is stored; a convective liquid layer; and a floating crust layer of approximately the same composition as the nonconvective layer that also contains a significant volume of gas.

Figures 4.1(b) and (c) illustrate the waste configuration in typical flammable gas SSTs. The main difference among the three configurations is the amount of free liquid available. Figure 4.1(b) represents waste configuration 1 (see Section 2.1). A shallow layer of supernatant liquid, possibly with a thin foam or even a thin crust floating on top, overlies the settled solids. Where it exists at all, the liquid layer is much thinner than the convective layer in any DST. The saltcake under the liquid is also usually coarser-grained than the solids in a DST, and there may be a layer of insoluble, clay-like sludge on the tank bottom. Figure 4.1(c) illustrates the effect of removing liquid (i.e., by pumping out a salt well). The free liquid level is below the top of the solids, creating a layer of moist but unsaturated saltcake. This view represents waste configurations 2 and 3.

Figure 4.1(d) represents the waste configuration discovered in recent core samples from Tank A-101.^(a) The entire solid waste column is apparently buoyant and floats on a deep layer of liquid. Whether this situation occurs in other tanks remains to be seen. In any of these situations, gas is stored only in liquid-saturated solids. In dry solids, flammable gas is diluted by diffusion and cannot accumulate.

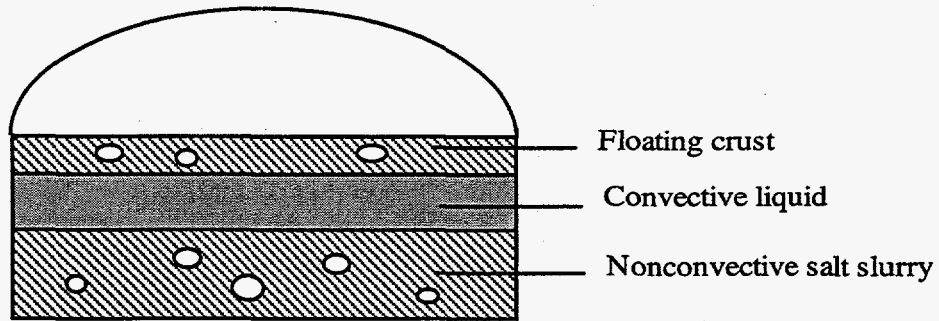
The nature of plausible mechanisms for large gas releases from SSTs containing sludge and salt cake as shown in Figure 4.1(b) and (c) has been the subject of much speculation. To begin focusing the speculation and developing a coherent theory, two meetings were organized by P. A. Gauglitz (PNNL) on May 18 and June 5, 1995, to discuss SST gas retention and release mechanisms.^(b) The classic buoyant displacement of the contents of an SST was considered unlikely but possible.

Besides an energetic displacement, the consensus of those attending the May 18 meeting was that the mechanisms that might cause a large, rapid release of retained flammable gas in SSTs are the following, in order of likelihood of large release:

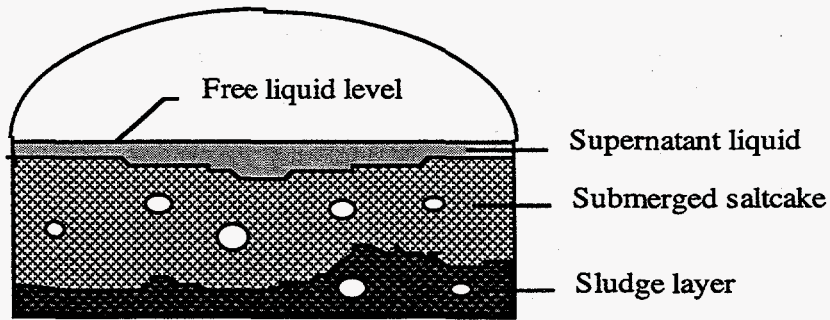
1. Local gas bubble cascade
2. Mud pot - chimney to dendritic bubble region
3. Local disruption ("intrusion") causing general release
4. Fracture of "dry" waste or dryout of surface saltcake.

^(a) Shekarriz A, DR Rector, MA Chieda, and JM Bates. September 1996. *Preliminary Retained Gas Sampler Measurement Results for Hanford Waste Tank 241-A-101*. Letter report TWS-MIT-093096, Pacific Northwest National Laboratory, Richland, Washington.

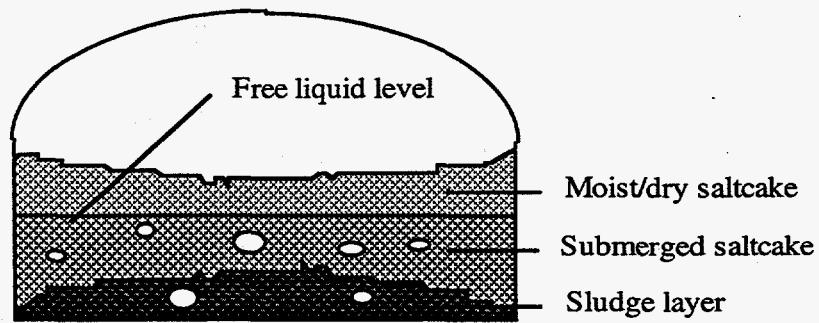
^(b) Gauglitz PA. June 8, 1995. *Flammable Gas Retention and Release in SSTs - Summary of Meeting*. Meeting notes, Pacific Northwest Laboratory, Richland, Washington.



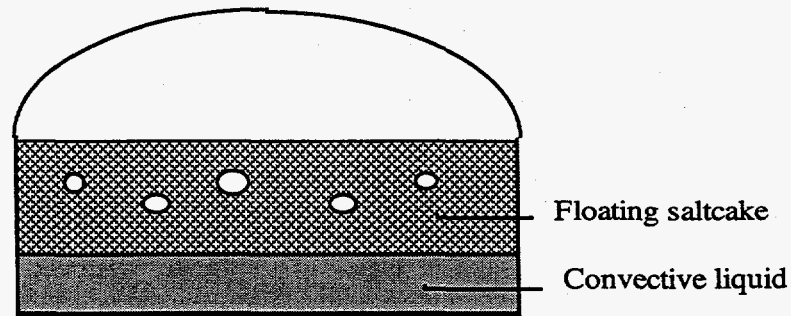
a. Typical Double Shell Tank



b. SST with Supernatant Liquid



c. SST without Supernatant Liquid



d. SST with floating saltcake

Figure 4.1. Basic Waste Configurations

These mechanisms were initially studied at PNNL during the remainder of the summer of 1995^(a) and during FY 1996. Gas releases caused by seismic events and salt-well pumping were also investigated experimentally and analytically, and the results are given in this section.

Section 4.1 discusses buoyant displacement and criteria for determining whether gas release will occur. Section 4.2 deals with gas release from connected hydro-dendritic and litho-dendritic bubble regions, covering all aspects of local gas bubble and "mud pot" release mechanisms. A preliminary analysis of seismic energy deposition and gas release is described in Section 4.3; and gas release during salt-well pumping is discussed in Section 4.4, which also includes a discussion of the proposed fracture and dryout gas release mechanisms. Experiments simulating gas releases from local disruptions are covered in Section 4.5.

4.1 Buoyant Displacement

Gas releases in DSTs occur by buoyant displacement (the terms "rollover" or "Rayleigh-Taylor instability" have historically been applied to this mechanism). The accepted model for a buoyant displacement (Allemann 1993) assumes that a region, or 'gob,' of the nonconvective layer accumulates gas until it becomes buoyant under the local hydrostatic pressure and rises to the surface. The expansion of the gas during the rise will produce a waste level rise if it occurs slowly or if the gas is not released immediately. At the surface, the gob disintegrates to some degree, and gas is released until what remains of the gob returns just to neutral buoyancy at the surface. This causes the sudden level drop that is the signature of a buoyant displacement. Then the waste sinks slowly back to the bottom, with the gas it still contains compressed. This final process yields the slower level decline that occurs days or even weeks after the actual release. The model predicts that only the initial level drop is accompanied by an actual release of gas into the headspace; thus, only the initial level drop should be used to compute the release.

Buoyant displacement events are usually identified by a sudden level drop following a long period of steady level rise. The initial drop is usually followed by a slower decline to a minimum level several days or even a couple of weeks after the main event. Often there is an accelerated or even abrupt level rise just before the event. The waste level must be measured by an FIC contact probe or Enraf buoyancy gauge (since about 1995) to characterize buoyant displacements. The manual tape or other devices are suitable for identifying, but not quantifying some of the larger releases. The most effective and accurate means of characterizing gas releases is by head space gas monitoring; however, gas monitoring has been available only in the last couple of years and can serve only to guide the calculation of release volume from level change.

Buoyant displacements proceed at widely varying rates depending on the amount and type of waste involved. Large releases that are energetic enough to liquefy the rising gobs completely may take only a few minutes; such behavior was typical of SY-101. A thick crust may reduce the rate of release if the gobs are not able to break through it, as in AW-101. (See Stewart et al. [1996] for a complete description of gas release history of DSTs on the FGWL.)

The key to understanding and predicting buoyant displacement behavior is knowing the amount of potential energy expended in the process. The potential energy available depends on the amount of gas in the nonconvective layer and the depth of supernatant liquid the solid mass must rise through. For a gas release to occur, sufficient energy must be released to break up the gob in which the gas is trapped. Thus if the supernatant liquid is not deep enough, no gas will be released

^(a) Allemann RT. October 1995. *A Discussion of Some Mechanisms for Sudden Gas Release from Single-Shell Waste Tanks at Hanford*. Letter report PNL-WTS-101095, Pacific Northwest Laboratory, Richland, Washington.

even though the nonconvective layer becomes buoyant and floats to the surface. Section 4.1.1 describes a series of experiments using clay simulants that shows this very convincingly. Section 4.1.2 provides the theory for this behavior and a criterion for gas release during buoyant displacements. The possibility of such releases occurring in SSTs is discussed in Section 4.1.3.

4.1.1 Experimental Observation of Buoyant Displacements

A series of experiments was conducted to qualitatively demonstrate differences in the dynamics of buoyant displacements between wastes with relatively deep and those with shallow overlying supernatant layers. It has also been argued that thinner nonconvective layers produce smaller gobs of buoyant waste; a single experiment with a thin nonconvective layer was conducted to observe this behavior.

Buoyant displacements were observed in bench-top experiments with waste simulants that mimic the behavior of actual tanks with deep supernatant layers. The effect of supernatant layer thickness was then determined by conducting pairs of experiments in which the only difference was the depth of the supernatant layer. While the small size of the bench-top experiments affects buoyant displacement behavior, the simulant physical properties can be adjusted to compensate. This approach does not seek to scale the experimental parameters exactly but to mimic the mechanism qualitatively through the choice of simulants.

Figure 4.1.1 is a schematic of the experimental apparatus consisting of a test vessel and two video cameras. The test vessel diameter is approximately 27 cm; the diameter varied slightly from the bottom of the vessel to the upper layer of the supernatant. The waste simulant was a bentonite clay and water mixture with a small amount of hydrogen peroxide (H_2O_2) added to generate gas in situ. The hydrogen peroxide decomposed over a few hours through its interaction with the clay, producing oxygen bubbles that were retained in the bentonite clay layer submerged below a supernatant layer of water.

To begin each experiment with the appropriate configuration of supernatant liquid above a settled solids layer, the simulant was added to the test vessel first, followed by deionized water, added carefully to the desired thickness. The simulant then began to retain gas bubbles, become buoyant, and eventually to rise through the supernatant liquid.

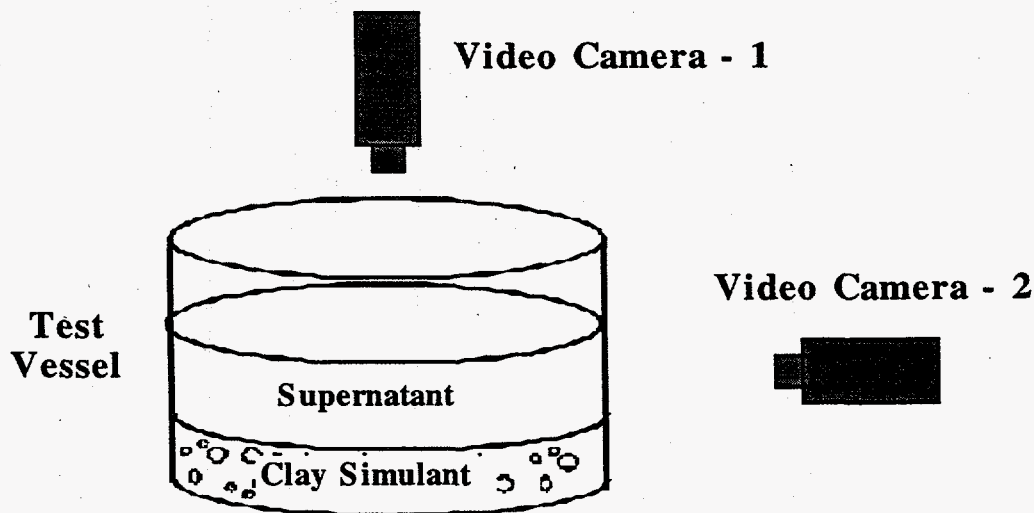


Figure 4.1.1. Schematic of Apparatus for Observing Buoyant Displacements

The change in the level of the supernatant from its initial level ($\Delta H_{\text{supernatant}}$) indicated the amount of gas that was retained. The supernatant level was used rather than the solids level because the latter was not uniform over the cross-section of the test vessel (except at the beginning of the experiment). The void fraction retained in the nonconvective layer was calculated as

$$\alpha = \frac{\Delta H_{\text{supernatant}}}{H_{\text{solids}}^0 + \Delta H_{\text{supernatant}}} \quad (4.1.1)$$

where the initial solids layer thickness is H_{solids}^0 . In this calculation of the void fraction, we have neglected the initial gas content in the bentonite simulant, which was probably a few percent void.

Video images were captured with color zoom video cameras (Sekai ISC-800A), which generated S-VHS resolution video images (460 horizontal TV lines). These video images were recorded on either a S-VHS recorder (Mitsubishi HS-S5600) or a Betacam-SP recorder (Sony UYW-1400A). While the video images of the buoyant displacements in progress are the most instructive data from these experiments, a series of still images also was generated from the video recordings with a Sony UP-5600MD color video printer.

The first pair of tests (1a and 1b) used a 67-Pa simulant that appeared to be too stiff to produce a spontaneous event representative of those observed in tanks. A second pair of tests (2a and 2b) was conducted with a weaker simulant (14-Pa) that gave a visually more representative action compared with in-tank video of the last natural buoyant displacement in SY-101. The final test (3) investigated the effect of the solids layer thickness on buoyant displacement dynamics. In each of these experiments, a small amount of hydrogen peroxide (less than 0.5 wt% of the simulant) was mixed with the bentonite clay to generate gas bubbles. This was enough to give an ultimate void fraction of about 0.3 in the clay simulant, although the events occurred at a lower void fraction, as described in the next section. Test conditions are summarized in Table 4.1.

The experimental observations show that the buoyant displacements were quite energetic with a deep supernatant layer. With the weaker simulant (14-Pa), this energetic action also produced an immediate and substantial release of gas. For the stronger simulant (67-Pa) the displacement was energetic, but the bubbles were not easily released from the clay. Buoyant gobs stayed intact and floated for a while before releasing some of their bubbles. With thin supernatant there was essentially no gas released during or after the buoyant rise of the bubbly solids. For both the weaker and stronger simulants, the bubbly solids clearly did trade places with the liquid. However, this buoyant rise was very lethargic and did not provide sufficient agitation to release any gas

Table 4.1. Test Conditions for Buoyant Displacement Experiments

Case	Solids Depth (cm)	Liquid Depth (cm)	Yield Stress (Pa)	Void at Displacement	Energetic Action	Gas Release
1a	4.7	10.5	67	0.25 ^(a)	Y	small
1b	4.5	1.2	67	0.25 ^(a)	N	none
2a	4.8	10.1	14	0.14	Y	major
2b	4.8	1.1	14	0.20	N	none
3	1.5	10.15	14	0.19	N	none

^(a) Displacement initiated manually.

from the simulant. The most useful documentation of these results is the video image of the experiments; a summary video of these experiments is available.^(a) Details are shown below.

4.1.1.1 Results for 67-Pa Bentonite Simulant

Though the simulant was buoyant when the void fraction reached about 0.08, its strength appeared to hold it down. In this pair of experiments, the void fraction increased to nearly 0.25 without a buoyant displacement. To initiate an event, the clay was disturbed by inserting a spoon. Once the bubbly solids layer was disturbed, it did rise in both the thin and thick supernatant cases.

An energetic displacement occurred in the deep supernatant case. Essentially all of the bubbly simulant participated in the action, with individual gobs rising sequentially. Figures 4.1.2 and 4.1.3 are video images of the top view and side view of this event, respectively. At this early stage, two gobs have risen to the top of the vessel.

For the thin supernatant case, the buoyant rise was slow and nearly imperceptible, and essentially no gas was released during or after. Top and side views of this gentle process are shown in Figures 4.1.4 and 4.1.5, respectively. The figures show the entry point of the spoon (dark slash); the portion of the sludge that had risen is just left of this mark.

4.1.1.2 Results for 14-Pa Bentonite Simulant

In experiments with the weaker simulant (14-Pa), the buoyant gobs rose spontaneously with deep or shallow supernatant layers. Still, the void fraction increased beyond the point of neutral buoyancy in both experiments, which was about 0.07. Displacement occurred at a void fraction of 0.14 in the deep supernatant case (2a) and at 0.20 in the shallow supernatant case (2b).

For the deep supernatant case (2a) displacement was spontaneous and energetic, with individual gobs of bubbly clay bobbing up sequentially. In contrast to the companion experiment with 67-Pa simulant (1a), the weaker gobs released a large fraction of their bubbles as they spread over the surface. It appeared that essentially all of the bubbly solids participated in the event. Two top views and a side view of this action are given in Figures 4.1.6, 4.1.7, and 4.1.8, respectively. The first top view shows the first two gobs released, and the next one shows how the gobs disintegrated on the surface.

The buoyant rise was again slow, and nearly imperceptible in the thin supernatant case (2b), though it occurred spontaneously. There was essentially no gas released during or following the buoyant rise, as in the companion experiment (1b) with 67-Pa simulant. See Figures 4.1.9 and 4.1.10 for the corresponding top and side video images, respectively.

4.1.1.3 Results for Thin Layer 14-Pa Simulant

In this experiment (test 3), a thin nonconvective layer of about 1.5 cm was submerged beneath a deep supernatant layer. The 14-Pa simulant strength and supernatant layer thickness are the same as in test 2a, but the nonconvective layer is thinner. Similar to tests 2a and 2b, the void fraction increased to 0.19 followed by a buoyant rise of the bubbly solids. Observation of the buoyant displacement with this thin nonconvective layer showed that smaller gobs were released over a longer period of time, in comparison to test 2b. The top view of this behavior is shown in Figure 4.1.11.

^(a) Send requests to PA Gauglitz, MSIN P7-41, Pacific Northwest National Laboratory, PO Box 999, Richland, Washington, 99352.



Figure 4.1.2. Top View of Test 1a (67 Pa, deep supernatant)

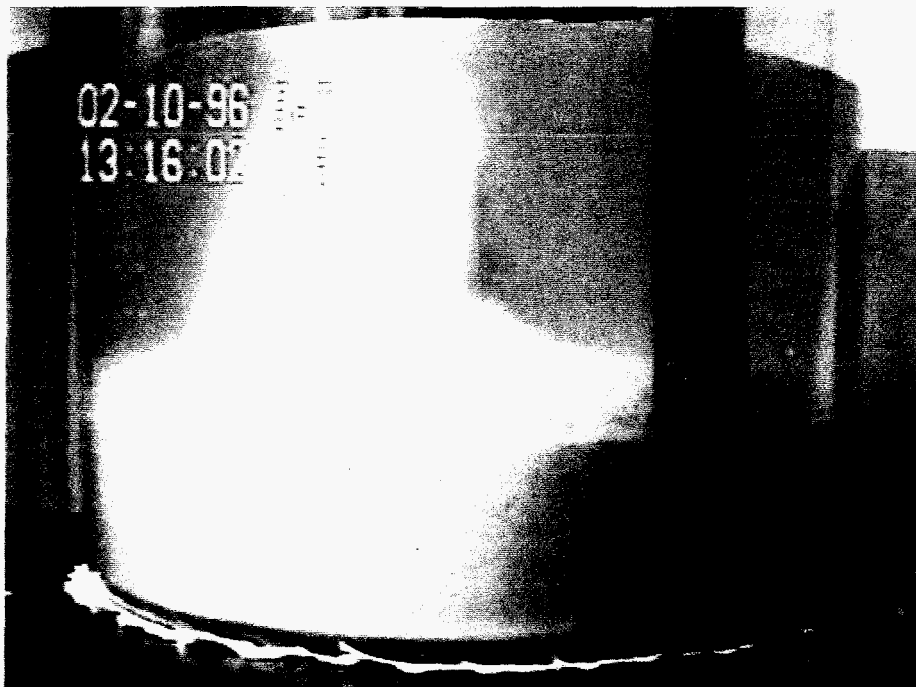


Figure 4.1.3. Side View of Test 1a (67 Pa, deep supernatant)



Figure 4.1.4. Top View of Test 1b (67 Pa, shallow supernatant)



Figure 4.1.5. Side View of Test 1b (67 Pa, shallow supernatant)

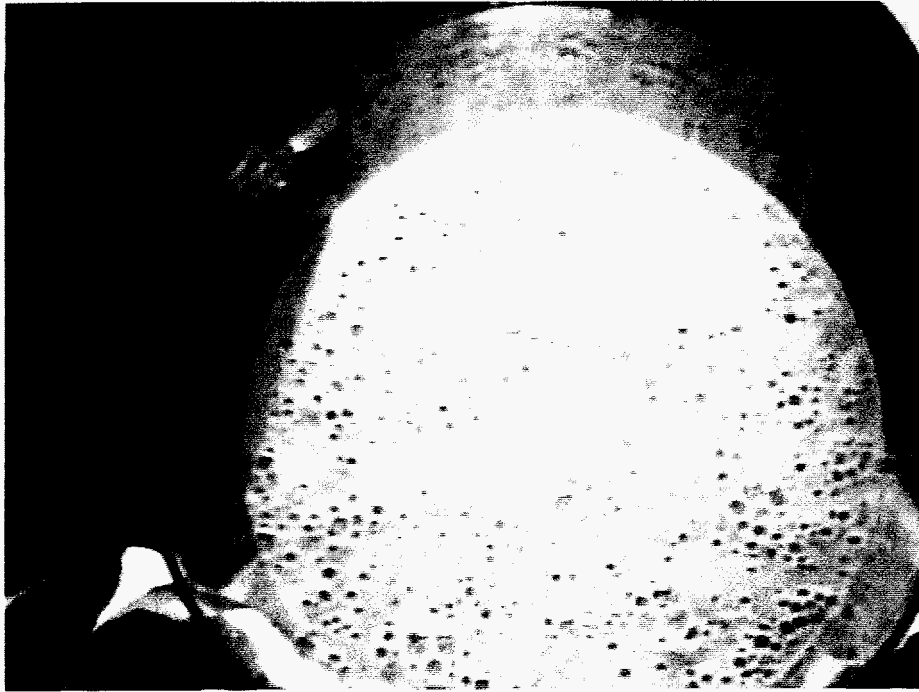


Figure 4.1.6. Top View of Test 2a (14 Pa, deep supernatant)

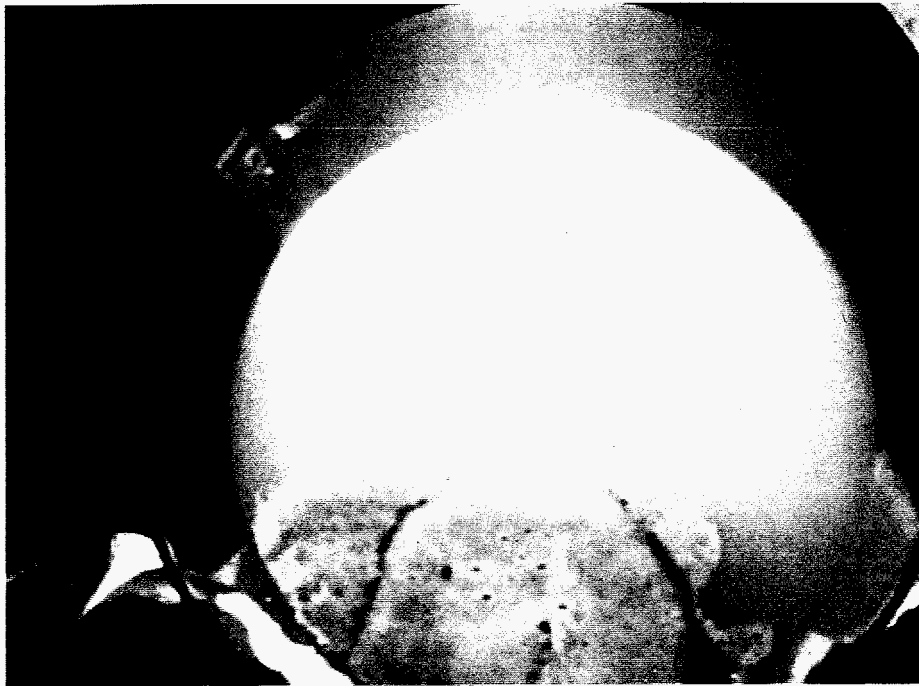


Figure 4.1.7. Later Top View of Test 2a (14 Pa, deep supernatant)



Figure 4.1.8. Side View of Test 2a (14 Pa, deep supernatant).

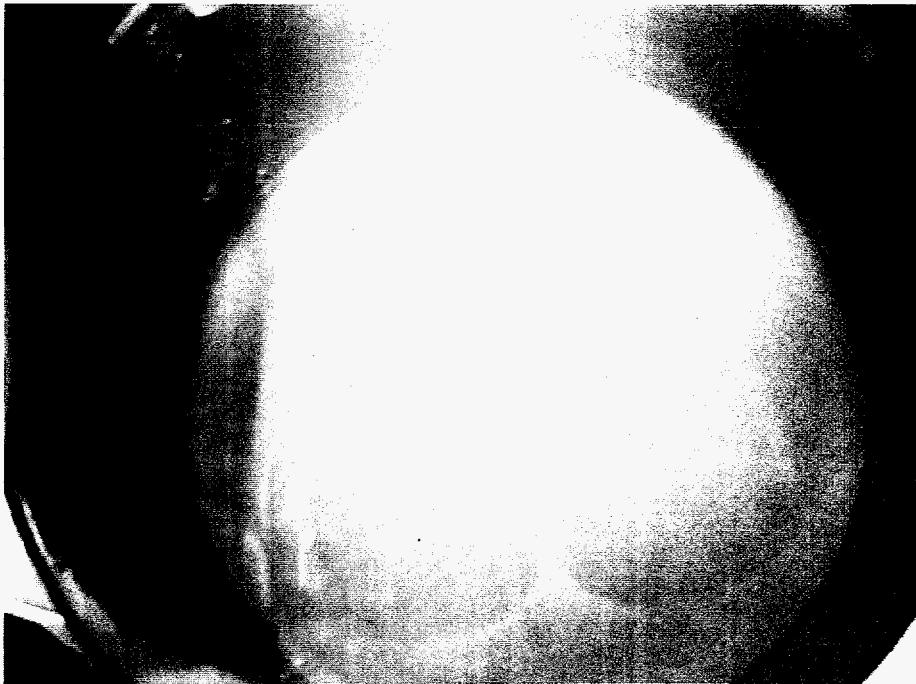


Figure 4.1.9. Top View of Test 2b (14 Pa, shallow supernatant)

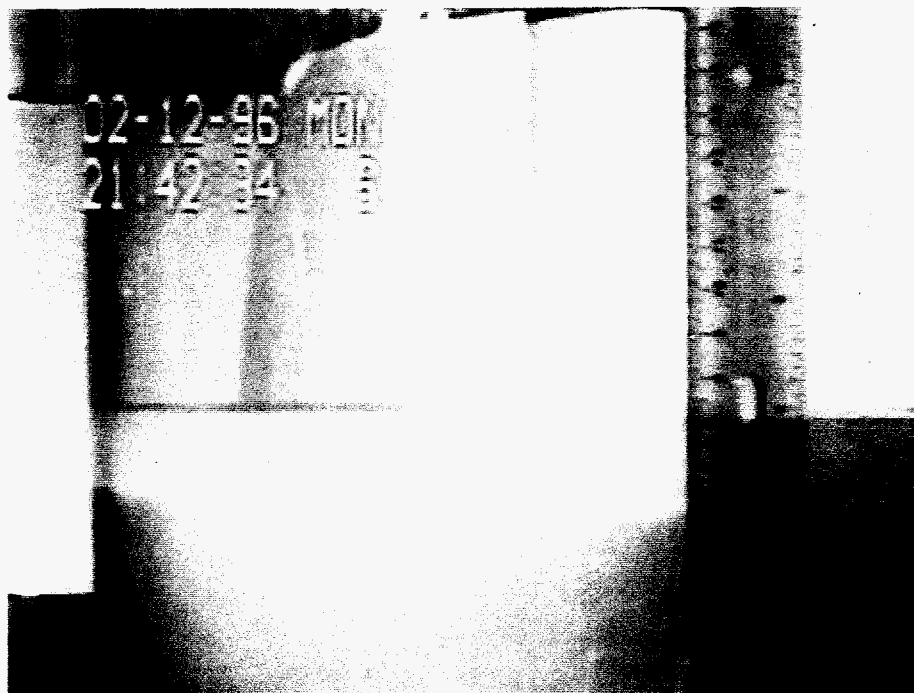


Figure 4.1.10. Side View of Test 2b (14 Pa, shallow supernatant)

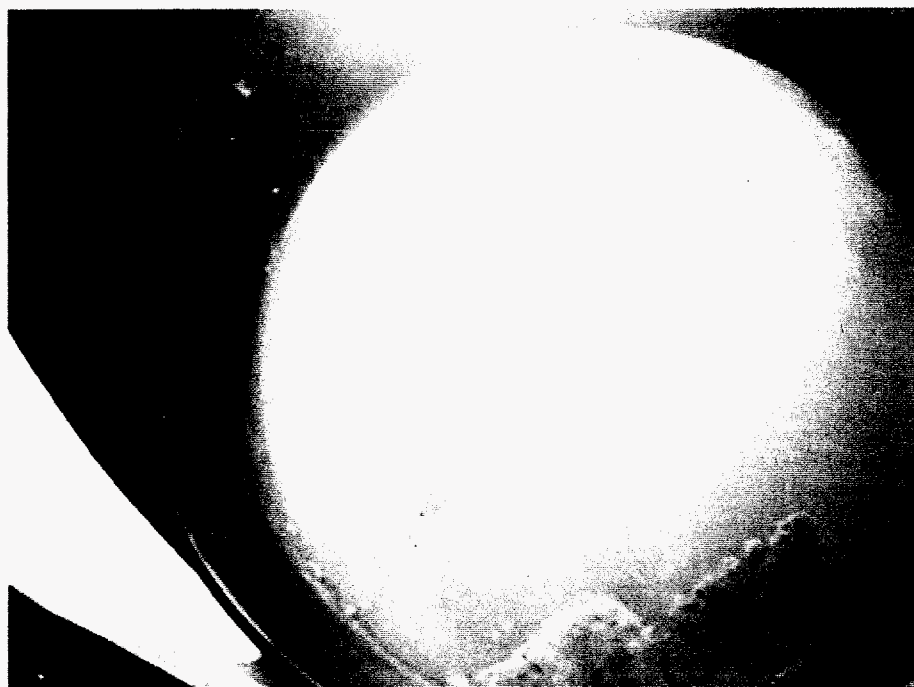


Figure 4.1.11. Top View Test 3 (14 Pa, thin layer)

4.1.2 An Energy Criterion for Buoyant Displacement Gas Release

During buoyant displacement events in DSTs such as SY-101, potential energy stored in the buoyant solids matrix is released and converted to kinetic energy. The excess energy released in this process disintegrates a portion of the rising gob, allowing some of the stored gas to escape. A gas release criterion is developed in this section stating that the total potential energy available must exceed the energy required to yield the buoyant solids matrix participating in the event. The model is applied to SY-101 (pre-pump conditions) and compared with the experimental data from Section 4.1.1. These comparisons show that the energy criterion can be used to predict whether gas release occurs during a buoyant displacement. The model is then applied to evaluate the propensity for large displacements in typical SSTs.

To calculate the energy available to be released during a buoyant displacement, consider an initial volume of buoyant, gas-retaining material, V_0 , as shown in Figure 4.1.12. This volume is composed of both de-gassed solids, V_s , and gas, V_{g0} . We assume that the material is buoyant enough with respect to the overlying supernatant liquid to begin to rise. In order to achieve this, the initial void fraction, α_0 , must be at or above the neutral buoyant condition, given by

$$\alpha_{NB} = 1 - \rho_L / \rho_{SL} \quad (4.1.2)$$

where α_{NB} is the neutral buoyant void fraction, ρ_L is the supernatant liquid density, and ρ_{SL} is the degassed density of the solid-liquid matrix in which gas is stored. It is possible that the initial void fraction is greater than the neutral buoyant void fraction because of the additional restraining force of the material strength.

Due to its buoyancy, the initial volume has potential energy that can be released during a displacement. The total stored buoyant energy can be calculated from the work done in raising the participating volume a distance, L , given by

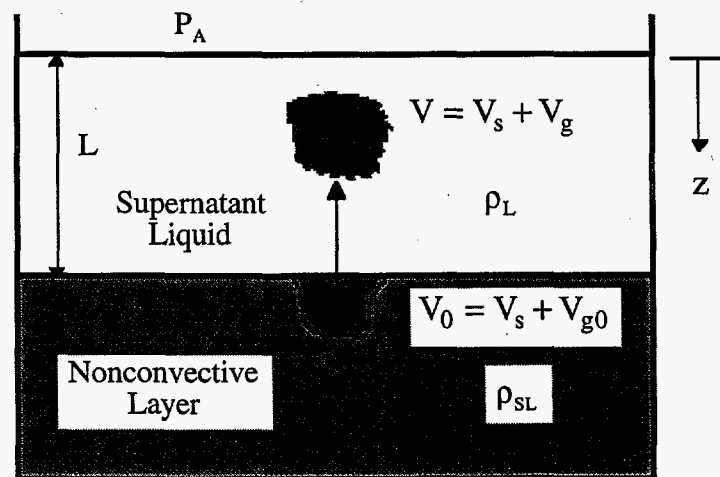


Figure 4.1.12. Geometry and Nomenclature for Displacement Model

$$E_b = \int_0^L F(z) dz \quad (4.1.3)$$

where $F(z)$ is the net buoyant force, neglecting the mass of the stored gas, which is given by

$$F(z) = (\rho_L V - \rho_{sL} V_s) g \quad (4.1.4)$$

Not all of this energy goes into yielding the participating volume; some will be dissipated due to viscous motion. However, it does represent the maximum energy available. Eq. (4.1.4) can be expressed in terms of known quantities with the following relations:

$$V_0 = V_s + V_{g0} \quad (4.1.5)$$

$$V(z) = V_s + V_g(z) \quad (4.1.6)$$

$$V_s = (1 - \alpha_0) V_0 \quad (4.1.7)$$

$$P(z) = P_A + \rho_L g z \quad (4.1.8)$$

$$V_g(z) = V_{g0} P(L) / P(z) \quad (4.1.9)$$

Eq. (4.1.9) assumes the retained gas undergoes an isothermal expansion process as the volume rises. By combining Eq. (4.1.2) and (4.1.5)–(4.1.9), Eq. (4.1.4) can be written as

$$F(z) = \alpha_0 \rho_L V_0 g \left(\frac{\gamma + 1}{\gamma + z/L} - k \right) \quad (4.1.10)$$

where the parameters γ and k are given by

$$\gamma = \rho_L g L / P_A \quad (4.1.11)$$

$$k = \frac{\alpha_{NB}(1 - \alpha_0)}{\alpha_0(1 - \alpha_{NB})} \quad (4.1.12)$$

The integral in Eq. (4.1.3) can now be evaluated with the aid of Eq. (4.1.10) to give the buoyant energy as

$$E_b = \alpha_0 V_0 P_A \gamma \left((1 + 1/\gamma) \ln(1 + \gamma) - k \right) \quad (4.1.13)$$

We assume that the nonconvective layer has a finite yield strength that must be overcome to release bubbles of gas. The structural and rheological properties of waste are, in general, complex and not yet well known; however, there are some basic features that allow us to estimate yield energy. The energy required to yield a volume of solids is equal to the work done on the volume by an externally applied force to deform it to the point of yielding. This is expressed mathematically as

$$E_y = V_s \int_0^{\epsilon_y} \tau d\epsilon \quad (4.1.14)$$

Here τ is the stress applied to the volume, and ϵ is the strain (relative elongation). The limit of integration is ϵ_y , which is the strain at failure. This integration can be performed if the stress-strain relation is known. For example, for a linear-elastic material the stress is proportional to the strain, with the constant of proportionality being the elastic modulus G . If the material is brittle and fails suddenly at strain ϵ_y , then the yield energy is $\tau_y^2/2G$, where $\tau_y = G\epsilon_y$ is the yield stress.

Colloidal salt slurries typical of DST waste have more complex stress-strain behavior than brittle, linear-elastic materials. Figure 4.1.13 shows stress-strain data for bentonite clay simulant at two different strain rates; the lower strain rate data are shown on the left plot.^(a) Three distinct regions can be seen: first, a linear region occurs for strains less than about 10%. As the stress increases above a certain critical value (about 190 Pa for the low strain-rate case and about 230 for the high strain-rate case), there is a sudden failure or relaxation. Beyond this point, a plastic region exists where the stress is approximately constant with strain. Finally, at a strain of about 1.6 for the low strain-rate case and 1.2 for the high strain-rate case, a thixotropic region is encountered. Here the sludge material is essentially flowing and no longer possesses solid-like properties. The fact that the thixotropic region begins at a nominal strain of approximately 1 is significant. For this strain, solid particles in the sludge are displaced approximately one diameter. In doing this, they lose their "memory" of their initial state, so there is no longer a restoring force.

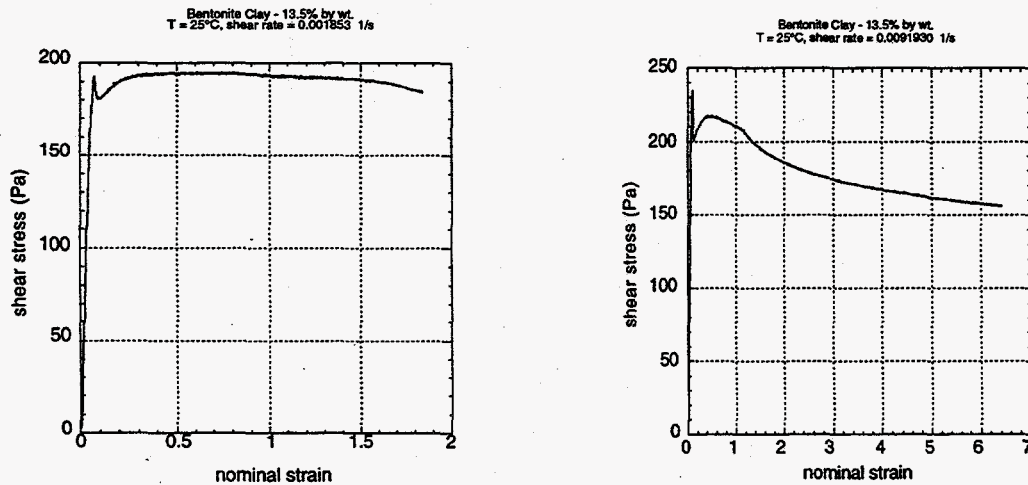


Figure 4.1.13. Stress-Strain Data for Bentonite Clay Simulant

We propose a model waste with the following, somewhat general, features:

1. Linear-elastic behavior occurs for small strain. The strain at elastic yield is 5–10%.

^(a) Data from internal letter report by JR Phillips (PNNL) entitled, "A Basic Survey of Simulant Materials for the Ball Rheometry Project." Pacific Northwest National Laboratory, Richland, Washington.

2. The stress is approximately constant over the plastic region. The value of stress is approximately equal to the yield stress, or material strength.
3. The thixotropic region begins at a strain of approximately 1.

With these assumptions, the energy required to yield the sludge is approximately $E_y = \epsilon_y V_s \tau_y$, where $\epsilon_y \approx 1$ is the strain at thixotropic transition. With $V_s = (1 - \alpha_0)V_0$ we can write the yield energy as

$$E_y = (1 - \alpha_0)V_0\epsilon_y\tau_y \quad (4.1.15)$$

Gas release will not occur if the buoyant energy available is less than that required to yield the sludge volume involved in the displacement. The ratio of the two energies is given by the ratio of Eq. (4.1.13) and (4.1.15) as

$$\frac{E_b}{E_y} = \frac{\alpha_0 P_A \gamma}{(1 - \alpha_0)\epsilon_y \tau_y} ((1 + 1/\gamma)\ln(1 + \gamma) - k) \quad (4.1.16)$$

If $E_b/E_y > \sim 1$, we expect a buoyant displacement to release some or most of the retained gas. Otherwise, we expect little or no gas to be released. Though the ratio is approximately unity for gas release, its precise value cannot be determined by modeling alone. The efficiency of the energy conversion process comes into play. Some of the buoyant energy is dissipated in processes other than yielding the rising gob, so more energy is required than just enough to yield.

The energy ratio given in Eq. (4.1.16) can be evaluated with the conditions of SY-101 before the mixer pump was installed; this tank had historically suffered violent, large-scale buoyant displacements that released over 50% of the gas stored in its nonconvective layer. Table 4.2 shows estimated model input values for SY-101 (pre-mixer pump). All cases assume a nonconvective layer density of 1700 kg/m³ and a strain at yield of 1.4. The yield strain is the average of the values from the sludge simulant shown in Figure 4.1.13. Case 1 is the base case with the initial void fraction at neutral buoyancy. The energy ratio for this case is 7.4, implying that, for this set of conditions, more than enough energy is available to yield all the solids and release a large fraction of its gas. This prediction is consistent with observed behavior for this tank.

In Case 2, the liquid density is reduced by approximately 10%, increasing the energy ratio by about 22%. In Case 3, the liquid depth is increased by approximately 10%, which increases the energy ratio by about 19%. For Case 4, the initial void fraction is increased above the neutral buoyancy condition by 3% (absolute void), which increases the energy ratio dramatically, about 250%, to a value of about 18. This implies that the initial condition for the void fraction is important in determining whether a gas release will occur. Evidently, a great deal of additional potential energy can be stored if the neutral buoyant condition is surpassed. In the final case, the yield stress is increased to 500 Pa, decreasing the energy ratio proportionally, since the yield stress appears as a linear multiplier in Eq. (4.1.16).

Experimental data can also aid in determining a more precise value for the required energy ratio. Table 4.3 shows model input values corresponding to the scaled buoyant displacement experiments described in Section 4.1.2. While buoyant displacement occurred in Case 1, little gas was released because the individual gobs, while rising to the surface, did not break apart and release their gas. The energy model gives an energy ratio of 2.6 for this case. In Case 2, the conditions are the same as in Case 1, but the liquid layer depth is reduced, no gas release is observed,

Table 4.2. The Energy Model Applied to Tank SY-101

Case	ρ_L (kg/m ³)	ρ_s (kg/m ³)	α_0, α_{NB}	k	L (m)	γ	τ_v (Pa)	E_b/E_y
1	1500	1700	0.12, 0.12	1.0	4.1	0.6	200	7.4
2	1450*	1700	0.15, 0.15	1.0	4.1	0.58	200	9.0
3	1500	1700	0.12, 0.12	1.0	4.5*	0.66	200	8.8
4	1500	1700	0.15, 0.12	0.77*	4.1	0.6	200	18.3
5	1500	1700	0.12, 0.12	1.0	4.1	0.6	500*	3.0

Table 4.3. The Energy Model Applied to Scaled Buoyant Displacement Experiments

Case	ρ_s (kg/m ³)	α_0, α_{NB}	k	L (m)	γ	τ_y (Pa)	E_b/E_y	Energetic	Gas Release
1	1087	0.25, 0.087	0.286	0.105	0.010	67	2.6	Y	N
2	1087	0.25, 0.087	0.286	0.012	0.0012	67	0.30	N	N
3	1070	0.15, 0.07	0.426	0.101	0.0099	14	5.2	Y	Y
4	1070	0.20, 0.07	0.426	0.011	0.0011	14	0.81	N	N

and the action is very gentle and gradual. The model predicts an energy ratio of 0.3 for this case. In Cases 3 and 4, a weaker simulant was used. A large gas release was observed in Case 3, with a predicted energy ratio of 5.2. In Case 4, the liquid layer was reduced, and again the process was very gentle; some gas was released, but the mechanism appeared to be percolation rather than displacement. The energy ratio for this case is 0.81, consistent with observed behavior.

The energy model gives consistent predictions for both the SY-101 conditions and the scaled experiments. We conclude that an energy ratio of between 5 and 10 corresponds to buoyant displacement with large gas release (over 50% of the stored volume). The scaled experiments suggest a transitional energy ratio above 2.6. A relatively conservative criterion for gas release due to buoyant displacement can therefore be defined as

$$E_b/E_y > 3 \quad (4.1.17)$$

We now apply the energy model to determine the propensity for a buoyant displacement-induced gas release in SSTs. The estimated and measured properties of A-101, as they were known in mid-1996, prior to the latest core samples and issuance of the revised *Historic Tank Contents Estimates* (Brevick 1996) are used as inputs representing an SST most likely to experience a buoyant displacement. Although the inputs are now known not to match A-101, they still represent conditions more likely to release gas in a displacement than any other SST.

Table 4.4 presents the input values and results of the energy model. Case 1 corresponds to the best-estimate base case; references for the input values are shown. Values without references are either calculated or assumed. The energy ratio for Case 1 is found to be 0.033, which is much

Table 4.4. The Energy Model Applied to Tank A-101

Case	ρ_L (kg/m ³)	ρ_s (kg/m ³)	α_0	α_{NB}	k	L (m)	γ	τ_v (Pa)	E_v/E_y
1	1450 ^a	1530 ^b	0.055	0.055	1.0	0.4 ^c	0.057	200	0.033
2	1450 ^a	1530 ^b	0.055	0.055	1.0	1.0*	0.14	200	0.19
3	1300*	1530 ^b	0.177	0.177	1.0	0.4 ^c	0.051	200	0.098
4	1450 ^a	1530 ^b	0.10*	0.055	0.52	0.4 ^c	0.057	200	1.15

$\epsilon_y=1.4$ for all cases.
(a) Per telephone conversation with W. Kubic (LANL) on April 17, 1996.
(b) *Safety Assessment for Salt Well Pumping Operations in Tank 241-A-101*. WHC-SD-WM-SAD-034, 4/15/96.
(c) *Historical Tank Contents Estimate for the NE Quadrant of the Hanford 200 E Area*. WHC-SD-WM-ER-349 6/94.

less than 3, implying that a displacement-induced gas release is not possible. For the second case, the liquid level is increased 250% above the reported value, and the energy ratio is 0.19, still indicating no gas release. In the third case, the liquid density is decreased by 10%, producing a very large neutral buoyancy void fraction of 17.7%. Even under these conditions, the energy ratio is less than one. The last case shows that the energy criterion is still not met (energy ratio <3) with initial void fraction of 0.1, almost twice the neutral buoyancy value.

The recent RGS measurements (which were discussed briefly in Section 3.2) indicate that A-101 has nonconvective void fractions well above 10%. However, all the gas was found in the upper two-thirds of the waste and essentially none in the lower region, which was found to be liquid. The recently revised historical tank content estimates also predict the solids layer to be lighter than the liquid, so the solids are already buoyant even in the absence of gas. The energy model states that this configuration has essentially no excess potential energy available and is therefore much more stable than one with a shallow supernatant liquid layer.

4.1.3 Conclusions on Buoyant Displacement

From both the analytical and experimental results described above, it is clear that buoyant displacement can occur whenever a gas-bearing solids layer becomes buoyant with respect to the overlying liquid layer. When this happens the solids layer, or a portion of it, rises to the top with the liquid sinking down to replace it. The volume of gas released in this process depends on the amount of potential energy expended. The available potential energy in turn depends on the depth of supernatant liquid present. If the supernatant depth does not permit an energy release sufficient to yield most of the solids layer, little of the trapped gas will be released. Thus a necessary condition for large gas releases via the buoyant displacement mechanism is the presence of supernatant liquid. In fact, the depth needs to be roughly that of the nonconvective layer.

Significant supernatant liquid layers currently exist only in the DSTs. The single-shell flammable gas tanks have, at most, 40 cm of supernatant liquid. The shortage of supernatant suggests that, even if a buoyant displacement is possible, the gas release is likely to be limited (as shown in the scaled experiments for thin supernatant layers). From this we conclude that buoyant displacement, accompanied by a release of much of the retained gas, is not a plausible gas release mechanism in SSTs.

4.2 Gas Percolation from Connected Dendritic Regions

The mechanism for gas release from porous media was originally proposed as the 'mud pot' chimney. In the mud pot scenario, the gas is stored in the form of dendritic bubbles that form a finely distributed connected phase held some distance under the surface by a sealing region where bubbles remain spherical. At some point a crack, channel, or chimney is assumed to be opened through the sealing layer, and the pressurized dendritic gas region is suddenly provided with a path to the surface; this hypothetical mechanism might result in a relatively large release. The gas passing through the liquid in the upper layers makes the surface look like a bubbling mud pot. Participants at both of Gauglitz' meetings (see Section 4.0) described possible evidence of such mud pots in photographs of the waste surface in many SSTs. This is now specified as one type of 'percolation' mechanism, to better describe the physics.

Gas percolation release occurs when gas bubbles stored in the waste connect into dendritic structures, migrate upward, and eventually break through to the surface. The percolation release is an event that can occur without any external force or object disrupting the waste. (Disruption releases are described in Section 4.5.) Percolation events were originally thought to result in a fairly large release; however, analyses now show that they are much more limited.

Dendritic bubbles may be either particle-displacing or pore-filling, as discussed in Section 3. Particle-displacing bubbles occur most often in waste layers that are under little hydrostatic pressure or that have low yield strength and small pore size. The particle-displacing bubbles may be referred to as hydrostatic if they have not merged into networks, or hydro-dendritic if they have. The other type of bubbles, those that are confined to the pore volume, often appear in deep layers of waste or in waste that has large pores and high yield strength. These bubbles, which displace only the interstitial liquid, exist as pore-filling networks and may be referred to as litho-dendritic bubbles, because they assume a dendritic shape and are confined to the pores between particles by the lithostatic load. The maximum gas retention in pore-filling bubbles is limited by the waste's porosity. The upper limit on gas retention by particle-displacing bubbles is somewhat higher, because porosity is not relevant for this bubble type.

Gauglitz et al. (1994) demonstrated the formation of the three types of bubbles in graduated cylinders containing fine sand (relatively large particles compared to waste) and sugar water in which carbon dioxide was generated by yeast. A lower layer of litho-dendritic bubbles formed below a "fractured" mid-layer where the gas was held in large hydro-dendritic fissures. The topmost layer contained separated round (hydrostatic) bubbles.

The dynamics of a percolation gas release from pore-filling or particle-displacing bubbles are different. When a connected region of litho-dendritic bubbles migrates upward, the flow of gas is limited by the rate at which liquid can flow in to replace it. When a particle-displacing bubble network moves, gas flow is not limited by the replacement liquid flow, because the bulk waste collapses into the volume the gas had occupied. The dynamics of these processes are discussed below.

4.2.1 Configuration of the Connected Litho-Dendritic Bubble Region

As was discussed in Section 3.1, pore-filling (litho-dendritic) bubbles can only be present in regions of the tank where the combination of the lithostatic pressure and waste strength is great enough to prevent bubbles from pushing the particles apart. The condition is expressed in terms of a Bond number in Eq. (3.1.1). In a typical saltcake, litho-dendritic bubbles exist only at depths of

a few meters below the waste surface. Litho-dendritic bubbles are not expected to be present at all in sludge tanks since their smaller pore diameter is easier for gas bubbles to push apart.

The first step in estimating the potential gas release is to establish how large a volume of waste containing litho-dendritic bubbles can participate in a percolation release. Pore geometry, hydrostatic head, and capillary effects are the main phenomena that act to hold litho-dendritic bubbles within the waste and separate from one another. We can represent these effects schematically, as shown in Figure 4.2.1.

Here a pore contains a bubble that has begun to extend out and up through three outlet pores located at different depths. Each of the three gas-liquid interfaces has a different curvature, determined by the interfacial contact angle and the irregular angles of the pore surfaces. Since the pressure in the gas is essentially uniform, each interface must satisfy the relationship

$$\rho_L g h_1 + 2\sigma/r_1 = \rho_L g h_2 + 2\sigma/r_2 = \rho_L g h_3 + 2\sigma/r_3 \quad (4.2.1)$$

Thus, as the gas bubble grows, the depths (h) and curvature radii (r) of the liquid-gas interfaces continually readjust themselves to maintain uniform gas pressure throughout the bubble. The deeper interfaces, therefore, must be less curved than the upper ones. If the local pore geometry in a deeper leg of the bubble forces the curvature to be too small for the depth, that leg is pinched off. If the curvature in an upper leg is too large for the bubble height, then the hydrostatic pressure pushes gas out that leg until the center of mass of the whole bubble moves up to some new equilibrium location. The gas fraction at which this occurs is the percolation threshold.

There is, therefore, a natural limit on the vertical extent, Δh , of a litho-dendritic bubble. Taking legs 1 and 3 in Figure 4.2.1 as the top and bottom, respectively, and solving Eq. (4.2.1) for the depth difference, the limit on vertical extent is given as

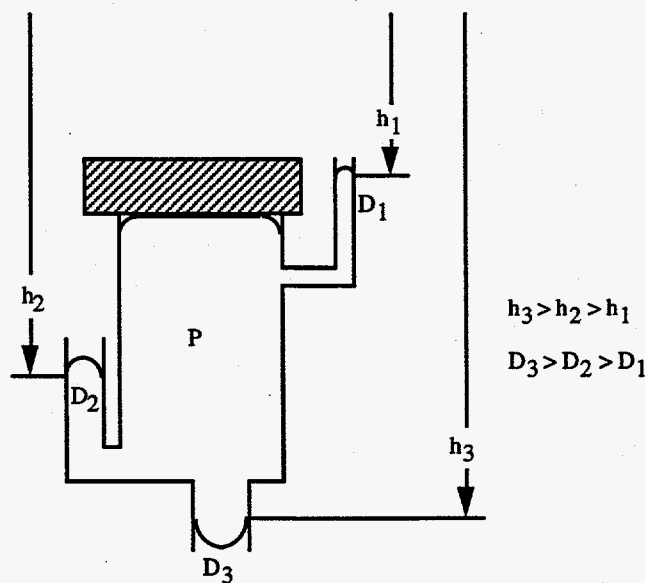


Figure 4.2.1. Schematic of an Equilibrated Bubble

$$\Delta h = h_B - h_T = (2\sigma/\rho_L g) (1/r_T - 1/r_B) \quad (4.2.2)$$

where

- h_B = depth at the bottom of the bubble
- h_T = depth at the top of the bubble
- r_B = radius of curvature of the largest interface at the bottom of the bubble
- r_T = radius of curvature of the largest interface at the top of the bubble.

The minimum radius of curvature of an interface is approximately equal to the local pore radius. The maximum radius of curvature is infinity. Taking these as bounds for the top and bottom radii, respectively, the upper limit on the vertical extent of a litho-dendritic bubble can be stated as

$$\Delta h = 4\sigma/\rho_L g D_p \quad (4.2.3)$$

where

- D_p = pore diameter (m)
- σ = surface tension (0.08 N/m)
- ρ_L = liquid density (1400 kg/m³)
- g = gravity (9.8 m/s²).

Figure 4.2.2 shows the relationship between the maximum litho-dendritic bubble height (Eq. 4.2.3) and the condition for the existence of litho-dendritic bubbles (Eq. 3.1.1). The pore diameter for sludges is probably on the order of one micron (Gauglitz et al. 1994). Hence, litho-dendritic bubbles are not possible in sludges, even in full tanks of 10 m depth. In a 30-micron salt slurry, litho-dendritic bubbles could exist below about 2.5 m with a maximum height of 80 cm. For coarse saltcake, supposing a pore diameter of 100 microns, the maximum vertical extent of a litho-dendritic bubble is found to be about 0.25 m, existing below a depth of 0.5 m. Based on this discussion, we take the practical maximum height of a litho-dendritic bubble to be 1 m.

The horizontal extent of a litho-dendritic bubble is more difficult to analyze. It seems likely that vertical motion by percolation is very local; gas fingers up through the waste as the main bubble moves, leaving small breakaway bubbles behind as lower legs pinch off. This would tend to break up a large horizontal extent. If a bubble is too much wider than it is deep, it is unlikely that a local upward migration could carry the entire bubble upward. Similarly, a very wide bubble would be more likely to begin percolating at several locations, thereby breaking up. Irregularities in the waste will tend to disrupt horizontal growth by encouraging upward movement locally.

Taking all these ideas together, it does not seem possible to sustain a bubble wider than its height by more than a small factor. This means that our limiting, 1-meter-deep litho-dendritic bubble could be a few meters in diameter at most.

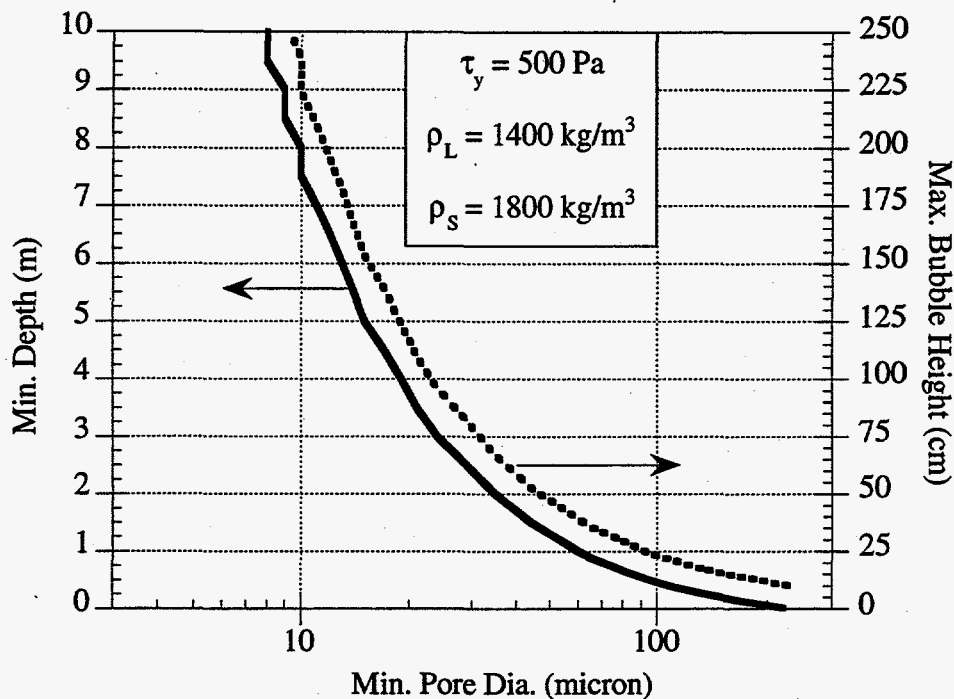


Figure 4.2.2. Limitations on Litho-Dendritic Bubbles

4.2.2 Dynamics of Litho-Dendritic Percolation

In a pore-filling bubble, the gas in the spaces between the solids has displaced liquid; hence it is under the pressure of the liquid head, not the solid weight. (The solids are supporting themselves by virtue of the particles touching each other.) If a dendrite branch then extends itself, the flow of gas in the region connected to that branch is driven by the hydrostatic pressure difference across the height of the bubble. The movement of gas into the extending branch is resisted mainly by the pressure drop of the flow of liquid through the interstices to displace the gas.

Litho-dendritic bubbles exist only in the lower layers of the waste. They are capped by a layer of particle-displacing bubbles. Therefore, direct release from the litho-dendritic layer to the dome space is not possible. Instead, the gas percolates to the top of the litho-dendritic layer and forms a fracture bubble at the bottom of the layer containing particle-displacing bubbles. The fracture bubble eventually escapes by percolation of particle-displacing bubbles. (The releases from the particle-displacing bubbles themselves are discussed in Section 4.2.3.)

Once a bubble breaks through to the top of the litho-dendritic layer, the gas in it flows into a fracture bubble as liquid flows into the litho-dendritic bubble volume to replace it. However, not all the gas can be expelled. Consider the percolation processes in more detail, as shown in Figure 4.2.3. A certain gas fraction is required before gas can flow over any significant distance (Dullien 1992; Li and Yortsos 1995), as shown in Figure 4.2.3(a). This percolation threshold, 15–40% of the pore space (or 6–16% void fraction, assuming a 40% porosity), is the minimum

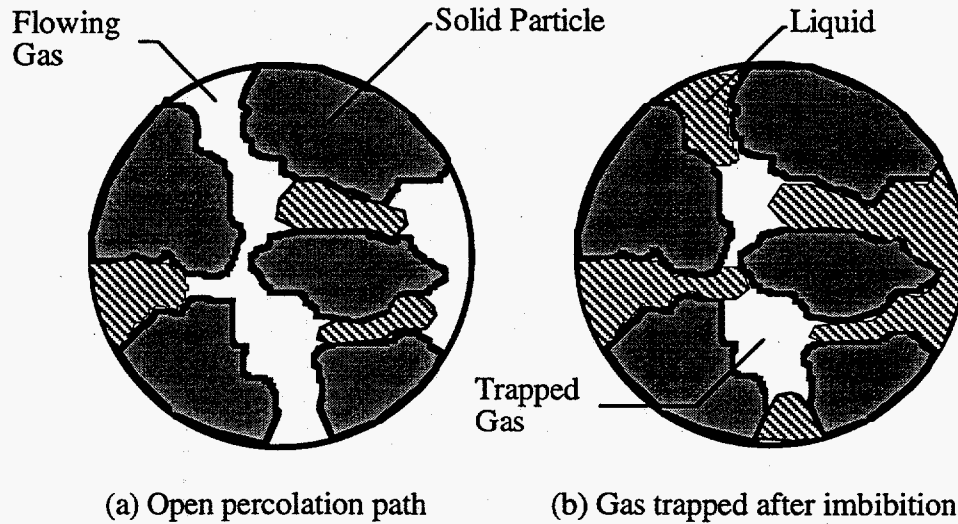


Figure 4.2.3. Maximum and Minimum Gas Fractions

possible gas fraction that allows the gas to connect and flow. As the bubble expands, a similar small amount of liquid, on the order of 10–20%, remains trapped in the pores and is not displaced by the inflowing gas (maximum void fraction $\approx 32\text{--}36\%$). Then, after percolation begins and gas is displaced by liquid, an irreducible gas fraction, roughly equal to the percolation threshold, remains behind as shown in Figure 4.2.3(b) (minimum void fraction again 6–16%). Therefore, the maximum fraction of gas that can be released is 50–80%.

Except for an initial pulse to equalize the pressure, the imbibition of liquid into the lithodendritic bubble is the limiting process for the flow of gas upward. The Ergun equation allows a calculation of the initial maximum flow rate at which the liquid, under its hydrostatic head, can infiltrate (drain) into the bubble through a porous medium. The standard Ergun equation (McCabe and Smith 1976) is

$$-\frac{\Delta P}{\rho_L L} = \frac{1 - \alpha}{\alpha^3} \frac{V_0^2}{\Phi_s D_p} \left[\frac{150 \chi \mu (1 - \alpha)}{\rho_L V_0 \Phi_s D_p} + 1.75 \right] \quad (4.2.4)$$

where

- ΔP = bubble hydrostatic pressure difference, N/m^2
- V_0 = average flow velocity (m/s)
- ρ_L = liquid density, 1400 kg/m^3
- L = layer thickness, the limiting bubble height
- α = porosity, 0.4
- Φ_s = sphericity, 0.7 for irregular particles
- D_p = particle diameter, $3 \times 10^{-5} \text{ m}$ for typical saltcake
- χ = tortuosity, $2 < \chi < 10$, assume 3
- μ = liquid viscosity, $0.024 \text{ Pa}\cdot\text{s}$

To relate the potential release rate of gas out of the litho-dendritic layer to the limiting bubble height and particle diameter, we let L represent the maximum height from Eq. (4.2.3) and compute the bubble hydrostatic pressure difference over that height. Applying this assumption and rearranging, Eq. (4.2.4) yields the following quadratic in $1/V_0$:

$$\left[\frac{\alpha^3 g \Phi_s D_p}{1 - \alpha} \right] \frac{1}{V_0^2} - \left[\frac{150 \chi \mu (1 - \alpha)}{\rho_L \Phi_s D_p} \right] \frac{1}{V_0} - 1.75 = 0 \quad (4.2.5)$$

We also assume that the bubble being released is an oblate spheroid with an aspect ratio of 3 (three times as wide as it is high) at its maximum void fraction. The volume and surface area of the bubble are computed from the limiting height expressed by Eq. (4.2.3). During percolation, liquid flows into the bubble's lower surface, while gas flows out the top. The maximum volumetric flow rate is the product of half the spheroid's surface area and the velocity from Eq. (4.2.5). It turns out that the increase in velocity with pore size is almost exactly canceled by the decrease in maximum bubble size, so the volumetric flow rate is independent of pore size. For the parameters listed above, the gas flow rate is $0.003 \text{ m}^3/\text{hr}$, two orders of magnitude less than the most conservative passive breathing rate of about $0.33 \text{ m}^3/\text{hr}$ (0.2 cfm).

The bubble release time, computed from the flow rate and volume, and releasable gas volume are plotted against pore diameter in Figure 4.2.4 for the parameter values listed above. The straight lines are indicative of the uniform flow rate. For our typical saltcake with a pore diameter of about 30 microns, the largest possible litho-dendritic bubble could contain 0.73 m^3 (26 ft^3) and would require a minimum of about 250 hours to release into the hydro-dendritic layer above. A coarser, 100-micron saltcake would require only about seven hours to release, but its volume would be only about 0.02 m^3 (0.7 ft^3).

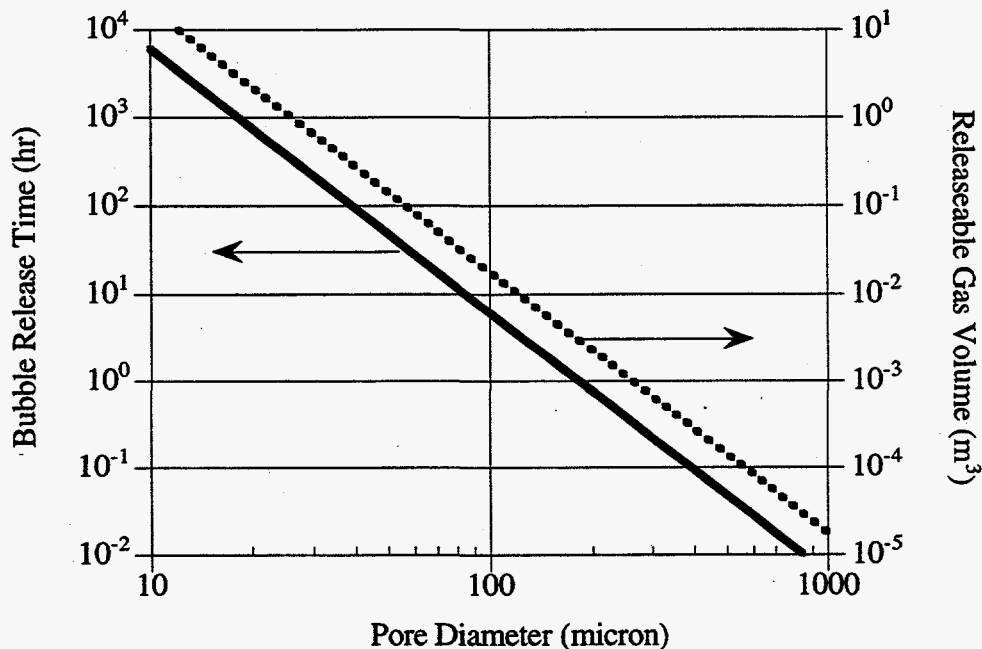


Figure 4.2.4. Litho-Dendritic Bubble Release Time and Volume

The above calculation shows that the potential releases from pore-filling, litho-dendritic bubbles are inconsequential in themselves. A direct release from the litho-dendritic layer to the dome space is not possible and, even if it were, the volumetric flow rate is several orders of magnitude less than the tank ventilation rate. However, the gas discharged into the bottom of the particle-displacing bubble layer can be released through mechanisms peculiar to that layer.

4.2.3 Particle-Displacing, Hydrostatic Bubbles

In the upper layers of the waste, where lithostatic pressure offers less resistance to bubble expansion, bubbles can expand in the pores and displace waste particles. Small pore sizes (meaning higher capillary pressures) and low yield strength also favor the formation of particle-displacing bubbles rather than the litho-dendritic bubbles that only displace interstitial liquid. Discrete, more-or-less round, particle-displacing bubbles are referred to as hydrostatic bubbles; when they depart from roundness and assume a dendritic shape, they are called hydro-dendritic bubbles. These may merge with each other and form networks similar to litho-dendritic bubbles. Hydro-dendritic bubbles are discussed in Sections 4.2.5 and 4.2.6.

As discussed in Section 4.2.1, particle-displacing bubbles are expected to be possible only in the top 2.5 m (approximately) of the nonconvective layer of saltcake tanks. In sludge tanks, however, particle-displacing bubbles can probably exist throughout the entire waste column.

There are two basic constraints on the size of hydrostatic bubbles: 1) a bubble can be approximately spherical only when the forces defining its surface are dominated by surface tension, and 2) a bubble can grow no larger than the size at which its buoyancy exceeds the ability of the waste to hold it in place.

The first criterion is described by Gauglitz et al. (1996). When bubbles grow in a deformable material, the two main forces resisting growth and thereby controlling bubble shape are surface tension and the strength of the material. If surface tension dominates, the bubble will bend to remain roughly spherical. When the waste strength dominates, the bubble displaces the weakest segment of its surface, following the path of least resistance and evolving into some dendritic shape. Simple scaling of the relative importance of strength to surface tension gives the following criterion for existence of round bubbles.

$$\frac{\tau_y D_b}{\sigma} < 1 \quad (4.2.6)$$

Where τ_y is the yield stress, σ is the surface tension, and D_b is the bubble diameter. Solving for the bubble diameter gives the limiting round bubble size as

$$D_b < \frac{\sigma}{\tau_y} \quad (4.2.7)$$

Laboratory experiments by Gauglitz et al. (1996) with clays and samples of tank waste, including both saltcakes and sludges, indicate that when $(\tau_y D_b/\sigma) < 1$, bubbles are round, and when $(\tau_y D_b/\sigma) > 1$ bubbles become flattened into fracture-like shapes that lie along a horizontal or nearly horizontal plane. For example, the largest spherical bubbles observed in a clay with a yield

strength of 67 Pa had a diameter less than about 2 mm which is consistent with Eq. (4.2.7). Bubbles of more than about a centimeter in diameter have not been observed experimentally.

In the second criterion, the ability of the material to restrain the bubbles buoyancy limits the size. Numerous researchers have treated the case of a solid sphere immersed in a Bingham fluid (Chhabra and Uhlherr 1986) and found that a criterion for incipient motion can be expressed in terms of a critical gravity-yield number, Y_G :

$$\frac{\tau_y}{\rho_w g D_b} > Y_G \quad (4.2.8)$$

where ρ_w is the average waste density and g is the acceleration of gravity. The limiting diameter is expressed as

$$D_b < \frac{\tau_y}{\rho_w g Y_G} \quad (4.2.9)$$

Chhabra and Uhlherr (1986) state that the number Y_G is typically less than 0.1 when the Bingham yield stress (determined from the stress-versus-strain rate rheogram extrapolated to zero motion) is used in place of the static shear yield strength. The number Y_G is estimated at about 0.2 when the shear yield strength τ_y is measured by static methods such as vane torsion. The latter, larger value of Y_G is more appropriate for use with yield strengths as measured at Hanford (by static methods).

The 0.2 value for Y_G is also consistent with simple force balances. Assuming the bubble buoyancy force is resisted by the shear stress acting over a cylindrical area tangent to the bubble perimeter results in $Y_G = 0.17$. Assuming that buoyancy is resisted by the normal yield stress acting on twice the projected area and multiplying the shear stress by $\sqrt{3}$ to convert to normal stress gives $Y_G = 0.19$.

Figure 4.2.5 shows the limiting bubble diameters derived from Eq. (4.2.7) and (4.2.9) plotted versus yield stress for a waste density of 1800 kg/m³ and a surface tension of 0.08 N/m. The plot represents a map of particle-displacing bubble behavior. The triangular shaded area satisfies both the criteria: the bubbles are round and the waste is sufficiently strong to prevent them from rising. As bubbles grow along the vertical axis, those in relatively strong material, $\tau_y > 100$ Pa, will first become dendritic, then relax by percolation (see Section 4.2.5). Bubbles in very weak material, say $\tau_y < 10$ Pa, will remain round until they grow to the point that the material can no longer hold them.

In the range of yield stress from about 20 to 100 Pa is a transition region where bubbles may depart significantly from spherical but remain as discrete bubbles without becoming truly dendritic. In this region, indicated by the cross-hatch shading on Figure 4.2.5, bubbles still escape by rising through the medium rather than by percolation. In the experiments of Gauglitz et al. (1996), this transition region produced vessel-spanning bubbles in both 31-Pa and 67-Pa clays in 2.6-cm diameter columns. When the vessel diameter was increased to 30 cm, vessel-spanning bubbles were not observed; instead, 67-Pa clays underwent releases in which the rise of a few bubbles triggered the release of most of the gas in the column. Such bubble-rise cascade releases were not seen in 147-Pa clays in a 2.6-cm-diameter vessel, or in 200-Pa clays in a 30-cm-diameter vessel. In these cases hydro-dendritic bubble networks formed and provided continuous gas release.

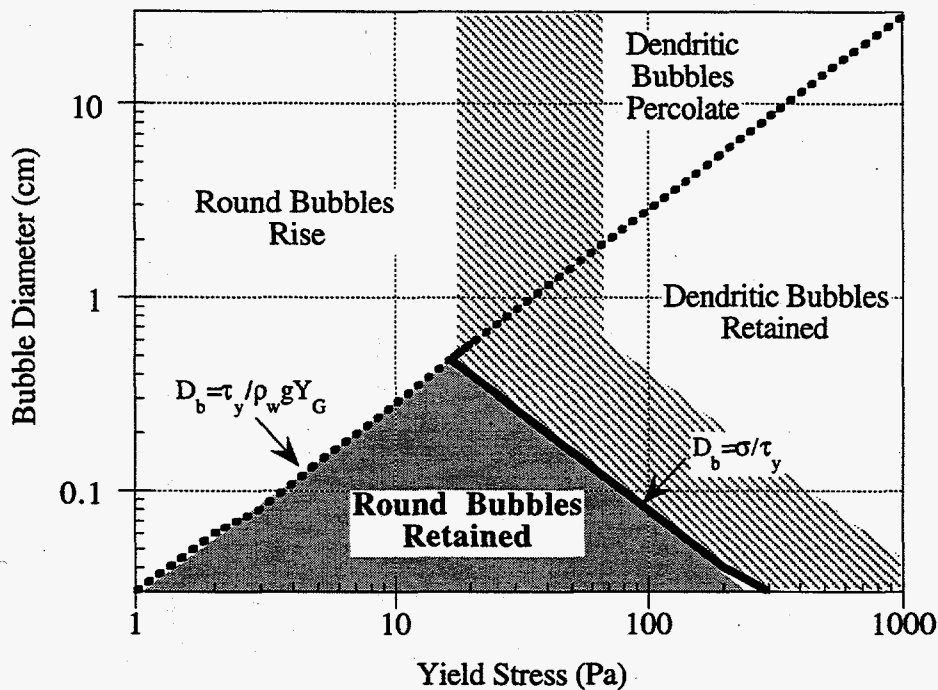


Figure 4.2.5. Particle-Displacing Bubble Behavior Map

We conclude that hydrostatic bubble releases are expected only in waste with yield stress less than about 100 Pa, and that the largest individual bubbles will be less than 1 cm in diameter.^(a)

4.2.4 Dynamics of Hydrostatic Bubble Release

Gas release occurs when an isolated hydrostatic bubble becomes large enough to overcome the yield strength of the waste and rise. The maximum release comes when a near-maximum bubble near the tank bottom begins to rise and starts a cascading with other bubbles it collects by contact or the disturbance of its passage on the way up. Gauglitz et al. (1996) found that in fairly dilute clay simulants with yield stress of 3.4–6.4 Pa, hydrostatic bubbles on the order of 1 mm diameter were released in upward cascades while bubbles of 0.5 mm diameter or less were retained. Bubble cascade releases were also observed for a 67-Pa clay simulant in larger vessels.

To evaluate the potential gas release volume from such a cascade, assume a bubble with an initial diameter of D_0 , begins to rise from a depth of H_0 , and the waste above it contains a uniform

^(a) Earlier calculations used Eq. 4.2.9 with a yield stress of 6700 Pa (Herting et al. 1992) to predict that spherical bubbles over 1 m in diameter could exist in SY-101 waste. This ignores the condition of Eq. 4.2.7 and grossly overestimates the strength of SY-101 waste. Herting also give shear strengths of 370–450 Pa at tank temperatures, which is consistent with ball rheometer measurements in other tanks (Stewart et al. 1996). The high yield stress values do not accurately represent the actual waste properties.

distribution of other bubbles, also of diameter D_0 , at a void fraction of α_0 .^(a) As the bubble rises it expands under the influence of decreasing head and sweeps through the field of stationary bubbles above it, acquiring gas from all the bubbles whose centers are within its region of influence. Based on the streamlines around a sphere in a Bingham fluid computed by Beris et al. (1985), we define the area of influence swept by the rising bubble as twice its diameter, D . The change in rising-bubble volume V (including both expansion and gas acquisition) in a small increment of height dh at depth h is

$$dV = \left[V \left(\frac{\rho_w g}{P_0 + \rho_w g h} \right) + \frac{\pi}{4} (2D + D_0)^2 \alpha_0 \right] dh \quad (4.2.10)$$

where ρ_w = waste density (kg/m^3)
 P_0 = standard atmospheric pressure (101300 Pa)
 D = rising bubble diameter ($D = [6V/\pi]^{1/3}$)
 D_0 = initial and stationary bubble diameter (m)

Eq. (4.2.10) can be numerically integrated over the waste depth to find the potential gas release volume from a bubble cascade. The results are plotted in Figure 4.2.6 for waste depths of 1, 3, 5, and 8 m, assuming a uniform 30% gas fraction and 1800 kg/m^3 waste density.^(b) The uniform high void fraction makes this a very conservative model.

The figure shows that the potential gas release depends more on waste depth than bubble size. The gas release volume for 8-m waste depth is on the order of 100 m^3 , a 12% fraction of the total gas content of 980 m^3 . This hypothetical release would have an equivalent bubble diameter at the surface of about 6 m and would have swept a 40° conical volume of waste. This represents an event of magnitude similar to the large rollovers in SY-101. The release volume falls off quickly with shallower waste; a 5-m tank would release about 20 m^3 (3% release fraction) and a 3-m tank only about 4 m^3 (1% release fraction).

Though the above calculations show that the bubble cascade release can result in relatively large releases, this mechanism is really just a theoretical demonstration and not a prediction of actual tank behavior. Bubble cascades have only been observed in the laboratory under conditions of uniform and very rapid bubble growth in the absence of significant hydrostatic pressures. Even they only occur in simulants much weaker than any actual SST waste is expected to be. The volume calculations also assume a uniform condition that does not exist in the SSTs. The only situation with a potential for a bubble cascade release might be that of initially filling a tank with a liquid that develops a small yield stress while generating gas at a very rapid rate.

^(a) A uniform void fraction and bubble size requires the gas generation rate to increase linearly with depth in proportion to the hydrostatic pressure. Actually, bubbles at higher elevations would grow faster and release sooner than those at the bottom.

^(b) The 30% void fraction is chosen to correspond with that seen in actual low-strength tank wastes whose gas retention was measured under laboratory conditions. The data may be seen in Figure 6.2 of Gauglitz et al. (1996).

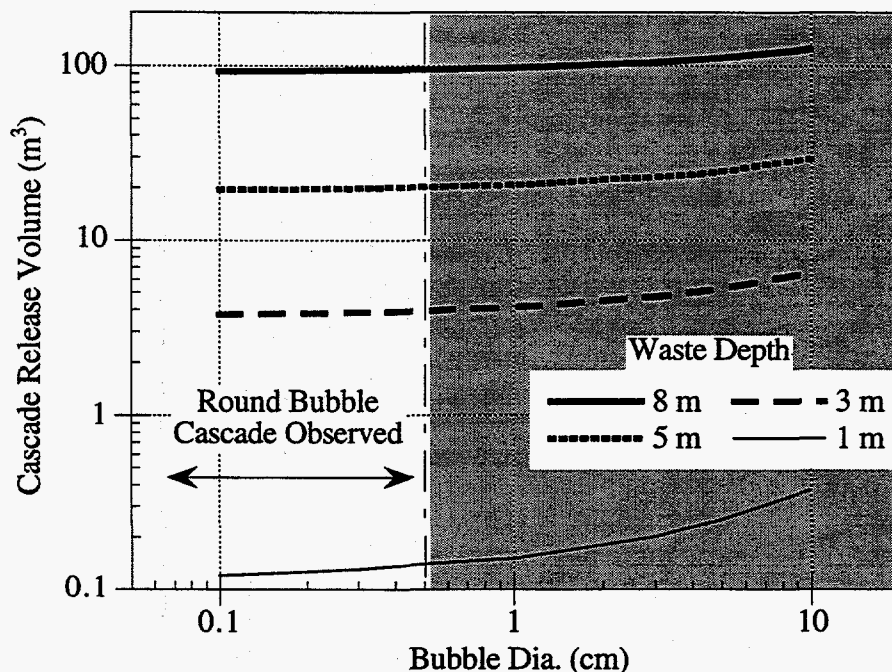


Figure 4.2.6. Round Bubble Cascade Gas Release Volume Versus Bubble Diameter

4.2.5 Particle-Displacing, Hydro-Dendritic Bubbles

Hydro-dendritic bubbles occur only in wastes with yield stress above about 150 Pa. The waste strength causes the formation of hydro-dendritic bubble networks for two reasons. First, the yield strength constrains round, hydrostatic bubbles to grow into flattened, slit-like shapes. Second, when this change occurs the bubble size is substantially smaller than the minimum size required for bubble rise.

A hydro-dendritic bubble can continue to grow vertically as long as it is neither pinched off nor filled with liquid that has drained into it. To satisfy this condition, the bubble height must be less than that for which the waste yield strength can bear the hydrostatic pressure difference across the bubble. It turns out that Eq. (4.2.9), the criterion for the maximum diameter of a hydrostatic bubble for a given yield stress, also defines the maximum vertical extent of a hydro-dendritic bubble (Brewster et al. 1996). The maximum hydro-dendritic bubble height in a 500-Pa waste, for example, is just over 10 cm (see Figure 4.2.5).

Also, to keep from being filled by leaking interstitial liquid, the walls of the hydro-dendritic bubble network must make the same balance between capillary pressure and hydrostatic head as for litho-dendritic bubbles discussed in Section 4.2.1. In saltcake, the maximum vertical extent of a hydro- or litho-dendritic bubble is 1.2 m. In sludge, with its finer particles, the maximum vertical extent could easily be many meters so that capillary pressure effectively does not constrain the size of hydro-dendritic bubbles.

It is interesting to note the wide disparity in the limiting heights of hydro- and litho-dendritic bubbles. This means that, when a limiting litho-dendritic bubble first penetrates an overlying hydro-dendritic region above it, the hydrostatic pressure of the entering gas will be greater than can be supported by a single hydro-dendritic bubble. This is very likely what produces the 'fracture' bubbles in the gas retention experiments of Gauglitz et al. (1994, 1995).

Logical constraints on the horizontal extent of a hydro-dendritic bubble are developed in the same way as for litho-dendritic bubbles in Section 4.1. At this time we assume the maximum horizontal extent of a hydro-dendritic bubble is thrice its vertical limit and that the overall shape of such a limiting bubble is an oblate spheroid.

4.2.6 Dynamics of Hydro-Dendritic Bubble Percolation

Gas release occurs when a hydro-dendritic bubble propagates through to the waste surface and gas percolates through it. The case of such a percolating network is treated in this section.

Gauglitz et al. (1996) performed experiments which clearly demonstrated gas percolation through a network of hydro-dendritic bubbles in stronger clay simulants. As discussed in Section 3.1.1, the bubbles in one region of the simulant column become dendritic as they expand, then contract as they reach the percolation threshold and discharge part of their gas into a higher region which in turn expands and eventually discharges. Upward gas motion in this irregular cascade is clearly visible. The contracting bubbles do not collapse completely. The column grows by this process until it becomes quasi-stationary and releases gas nearly continuously but at varying rates.

A model for hydro-dendritic percolation release was developed at Oxford University during the 29th European Study Group (Brewster et al. 1996). The Oxford model represented the waste as a set of discrete layers, each of which accumulated gas both from generation and from the discharges of lower layers. Flow from each layer is controlled by a relative permeability that was set to zero below a percolation threshold void fraction α_c of 10% and varied as $(\alpha - \alpha_c)^2$ until a critical permeability was reached. At that point the bubble collapsed and discharged a fixed fraction (70%) of its gas to the layer above.

The results of this model showed the void fraction in all layers hovering about the critical value. However, release from a lower layer often triggered a sort of cascade where all the higher layers would exceed the percolation threshold. Cascades only involved about half of the column and releases were relatively small.

The Oxford model was reconstituted with several modifications to study potential release volumes from hydro-dendritic percolation in more detail. In the revised model, both the amount of gas available and the fraction of it that is actually discharged from each layer depends on how much of the gas might be connected to the discharge path. The fraction connected varies with the void fraction between a threshold at which connection begins and an upper limit where the entire volume is connected. Each layer is structured to model the maximum vertical extent of a single hydro-dendritic bubble column rather than a slice across the entire tank. The gasless volume of each layer in the column is set equal to that of a cylinder with diameter thrice its height. For a yield stress of 700 Pa, on the order of a thousand bubble columns might exist in a tank.

The gas volume before discharge V_{1i} , is computed by conservation of mass assuming isothermal processes:

$$V_{1i} = V_{2i} + \Delta t \dot{V} V_0 \frac{P_0}{P_i} + R_{i-1} \frac{P_{i-1}}{P_i} \quad (4.2.11)$$

where V_{1i} = the in-situ gas volume in layer i before discharge
 V_{2i} = the in-situ gas volume in layer i after discharge from the prior time step
 Δt = the time step in days
 \dot{V} = the standard volume of gas generated per day per unit volume
 V_0 = the gasless volume in each layer (assumed a cylinder with a diameter thrice its height as discussed above)

$$V_0 = \frac{\pi}{4} (3\Delta h)^2 \Delta h$$

Δh = the maximum bubble height (Eq. 4.2.9)
 P_0 = standard atmospheric pressure
 R_{i-1} = volume of gas discharged from the layer below (i-1) in this time step
 P_i = pressure in layer i (hydrostatic + P_0)

$$P_i = P_0 + \rho g h_i$$

ρ = bulk waste density (ungassed)
 g = gravity (9.81 m/s²)
 h_i = depth of layer i below surface (ungassed)

P_{i-1} = pressure in layer below (i-1)

The void fraction before discharge is computed by

$$\alpha_i = \frac{V_{1i}}{V_{1i} + V_0} \quad (4.2.12)$$

Gas discharge to layer above occurs only when the void fraction exceeds a lower percolation threshold α_L , and is limited to maintain a minimum gas fraction, α_{min} , to account for the gas that remains between particles even when the walls of the dendritic bubble have collapsed together.

Not all of the gas in a layer is interconnected and available for discharge. As the void fraction increases above α_L , the extent of interconnection β increases linearly from zero at the lower percolation threshold to 1.0 (all the gas is interconnected) at and above the upper percolation threshold α_H . Above the lower percolation threshold, the extent of interconnection is allowed to vary randomly between this linear prescription and 1.0 (see Eq. 4.2.14, below). The fraction of the total gas available and interconnected that is actually discharged to the next level is expressed by a factor, F that is allowed to vary between two values depending on the extent of connectedness. A stronger material should resist collapse more than a weaker one and thus have a lower discharge fraction. However this effect has not yet been quantified theoretically or experimentally. The discharge model is expressed by

$$R_i = \left(V_{1i} - \frac{\alpha_{\min}}{1 - \alpha_{\min}} V_0 \right) \beta_i F_i \quad (4.2.13)$$

α_{\min} = the minimum void fraction remaining after a gas discharge

β_i = fraction of gas in layer i that is interconnected and subject to percolation

$$\begin{aligned} \text{for } \alpha_i < \alpha_L & \quad \beta_i = \beta_R \Psi \\ \text{for } \alpha_i > \alpha_H & \quad \beta_i = 1 \end{aligned} \quad (4.2.14)$$

$$\text{for } \alpha_L \leq \alpha_i \leq \alpha_H \quad \beta_i = \frac{\alpha_i - \alpha_L + (\alpha_H - \alpha_i) \beta_R \Psi}{\alpha_H - \alpha_L}$$

α_L = lower percolation threshold

α_H = upper percolation threshold (at which 100% connection is achieved)

β_R = randomness factor: 0 - linear variation, 1 - random variation

Ψ = a random number uniformly distributed between 0 and 1

F_i = discharge fraction of interconnected gas in layer i

$$F_i = F_0 + \beta_i (F_1 - F_0) \quad (4.2.15)$$

F_0 = discharge fraction when connection begins

F_1 = discharge fraction at complete connection

The gas volume in the layer after discharge is the simple difference:

$$V_{2i} = V_{1i} - R_i \quad (4.2.16)$$

This model is one of many that can be developed; it has not been verified by comparing it with experiments or SHMS data and is not intended to predict tank behavior. There is no sound basis for many of the input parameters. Nevertheless, it should capture some of the more important features of the percolation physics and serve as a focus for discussion of a better model.

A base case is defined with the following parameter values:

Waste density	$\rho = 1800 \text{ kg/m}^3$
Waste depth	$H = 5 \text{ m}$
Bubble height	$\Delta h = 0.2 \text{ m}$ corresponding to a 700 Pa yield stress
Gas gen. rate	$\dot{V} = 0.00135 \text{ m}^3 \text{ gas/m}^3 \text{ waste/day}$ (twice the rate of SY-101)
Time step	$\Delta t = 3 \text{ days}$ (total time 3.9 years)
Lower perc. threshold	$\alpha_L = 0.24$ from examination of Gauglitz et al. (1996) data
Upper perc. threshold	$\alpha_H = 0.40$ from examination of Gauglitz et al. (1996) data
Randomness	$\beta_R = 1.0$
Lower disch. factor	$F_0 = 1.0$
Upper disch. factor	$F_1 = 0.7$ consistent with the Oxford model.

The results of the model expressed by Eq. (4.2.11-4.2.16) are consistent with those reported for the original Oxford model. The average void fraction hovers very close to the lower percolation threshold, regardless of other parameter values. Given a uniform gas generation rate in terms of mass, the lower levels accumulate gas volume much more slowly than the upper ones that reach the percolation threshold sooner and discharge more often. This means that when the bottom layer discharges, the gas in layers above will have been somewhat depleted by earlier releases and will be able to absorb some of the gas passing through. Thus the maximum volume released in a cascade is quite limited. Only a quarter to half of the discharges from the bottom layer cascade all the way to the surface.

The cumulative distributions of the release fraction for the base case and two variations for a simulated period of just under four years are given in Figure 4.2.7. In all cases the column release fraction is less than 10%. Reducing the upper percolation threshold from 0.4 to 0.3 increases the release fraction slightly. Setting the initial discharge fraction to zero shifts the distribution markedly toward lower release fractions without altering the maximum significantly. The distribution is undoubtedly strongly influenced by the choice of a uniform distribution for the random number in Eq. 4.2.15.

The effects of varying the upper discharge fraction, waste depth and bubble height on the maximum release volume and maximum release fraction are shown in Figures 4.2.8, 4.2.9, and 4.2.10, respectively. Increasing the upper discharge fraction above about 0.8 dramatically reduces the number of releases while increasing their magnitude. However, visual evidence from laboratory experiments (Gauglitz et al. 1996) would suggest a lower discharge fractions. The appropriate value probably varies with yield stress and possibly depth. Weaker material in deeper levels would have a higher discharge fraction.

Figure 4.2.9 shows that waste depth affects mainly the release fraction. The release volume is essentially constant, but the total gas volume stored in the column increases with depth, thereby reducing the release fraction. This somewhat counter-intuitive effect is due to the decrease in discharge frequency with depth. The upper layers discharge much more frequently than the lowest ones. This keeps the void fraction in the upper layers below the percolation threshold so they can absorb much of the gas discharged from the bottom layers.

Both the release and release fraction increase approximately linearly with bubble height as shown in Figure 4.2.10. The larger the bubble, the greater the volume it can discharge and the fewer bubbles can exist in the column. Therefore the release volume and release fraction both increase. However, larger bubbles require higher yield stress material, which might decrease the discharge factor and cancel out most of the effect.

In all the above results, it is important to note that 1) the maximum releases and release fractions are small, and 2) each represents only a single dendritic bubble column, not the whole tank. Therefore the overall fraction of a tank's total stored gas released in an individual percolation event is truly miniscule. However, on the order of a thousand such columns could theoretically exist in a tank with an average yield stress of 700 Pa, so discharge events might be relatively frequent. A low barometric pressure event might cause more than the usual number to discharge. A typical 1-2 m³ release as observed in the SHMS data from SSTs during the low pressure events of the winter of 1995-96 (Wilkins et al. 1996) would require 30-60 columns to discharge an average of 0.03 m³ of gas at close to the same time.

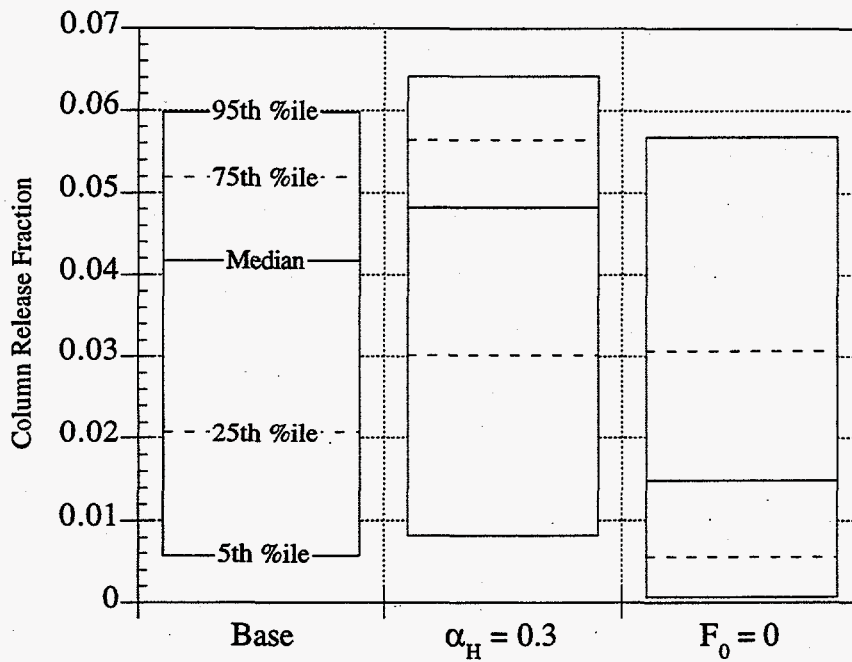


Figure 4.2.7. Cumulative Distribution of Hydro-Dendritic Release Fraction

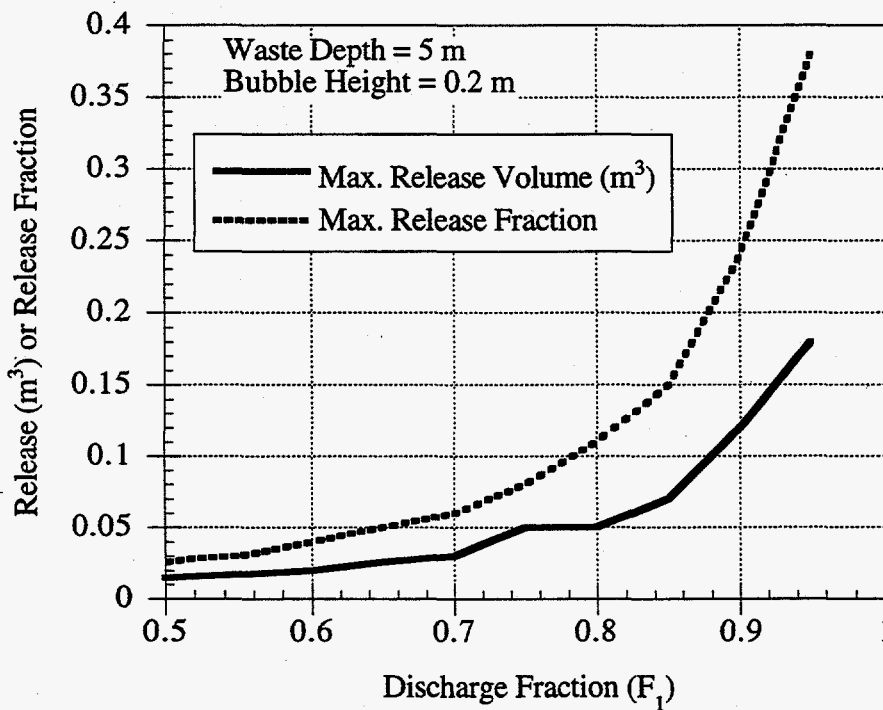


Figure 4.2.8. Effect of Discharge Fraction on Hydro-Dendritic Release

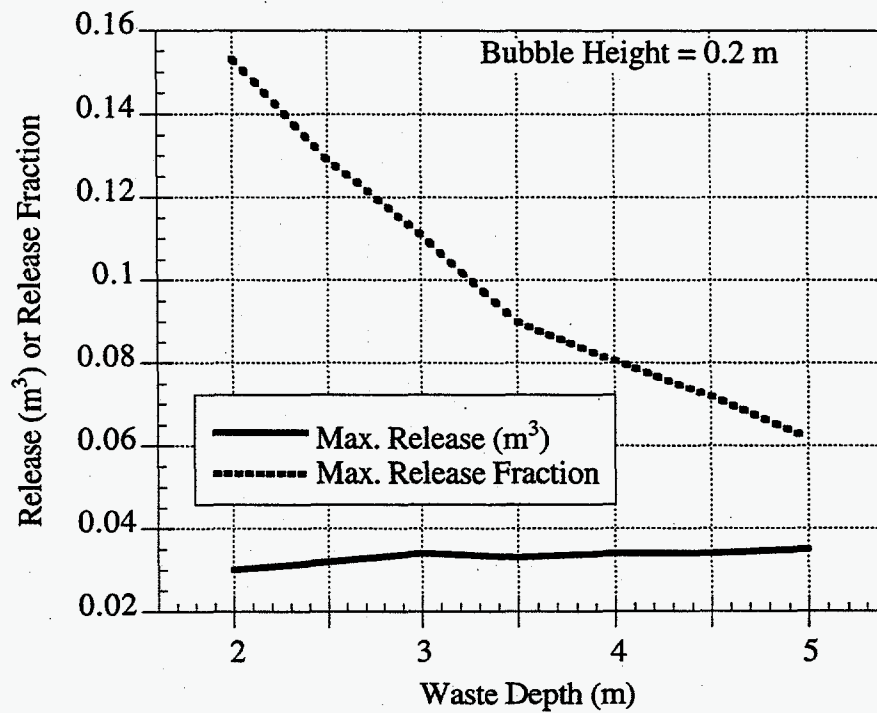


Figure 4.2.9. Effect of Waste Depth on Hydro-Dendritic Release

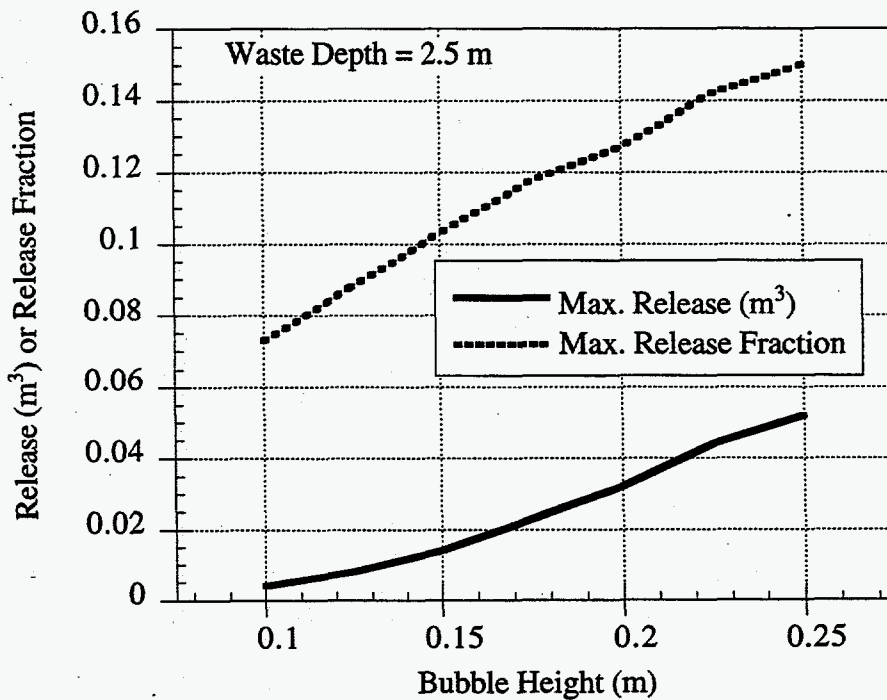


Figure 4.2.10. Effect of Bubble Height on Hydro-Dendritic Release

4.2.7 Conclusion on Percolation Release

Three release mechanisms have been discussed in this section: litho-dendritic (pore-filling) bubble percolation into a particle-displacing bubble region, a cascade of hydrostatic (round) bubbles, and hydro-dendritic (particle-displacing) bubble percolation cascades through to the waste surface. Of these, the one that releases the most gas and does so nearly instantaneously is the hydrostatic bubble cascade. The hydro-dendritic percolation cascade is most common and may explain the typical small releases seen in the SHMS data in SSTs. Litho-dendritic bubble percolation is inconsequential in itself because it occurs so slowly and does not have direct access to the waste surface.

Large hydrostatic bubble cascade releases are expected only in relatively weak waste with yield stresses less than about 100 Pa. The largest individual bubbles will be less than 1 cm in diameter. Though such a release could potentially be large, this mechanism is more a theoretical demonstration than a prediction of actual tank behavior. Bubble cascades have only been observed in the laboratory under conditions of uniform and very rapid bubble growth and in the absence of significant hydrostatic pressures. Even then they only occur in simulants much weaker than any actual SST waste is expected to be. The volume calculations also assume a uniform condition that does not exist in the SSTs. A possible situation with a potential for a bubble cascade release might be transferring a dilute slurry into a tank such that the waste develops a low yield stress while generating gas at a rapid rate.

The overall fraction of a tank's total stored gas released in an individual hydro-dendritic percolation cascade is miniscule but discharge events are probably frequent since over a thousand bubble columns might exist in a tank. A typical 1–2 m³ release as observed in the SHMS data from SSTs during the low pressure events of the winter of 1995-96 (Wilkins et al. 1996) would involve 30–60 columns to discharge an average of 0.03 m³ of gas at close to the same time.

A hydro-dendritic percolation cascade release could leave some marks of its occurrence on the waste surface. Entrained liquid or liquid-solid slurry brought to the surface repeatedly through the same vent could produce mud cones, such as those visible in SY-101 surface photographs (Figure 2.5). Venting under supernatant liquid layers or under deep layers of unsaturated waste might not leave a sign. The waste surface photographs discussed in Section 2 showed no surface features that positively indicated episodic gas releases of any kind. There were no large vents or fumaroles such as those found in SY-101 in any of the SSTs. Therefore, individual percolation events must generally be too small to disturb the waste surface or to transport heavy material to the surface with the gas. They have no potential for sudden release of a large fraction of the tank's stored gas inventory.

4.3 Earthquake-Induced Gas Release

In this section the behavior of tank waste during the earthquakes postulated for Hanford are investigated using spectrum vibration analysis. This method requires waste physical and structural property data that are not currently available; thus the results given at the end of this section should be considered as possible ranges of effects, not as specific predictions. They should not be considered a technical basis for a safety analysis.

The design basis earthquake (DBE) spectrum for Hanford, using the best-fit Newmark-Hall (1978) method, is shown in Figure 4.3.1.^(a) The shock spectrum envelopes the root-mean-square (RMS) acceleration history as a function of frequency; analytical equivalent time associated with the spectrum is 20 seconds. This spectrum describes a 1,000-year earthquake and has its "hook" set at 0.35g. The 100-year earthquake is a proportional curve with its hook set at 0.20g.

A generic waste model is used to evaluate the waste motion during the assumed DBE based on linear elastic theory. Elastic assumptions provide a means to characterize induced stresses and absorbed energy for a spectrum analysis. Waste is not extensively characterized for solid mechanics properties, but some data are available.

The estimated yield stress of the SY-101 nonconvective layer ranged around 500 Pa (Herting et al. 1992). Ball rheometer tests in six Hanford DSTs show somewhat lower nonconvective layer yield stresses, in the 100-300 Pa range. JR Phillips has evaluated a mildly stiff clay

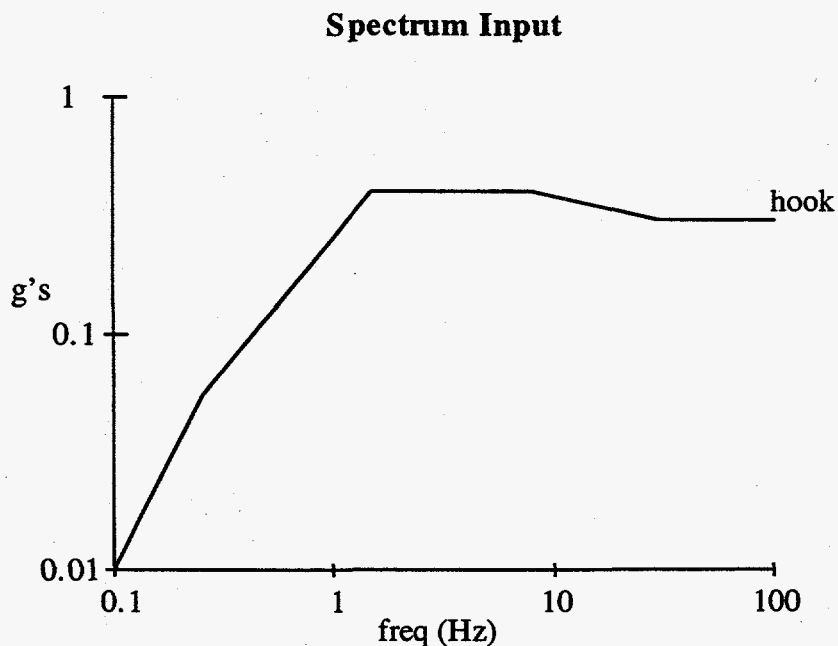


Figure 4.3.1. Design-Basis Earthquake Spectrum for Hanford

^(a) Weiner EO. *Design Basis Earthquake Time Histories for 1992 SDC-4.1*. WHC SD-GN-DA-30018 Rev. 12, Westinghouse Hanford Company, Richland, Washington.

simulant and determined that the shear modulus in the elastic strain regime is about 6 kPa.^(a) This simulant had a yield strain of 5%, for a yield stress of 300 Pa. A survey of thin waste simulants indicates the shear modulus is about 100 Pa and the yield strength around 20 Pa.^(b) The range of shear moduli assumed for this analysis was 100 to 1×10^5 Pa.

4.3.1 Stress Modeling of Waste for a Design Basis Earthquake

A simple finite element model of waste excitation was used to generate normal stresses. The spectrum excitation was assumed at the base of the tank. Three primary unknowns required to determine natural frequency and response were the modulus of elasticity, Poisson's ratio, and damping.

A series of parametrics was used to determine natural frequency for waste with a density of 1.7 gm/cm^3 and shear moduli of 300, 3,000, and 30,000 Pa. The equivalent Young's Modulus was computed from the shear modulus and the assumed Poisson's ratio of 0.5 (for normal stresses only). Two modes of vibration were evaluated: vertical motion due to an excitation applied at the bottom of the tank and lateral motion due to a rocking spectrum applied at the base. The lateral vibration model includes some adjacent ground structure to account for inherent restraint. A schematic of the modeling is presented in Figure 4.3.2(a) and (b). The models assume one-dimensional vertical and horizontal vibration.

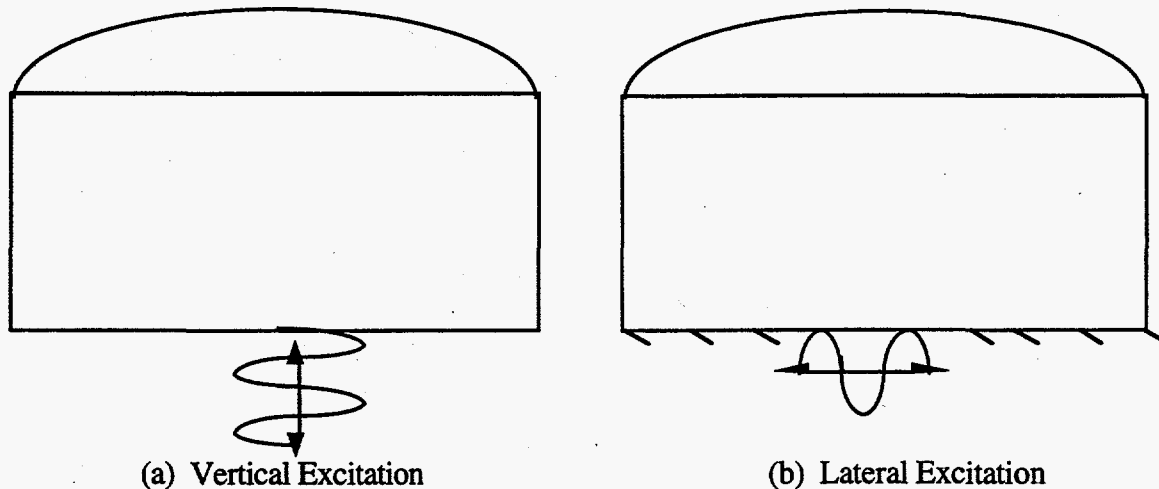


Figure 4.3.2. Excitation Modes for Tank Seismic Analysis

-
- (a) Phillips JR. May 1994. *A Basic Rheological Survey of Simulant Materials for the Ball Rheometer Project*. Memo, Pacific Northwest National Laboratory, Richland, Washington.
- (b) Phillips JR. June 1995. *NCAW Simulant Supernatant Liquid Viscometric Behavior*. Memo to GT Maclean, WHC. Pacific Northwest National Laboratory, Richland, Washington.

The method of computing the spectrum output is an analytical procedure outlined by Wheeler (1987). The natural frequencies of the systems are given by

$$f_n = C \sqrt{\frac{gY}{\rho L^2}} \quad (4.3.1)$$

where g is the gravitational constant (386 in./sec²), Y is the waste Young's modulus, ρ is the waste density, and L is the waste depth. The coefficient C is determined by the mode (vertical or horizontal excitation). For vertical motion, $C = 0.25$ (Avalone 1987); C for horizontal excitation was determined to be 0.188, based on a SAP7 (1980) finite element model. The natural frequencies obtained for the vertical and lateral excitations are shown in Figures 4.3.3 and 4.3.4, respectively, as a function of shear modulus and total waste height.

The peak displacement for the motion is

$$\delta = \frac{G}{(2\pi f_n)^2} \quad (4.3.2)$$

where G is response acceleration and, for a pure "white noise" spectrum, is

$$G = G_0 \sqrt{\frac{\pi}{2}} Q \quad (4.3.3)$$

with the amplification factor, Q , equal to 1 for a critically damped system. G_0 is the spectrum value of the acceleration at frequency f_n . Finally, the stress induced by the motion is obtained from

$$\sigma = \frac{\delta}{L} E \quad (4.3.4)$$

Normal stresses for a vertical excitation at critical damping were predicted for the assumed spectrum input of Figure 4.3.1. The resulting peak normal stresses halfway down the waste column as a function of waste thickness and shear moduli for vertical and horizontal excitation in a 1000-year earthquake are shown in Figures 4.3.5 and 4.3.6, respectively. Note that thicker wastes have a lower natural frequency but experience similar stresses. Figures 4.3.7 and 4.3.8 show the same stress predictions for a 100-year earthquake for vertical and horizontal excitation, respectively.

The vertical mode has a slightly higher natural frequency than the lateral because the lateral mode allows for displacements in both vertical and horizontal directions, which combine to produce a lower natural frequency. The vertical mode assumes vertical displacements only. The peak normal stresses are twice the average normal stresses over the waste height, because the stresses drop from a maximum at the restraint (floor) to zero at the free surface. The induced strain (and thus stress) is linearly dependent on the modulus of the material for a specified base load (g -load).

The induced stresses shown in these figures tend to be flat with respect to waste height because the natural frequency declines with increasing height (below 1.5 Hz), and spectrum acceleration follows suit. The induced stress from a spectrum shock is a static emulation of the dynamic response. The ratio of induced strain to static strain is proportional to the ratio of response spectrum load (in terms of acceleration) to 1g. Therefore, induced stresses from a spectrum shock are related to the static stress from an equivalent static load derived from the spectrum shock.

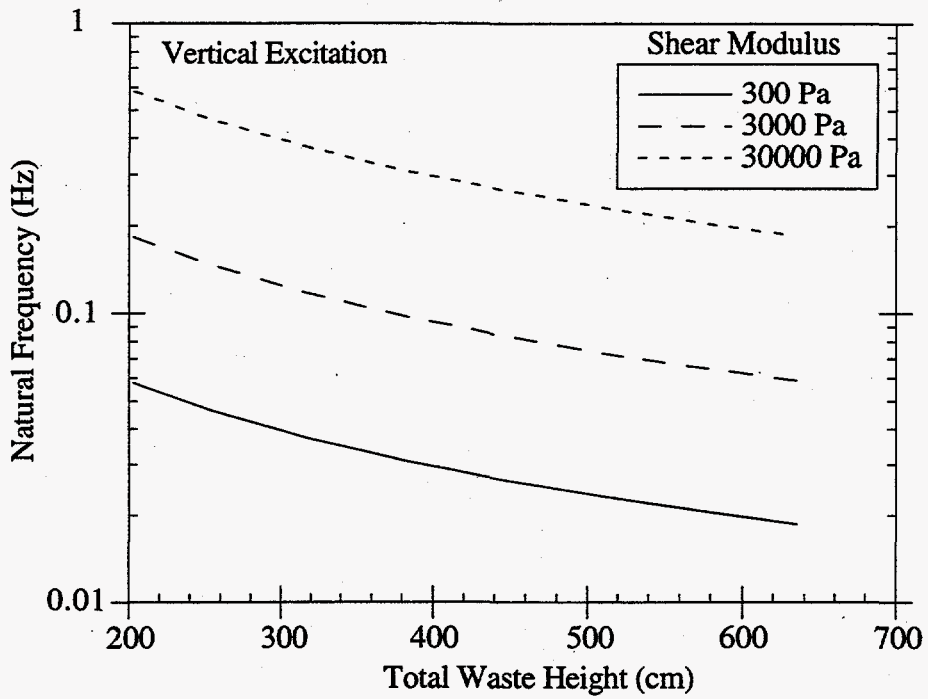


Figure 4.3.3. Natural Frequency Versus Overall Waste Height - Vertical

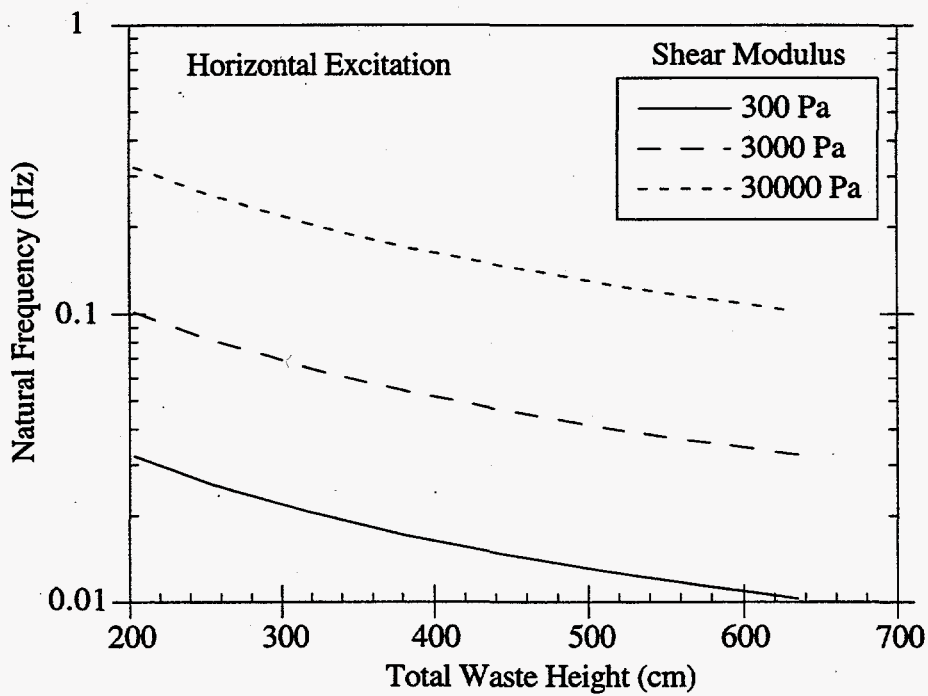


Figure 4.3.4. Natural Frequency Versus Overall Waste Height - Horizontal

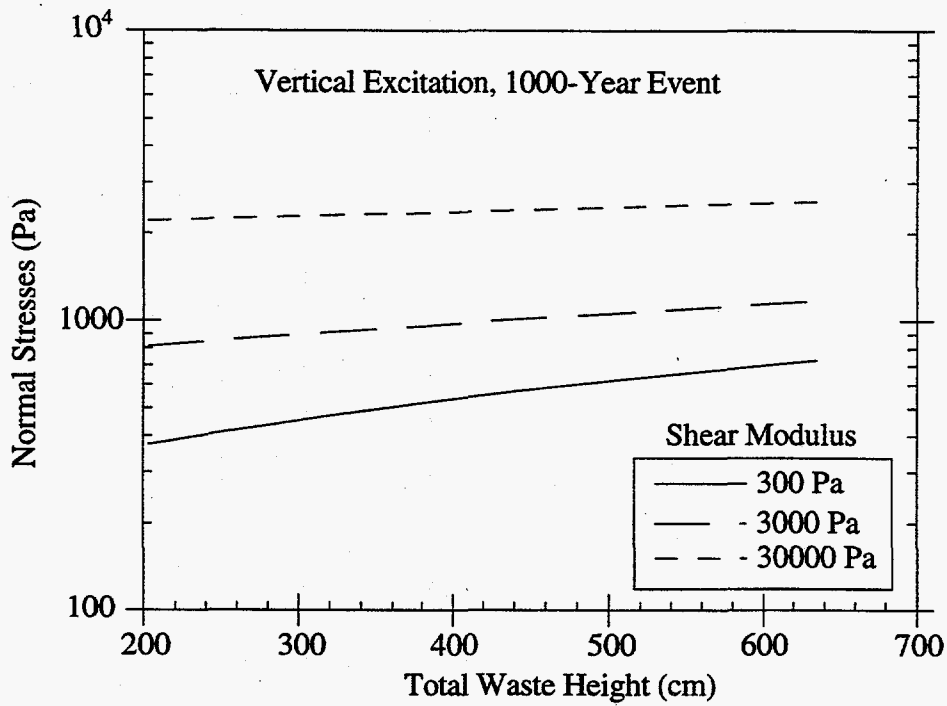


Figure 4.3.5. Peak Stresses at Mid-Depth - Vertical Excitation, 1000-Year DBE

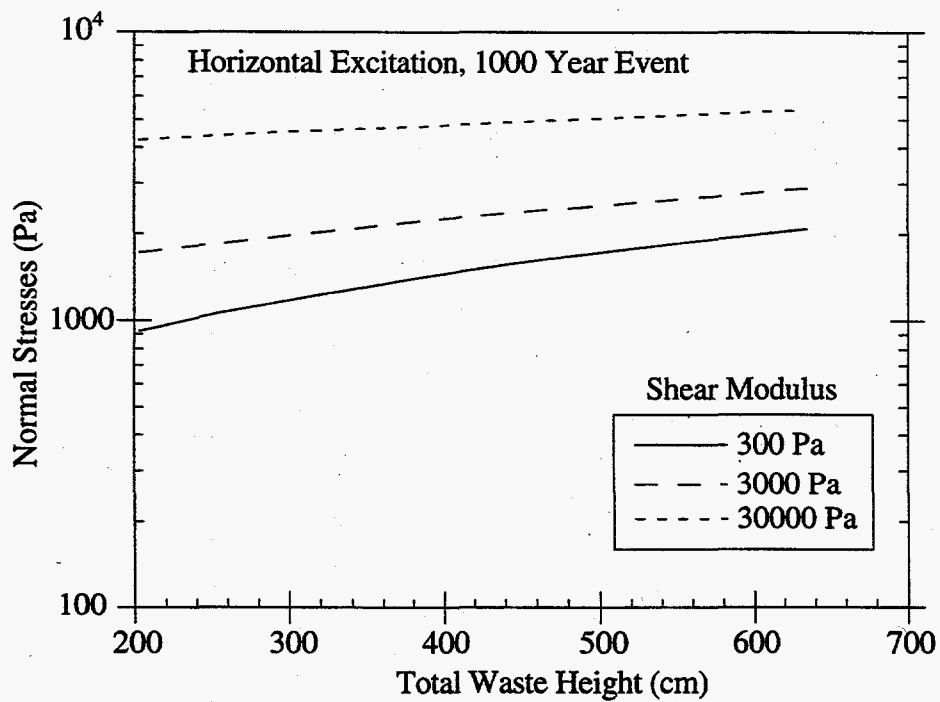


Figure 4.3.6. Peak Stresses at Mid-Depth - Horizontal Excitation, 1000-Year DBE

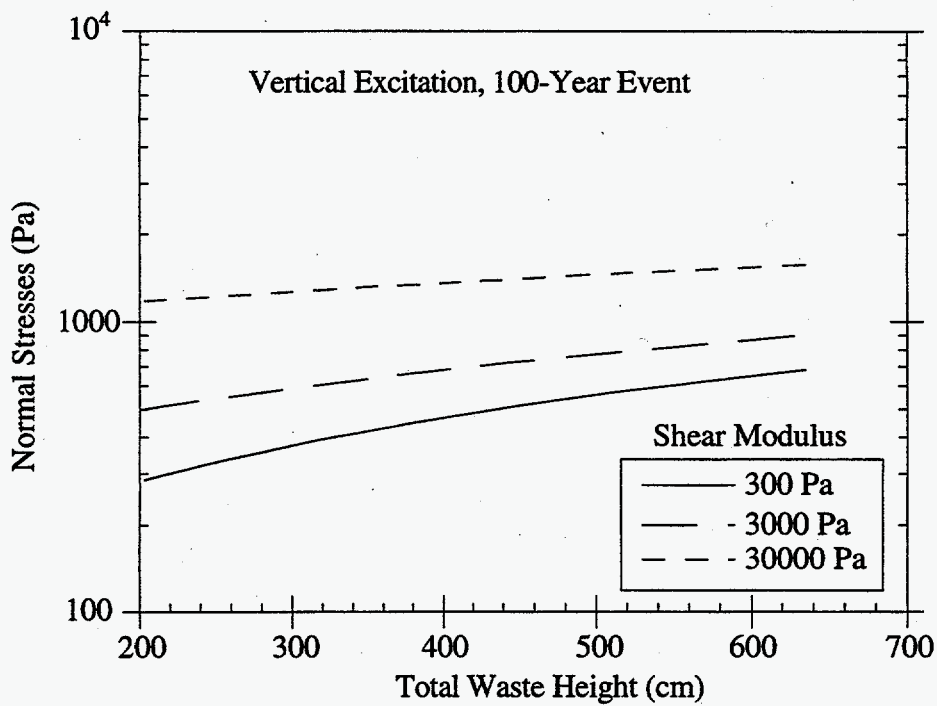


Figure 4.3.7. Peak Stresses at Mid-Depth - Vertical Excitation, 100-Year DBE

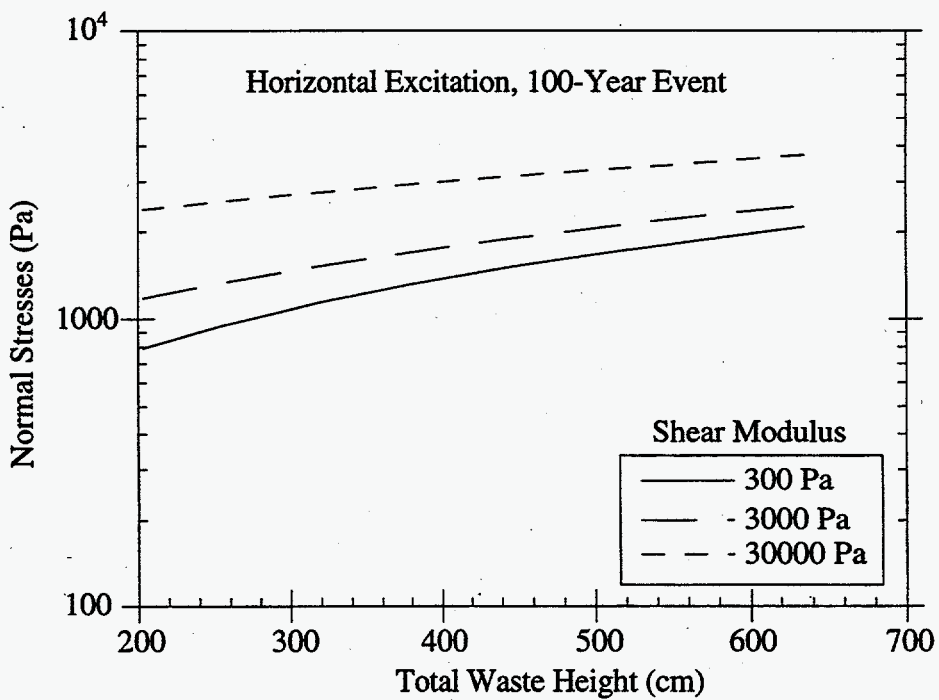


Figure 4.3.8. Peak Stresses at Mid-Depth - Horizontal Excitation, 1000-Year DBE

The magnitude of the induced stresses indicates that most of the waste could potentially yield (i.e., strains would exceed the elastic limit of ~5%). Horizontal excitation produces the highest induced stresses. For a 1000-year DBE, Figure 4.3.6 gives an average normal stress of about 5 kPa in a material with a 30-kPa shear modulus. Figure 4.3.8 indicates an induced stress of about 3 kPa for a 100-year DBE. Assuming a 5% elastic strain at yield, the 30-kPa waste has a yield stress of about 1.5 kPa, which is less than the induced stress in either DBE.

The major factor not yet discussed is damping. It is reasonable to assume that damping coefficients could be and probably are much greater than 1, especially as yielding is approached. Performing a single mode response spectrum analysis as a function of modal damping gives a curve of normal stresses versus damping coefficient. Figure 4.3.9 shows normal stresses in a vertical excitation for the given spectrum and natural frequencies for 200- and 650-cm waste depths. The critical damping coefficient is defined as 1. Coefficients greater than 1 imply an overdamped material. Phillips' data on simulants suggest that the wastes are overdamped. Stresses for overdamped waste properties are all below the critically damped value.

Attenuation is a direct consequence of damping, especially for overdamped systems. Dissimilar material interfaces as well as distributed gas bubbles tend to cause attenuation; attenuation factors can be orders of magnitude (Stewart et al. 1995). For the present analyses, no attenuation is assumed, which is very conservative.

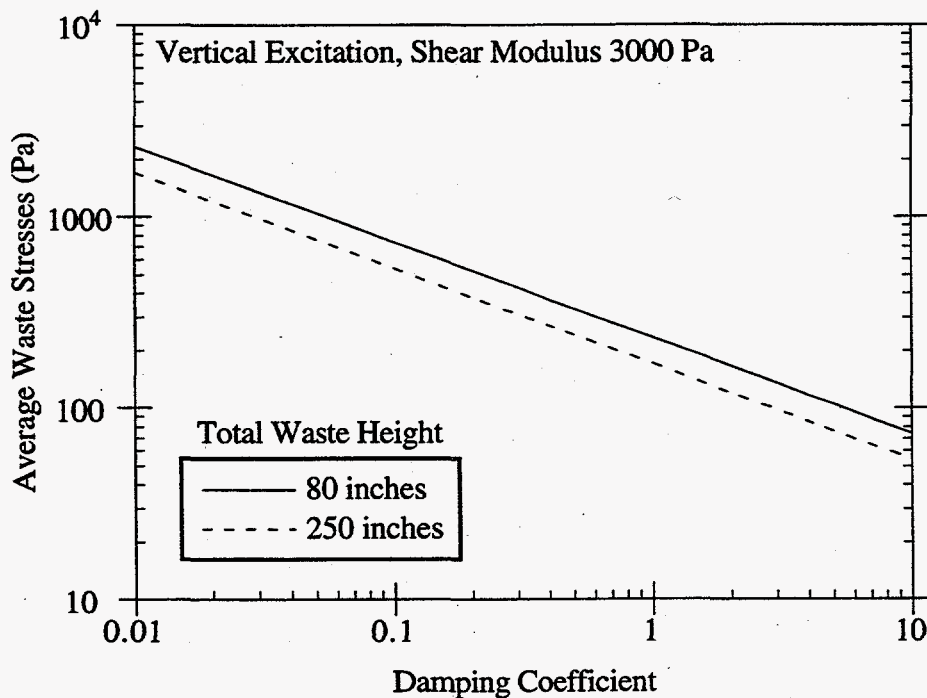


Figure 4.3.9. Average Waste Stresses with Damping Coefficient

4.3.2 Energy Developed in Waste for a Design Basis Earthquake

Potential gas releases induced by earthquakes depend only indirectly on the peak stresses. The real issue, in view of the development in Section 4.1.2, is how much energy is imparted to the waste compared with the energy required to yield it. The energy developed in waste can be formulated based on the elastic strain from the response spectrum. The generic model for strain induced with cyclic vibration is shown in Figure 4.3.10.

The maximum energy associated with the elastic strain occurs at the limit-induced strain. This energy is recovered as kinetic energy in a perfectly elastic material without damping. Depending on the degree of damping, some energy is dissipated in the material. For a critically damped material, all of the strain energy induced by one cycle is dissipated into the material. For this case, each new cycle begins with no accumulation of kinetic energy. The maximum strain energy is also equivalent to the peak kinetic energy, which is proportional to the velocity squared. Since the response of the waste varies with depth, the velocity profile of the waste is a function of the waste height. Therefore, the total energy dissipated in the waste during a single, critically damped cycle can be expressed as

$$E_n = 2 \int \frac{1}{2} \rho u^2 d\vartheta \quad (4.3.5)$$

where $d\vartheta$ is differential volume, equal to (unit area)* dh , and ρ is the waste density. The factor of 2 in front of the integral combines the compression and tension halves of each cycle. The integral of velocity squared over depth can be expressed as an average. The average u^2 for lateral motion is an integral of the predicted response over the x-y domain of the waste. The total energy input during the entire DBE is the product of the energy per cycle, the frequency of the cyclic strain (cycles/unit time), and the time, or

$$E_{DBE} = Cm(u_{avg})^2 f_n T \quad (4.3.6)$$

where the constant C is 1/2 for vertical excitations and about 1/3 for lateral motion, and m is the total waste mass. Finally, the energy per unit volume is

$$e_{DBE} = C\rho(u_{avg})^2 f_n T \quad (4.3.7)$$

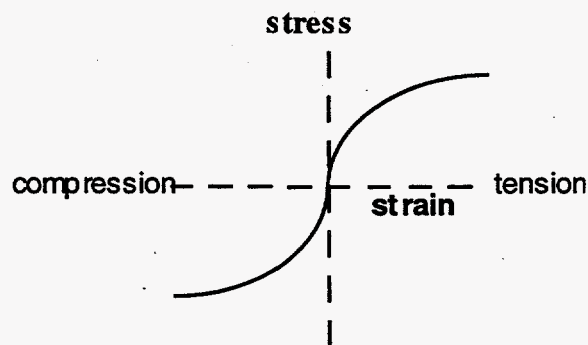


Figure 4.3.10. Strain Induced with Cyclic Vibration

The DBE has an equivalent time of 20 seconds associated with the spectrum. The response spectrum output from the one-dimensional analyses is used to obtain the specific energy absorbed by the waste as a function of waste height. The curves in Figure 4.3.11 are for the vertical excitation model, and Figure 4.3.12 presents the horizontal motion energy absorption for the 1000-year DBE. The material density is 1.7 gm/cm^3 , and the damping coefficient is assumed to be 1.

Energy imparted to the waste is proportional to the power density of the spectrum. For any natural frequency, the energy is a function of the square of the acceleration input. For the range of waste depths under consideration, the maximum average specific energy absorbed in the waste is shown to be about 27 ft-lb/ft^3 with a shear modulus of 30 kPa and a 200-cm (80-in.) overall height. The higher natural frequencies due to the high shear modulus incur larger spectrum input motion.

The waste is assumed not to yield in the energy absorption calculations shown in Figures 4.3.11 and 4.3.12; therefore, these curves are "yield-strength independent." If a yield strength is assumed, there is an upper limit to the displacement and velocity that can be attained at any spectrum input. The yield-limited displacement can be determined from Eq. (4.3.4) by

$$\frac{\delta_y}{\delta_{\max}} = \frac{\sigma_y}{\sigma_{\max}} \quad (4.3.8)$$

and the associated yield-limited velocity is

$$u_y = 2\pi f_n \delta_y \quad (4.3.9)$$

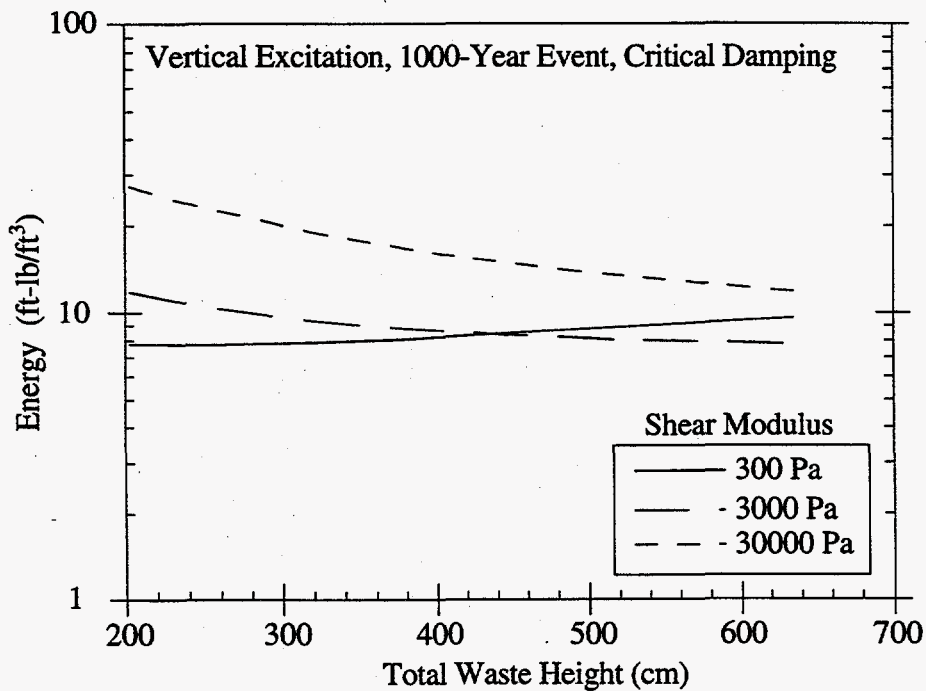


Figure 4.3.11. Average Absorbed Energy - Vertical Excitation

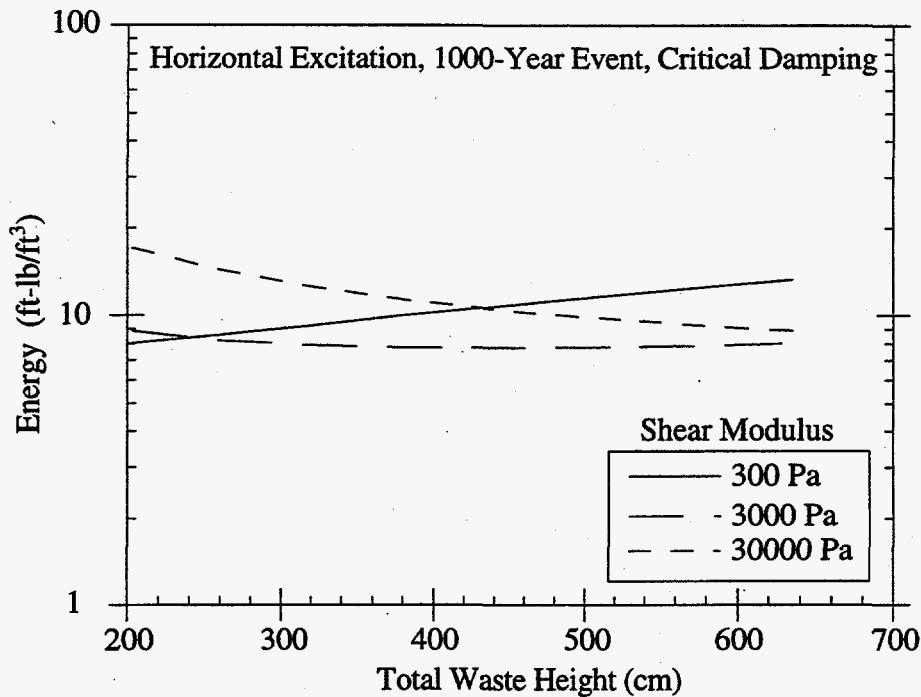


Figure 4.3.12. Average Absorbed Energy - Horizontal Excitation

Eq. (4.3.7) provides the means of computing the yield-limited energy based on the yield-limited velocities. To provide a simplified estimate of reasonable modulus-yield stress conditions, it is necessary to choose a yield strain for evaluation. Again, no comprehensive set of data exists for all wastes, but yield point strains for typical simulants fall in the 1–10% range. For evaluation purposes, we chose a 5% yield strain. In general, the yield-limited energy is proportional to the square of the velocity; however, assuming a constant yield-strain value also implies that the modulus is constrained by the assumed yield stress. A general relation for variation of yield-limited energy with modulus is derived from Eq. (4.3.4) as

$$e_y \propto u_y^2 f_n \approx (f_n \delta_y)^2 \approx f_n^3 \epsilon^2 \quad (4.3.10)$$

where ϵ is the assumed 5% yield strain. Since the natural frequency is shown to be proportional to the square root of the modulus in Eq. (4.3.1), the yield-limited energy is related to shear modulus, G , by

$$e_y \propto f^3 \propto G^{3/2} \quad (4.3.11)$$

Assuming an elastic limit yield point, an elastic excitation energy limit can be determined for waste of given height and modulus. However, the linear elastic strain energy limit is very conservative because it fails to consider energy absorption in plastic deformation beyond the elastic strain limit. Some approximate estimates of the upper limits of plastic deformation energy can also be made. The deformation limit for true yielding (where gas bubble release can occur) can be in the range of 100% strain (see Section 4.1.2). For strains of this magnitude, the linear elastic methods used to determine the modal excitation frequencies and energies are not formally

acceptable. Detailed elastic-plastic modal excitation and energy from DBE spectrum shock have not been performed at this point. Nevertheless, an approximate comparison of plastic deformation energy with elastic response can be made.

Figure 4.3.13 compares the energy deposited in the waste during 100-year and 1000-year DBEs with the energy required to yield the waste assuming both the elastic yield limit (5% strain) and plastic deformation limit (100% strain). The conditions represent horizontal excitation and 640 cm (250 in) waste depth. It is clear from the figure that a large earthquake can potentially yield most of the waste. Considering plastic energy absorption, waste with a shear modulus above about 3 kPa might withstand a 100-year DBE, while a modulus of 10 kPa is required for a 1000-year DBE. At 100% strain, the waste yield stress is equal to the shear modulus value.

4.3.3 Conclusion on Earthquakes

A seismic event has the potential to disturb the entire tank contents, possibly to the point of yielding and allowing a large fraction of the trapped gas to escape rapidly. Figure 4.3.13 compares the energy deposited in the waste during 100-year and 1000-year DBEs with the energy required to yield the waste assuming both the elastic yield limit (5% strain) and plastic deformation limit (100% strain). The conditions represent horizontal excitation and 640 cm (250 in) waste depth. Considering a tank whose waste has a yield stress of 500 Pa, which is typical of DSTs, a 100-year earthquake deposits about 3 ft-lb/ft³ in the waste. This is about six times the 0.5 ft-lb/ft³ required to yield the waste assuming plastic energy absorption and about the same energy ratio as occurred in the large buoyant displacement events that released on the order of 50% of the stored gas from SY-101.

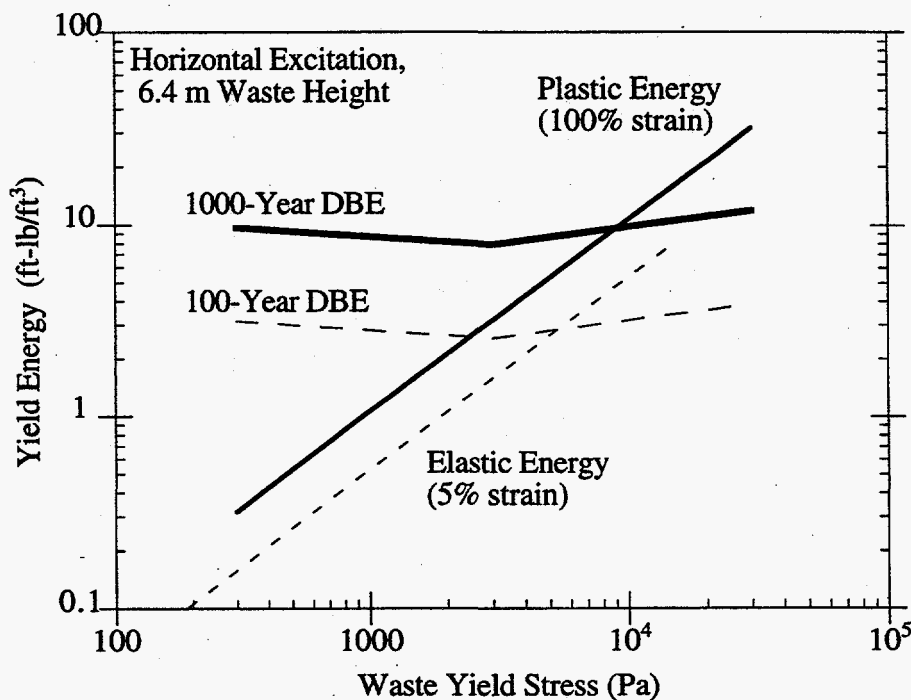


Figure 4.3.13. Yield Energy Limit, 640-cm Height - Horizontal

Thus if the analogy holds, a 100-year earthquake might cause a rapid release of ~50% of the stored gas in a typical DST. For a potentially stronger SST waste with yield stress of 1000–1500 Pa, a 1000-year earthquake is required to deposit the same relative energy for the assumed ~50% release. At the same time, for a yield stress above about 2500 Pa, yielding in a 100-year earthquake would be incomplete and gas release would be minimal. A 10,000-Pa material would survive a 1000-year event. This result is sketched in Figure 4.3.14.

We conclude that seismic events have the potential to create large, rapid gas releases in both DSTs and SSTs, although gas releases are expected to be larger in the former due to their somewhat weaker waste. Besides buoyant displacement in tanks with a deep supernatant liquid layer, earthquakes are the only other release mechanism with this potential. However, given the assumptions applied, the results of this analysis must be considered only tentative ‘ballpark’ possibilities, not as formal predictions.

4.4 Salt-Well Pumping

In this section, potential gas releases from salt-well pumping are discussed. Section 4.4.1 describes the salt-well pumping process and its effects on the waste along with some of the existing data from ongoing pumping campaigns (Caley et al. 1996). Sections 4.4.2 and 4.4.3, respectively, describe the results of a numerical modeling study and concurrent experimental studies (Peurrung et al. 1996). Section 4.4.4 describes a study of possible hydrogen retention that might occur in a ‘cavern’ postulated to occur due to waste subsidence following salt-well pumping. A summary of the conclusions is given in Section 4.4.5.

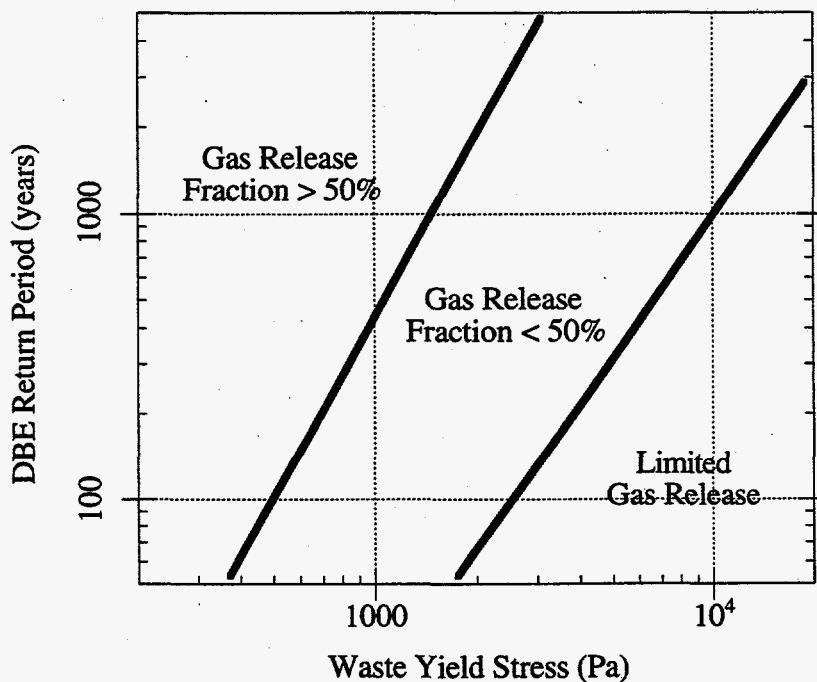


Figure 4.3.14. Possible Gas Release Fraction Versus Earthquake Severity

4.4.1 Salt-Well Pumping Process

In salt-well pumping, a portion of the interstitial liquid in the waste drains into, and is pumped out of, a screened well installed near the center of the tank. Pumping is complete when the liquid level reaches the zone in which capillary forces hold the liquid in place in spite of gravity. During pumping, the radial liquid profile in the waste has its lowest point at the well screen and its highest points at the tank walls. When the liquid level in the well falls too low to support pumping, the pump is shut off and the interstitial liquid is allowed to seek a uniform level across the tank by gravity and partially refill the well. Then the pump is started again, and the well is drained once again. In general, the well can be pumped dry much more rapidly than it can be refilled by liquid level equilibration, so salt-well pumping is an intermittent process.

When liquid drains out of the porous waste, the emptied pores are filled by air. Some of the gas already in the pores is exposed to the invading air and is thereby released to the head space. Other, unexposed gas beneath the interstitial liquid level expands under the decreased hydrostatic head and may migrate upward to be released at the surface. A substantial amount of the liquid continues to drain, releasing gas while the pump is off or running at low speed. More importantly, there is a delay between the exposure of retained gas and its transport to and through the head space, owing to the limited speed of diffusion. Thus gas releases are not necessarily concurrent with high pumping rates. This is clearly the case in the rather sparse salt-well pumping data description that follows and is also shown in the results of the analysis and experiments presented in Sections 4.4.2 and 4.4.3.

Flammable gas monitoring data are available only for the most recent salt-well pumping campaigns in Tanks BY-103, BY-106, BY-109, S-108, S-110, and T-104. The three BY tanks were monitored only for the last six weeks of salt-well pumping, meaning that any earlier gas releases were off the record.

Salt-well pumping apparently has different effects depending the waste type. Theoretically, the larger particle size in saltcake tanks should allow liquid to drain more readily into the salt-well screen than fine-grained sludges. Gas release during pumping depends on how rapidly liquid is removed. Therefore gas release from saltcake tanks should be more complete and more proportional to pumping rate than from sludge tanks. Caley et al. (1996) present some evidence that the gas volume actually increases in sludge tanks due to hydrostatic head reduction with relatively little release during pumping.

Tank S-108, which is predominately saltcake, and T-104, which is essentially 100% sludge, are selected to illustrate this effect. The measured flammable gas concentrations in the head space and the cumulative volume of liquid pumped for S-108 are plotted versus time from April through August 1996 in Figure 4.4.1. Figure 4.4.2 shows a close-up view of the flammable gas concentration and pumping rate from May through June. The same data are shown for T-104 in Figures 4.4.3 and 4.4.4, respectively. Salt-well pumping is currently ongoing in both these tanks.

One-dimensional simulations were first completed to investigate the salient features of the process and to compare with laboratory experiments. Later, a two-dimensional model was exercised to capture the effects of a nonuniform interstitial liquid level due to the radial inflow toward the well.

The one-dimensional simulations assumed that liquid was drained from a 20-ft depth of a porous medium similar to saltcake, using a constant, uniform flux from the entire bottom surface of the medium. These simulations illustrated that when drainage is sufficiently rapid, with a

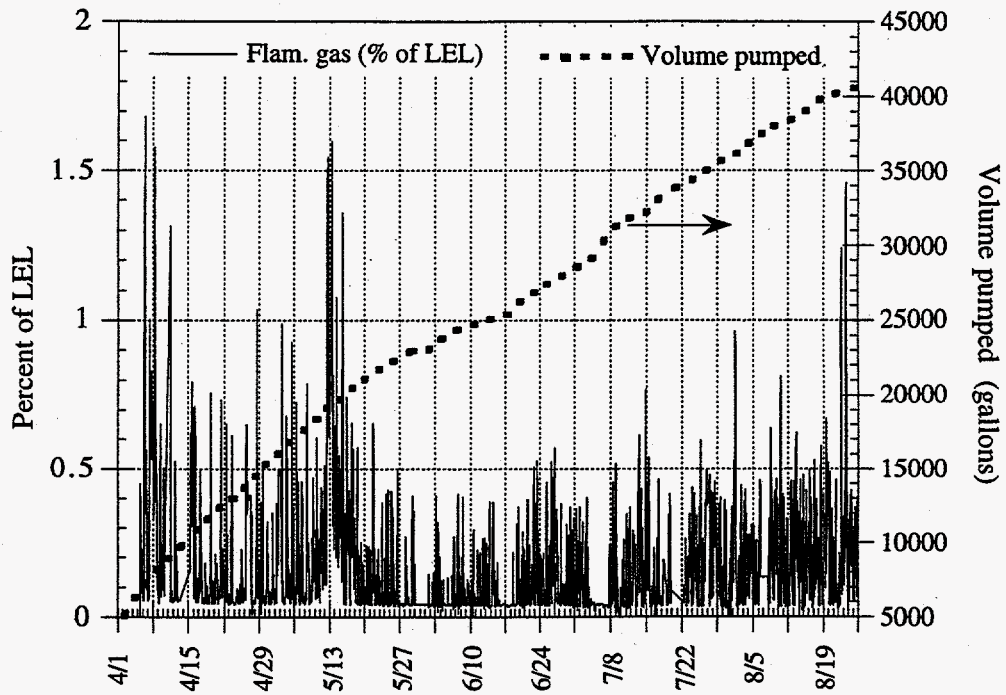


Figure 4.4.1. Salt-Well Pumping Data for Tank S-108: April–August 1996

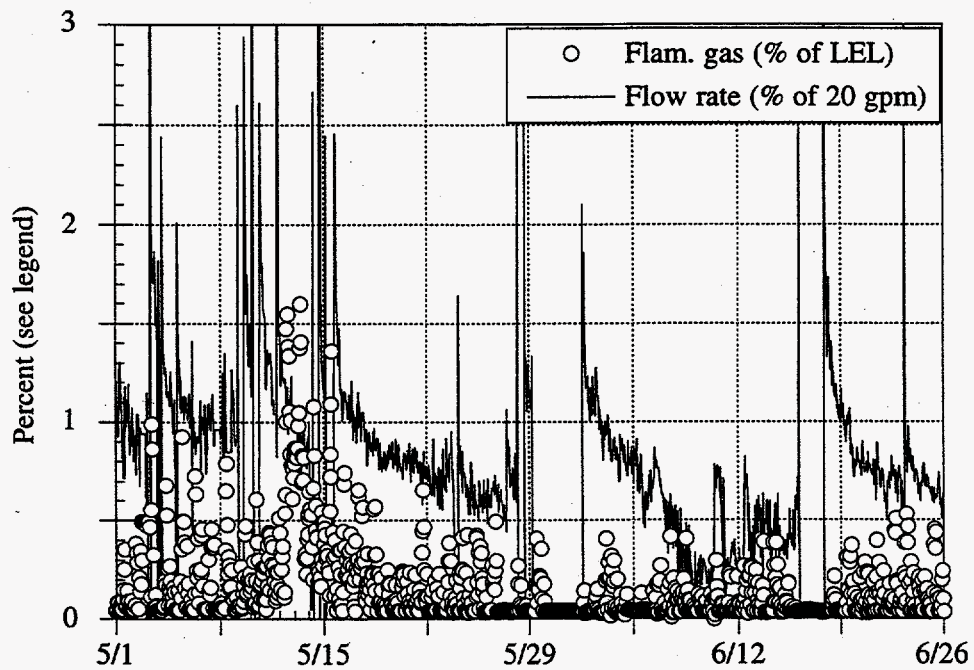


Figure 4.4.2. Salt-Well Pumping Data for Tank S-108: May–June 1996

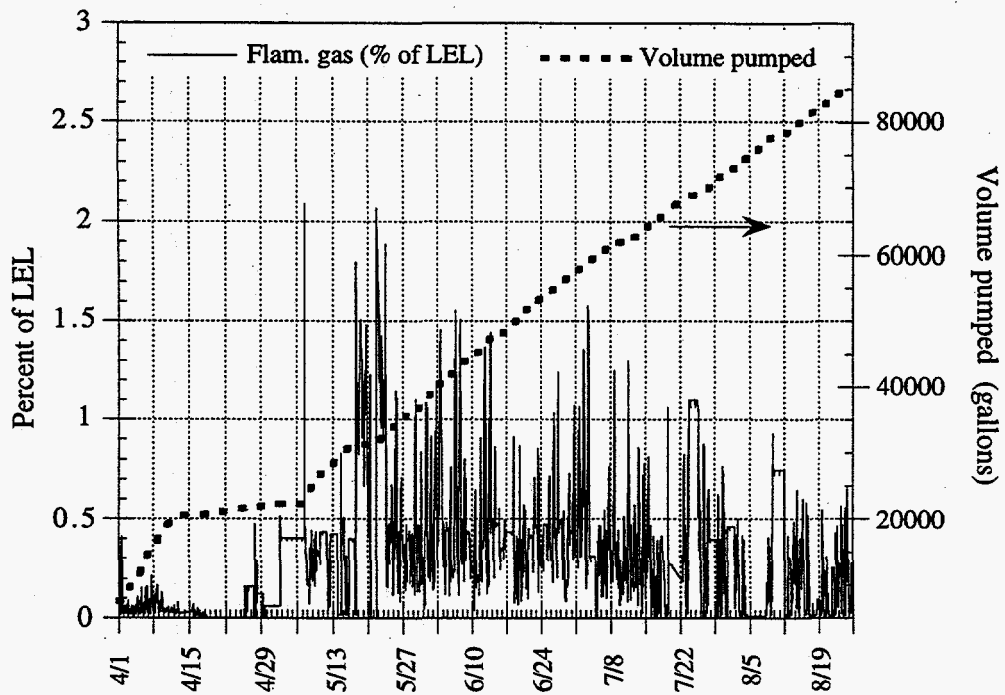


Figure 4.4.3. Salt-Well Pumping Data for Tank T-104: April–August 1996

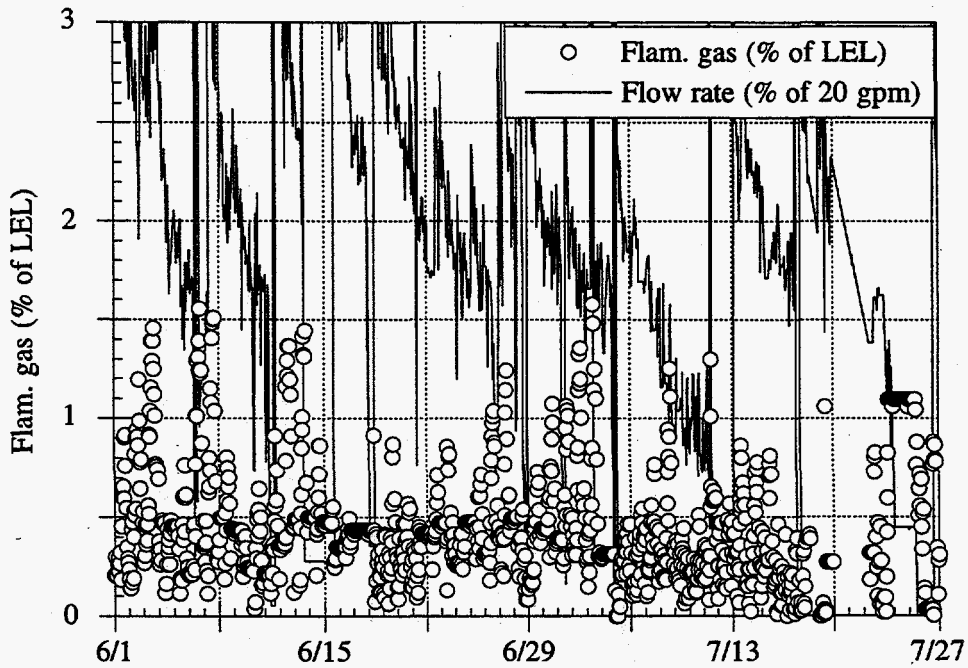


Figure 4.4.4. Salt-Well Pumping Data for Tank S-108: June–July 1996

drawdown time of 1 or 10 days, 90% or 40% (respectively) of the insoluble gas release is delayed until after pumping ends. This happens because the exposed gas cannot effectively counter-diffuse against the air flowing in to replace drained liquid. At a drawdown time of 100 days, gas release is dominated by diffusion; 90% of the insoluble gas release occurs during pumping and 10% after. In salt-well pumping of the waste tanks, the rapid-drawdown behavior might characterize the waste next to the salt-well screen, but most of the waste would follow the diffusion-controlled, slow-drawdown behavior.

The gas release rates were not substantially different whether expanding gas bubbles below the drained region connected to establish flow paths for gas escape or did not connect. This lack of effect depends heavily on the STOMP model's assumption of litho-dendritic bubble behavior, in which a percolating region releases only enough gas to maintain the material at its percolation threshold without releasing a larger fraction due to collapse of a hydro-dendritic bubble structure, as discussed in Section 4.2.

The STOMP model was also used for a two-dimensional simulation of a tank with the properties of A-101, as understood prior to the 1996 core sampling (see Sections 3 and 4.1.2 and the salt-well pumping safety assessment [WHC 1996b]), to represent a typical flammable gas SST. Both insoluble and soluble gases, representing hydrogen and ammonia, were included in the two-dimensional modeling. The waste was represented as 9.1 m (30 ft) deep with a centrally located salt well 0.3 m (1 ft) in diameter. A maximum instantaneous draining rate of 5 gpm was used, consistent with pumping limitations.

The simulation results indicated that only about half of the interstitial liquid would be drainable, owing to capillary forces, and that all of the drainable liquid would be removed in about 200 days. At the end of pumping, the pore space near the top of the saltcake would be about 65% filled with gas. Nearly all of the insoluble gas diffused out in the first 60 to 100 days of pumping, almost all escaping from the top of the waste, almost none through the well. The maximum insoluble gas release rate was predicted to be 4.2 m³/day (150 ft³/day) during the first ten days of pumping. The rate quickly fell below less than about 0.6 m³/day (20 ft³/day) after 25 days of pumping. The early maximum in gas release was not observed in the field data, except for the delay and slight decay shown in Figure 4.4.2 for T-104.

The soluble gas (ammonia) flux was much larger, 180 m³/day (6400 ft³/day) maximum, and continued at elevated levels (around 23 m³ or 800 ft³/day) long after the draining was essentially complete. The high release rates resulted from the extensive moist, unsaturated region produced by pumping, which provides an extremely high wetted surface area for mass transfer of a volatile solute from the liquid to the gas. This predicted ammonia release rate seems very high compared with the current operational experience; however, continuous ammonia monitoring has not yet been performed during pumping to allow direct comparisons.

It should be noted that the above results were based on a void fraction of 3% and a gas composed of 30% hydrogen and 15% ammonia, the latter in equilibrium with a liquid ammonia concentration of about 1 wt%. Preliminary RGS measurements in A-101, the same data cited in Section 3, indicated an in-situ void fraction of greater than 12% in the nonconvective layer, which was above the free liquid layer and contained 71.7% hydrogen and less than 1% ammonia. This more recent information implies that the hydrogen release during salt-well pumping could be 10 times that calculated under the current modeling assumptions, and the ammonia release could be 1/15 or less.

4.4.3 Experimental Results

Experiments to verify STOMP's one-dimensional model of salt-well pumping were performed in which liquid was drained from a packed column containing bubbles of insoluble gas (Peurrung et al. 1996). The effects of depressurization and fast and slow drainage were investigated. Thus the mechanisms of air invasion and bubble expansion, which played a part in the computational simulations, were both tested.

The experimental apparatus was a 2.5-cm diameter column packed to 75% of its height with 1-mm glass beads in water. Nitrogen spiked with 10,000 ppmv of SF₆ tracer was introduced by bubbling it through the bottom of the column. The volumetric gas content varied from 4–8% of the bead pack volume. Drainage experiments were carried out at a pressure of 2.4×10^5 Pa (20 psig); depressurization tests started at a pressure of 5.2×10^5 Pa (60 psig) and depressurized to 2.4×10^5 Pa (20 psig) at a constant rate over one hour. The initial (pressurized) gas saturation was set at about 70% of the maximum observed value, ensuring that on depressurization the bubbles would expand enough to connect with each other and form flow paths.

The experiments used either a 1.2-m-tall column packed with 0.91 m of beads or a 2.4-m-tall column with 1.8 m of beads. Doubling the packing height produced a roughly four-fold decrease in tracer release rate, in accordance with theory. Theory predicts that, once the draining stops, gas release is dominated by diffusion, which varies as the inverse of the diffusion distance squared. The dominance of diffusion following fast drainage was also confirmed with experiments that used air rather than helium as the invading gas. As predicted, a roughly five-fold increase in release rate was observed when helium was used.

Helium was used as the invading gas for the experiments whose results were compared with one-dimensional predictions made by the STOMP model. All of the model input parameters were independently measured or estimated; no adjustable parameters were used. The model predictions were in good accord with the data. Experiments were carried out, and the tests were modeled with STOMP for 5-minute "fast-drain," 5.5-hour "medium-drain," and 54-hour "slow-drain" cases.

The latter case approximately corresponds to conditions in waste tank salt-well pumping, as can be shown. A tank containing 9.1 m (30 ft) of wetted waste would hold about 370,000 gal. of liquid, of which about half, roughly 200,000 gal., might be drainable. The maximum diffusion distance in the drainable part of the tank would be 4.5 m (15 ft). From the standpoint of gas diffusion, which depends on the square of the diffusion distance, the time constant in such a tank would be 25 times that of the 0.9-m packed depth in the lab experiments. The drawdown times of 5 minutes, 5.5 hours, and 54 hours would therefore correspond to drawdown times of 2 hours, 6 days, and 56 days. The tank drainage rates would then be 1600 gpm, 24 gpm, and 2.5 gpm. Here the scaling was performed by keeping the same fraction of total liquid volume removed per unit of scaled time. The slow drainage rates are comparable to the more rapid rates used in tank salt-well pumping.

The match between the one-dimensional model predictions and the experimental data was good for all three drainage cases. In general, the model predicted slightly earlier gas release peaks than the experiments showed. However, the experimental and modeled rate constants for the diffusion-controlled part of the release were in good agreement. In the medium drainage cases the model somewhat overpredicted the fraction of gas released during pumping relative to that released after pumping.

There was also a good match between model and experiment in a depressurization test representing a factor-of-3 decrease in the hydrostatic head. The experimental release rates were rather noisy due to episodic releases of groups of bubbles. The model did not show this behavior because it treats retained gas as a uniform gas saturation, not as bubbles. Though some of the instantaneous experimental gas release rates were 50% higher than the modeled release rates, others were lower. The overall gas release fractions matched within a few percent, indicating that over the release period the high and low release rates balanced out. Gas releases would probably not show as high a percentage of variability in an actual waste tank, because no single bubble group would be as large a fraction of the entire gas content.

Comparisons with experiment showed that the STOMP simulation model succeeded both qualitatively and quantitatively at predicting one-dimensional insoluble gas release. Thus the model predictions of insoluble gas release in Section 4.4.1 are at least partially verified. The predictions of soluble gas behavior under salt-well pumping conditions have not yet been experimentally validated.

4.4.4 Gas Release from Caverns Formed After Salt-Well Pumping

It is possible that larger voids, or caverns, could form following salt-well pumping due to subsidence of the solid column when the partial support of buoyancy is removed with the liquid. Many tanks show deep depressions surrounding salt-well screens, and sudden large waste level drops are occasionally observed long after a salt-well pumping campaign ends (Caley et al. 1996). Such level drops could be considered evidence for the collapse of subsurface caverns. If the caverns contained high concentrations of flammable gas, a significant volume could be released in such a collapse. The calculation given below shows that diffusion of gas through the porous saltcake is quite sufficient to prevent flammable gas buildup in such a cavern.

Consider the accumulation of hydrogen in a hypothetical cavern in dry saltcake that might be created over a hydrogen-producing wet layer as a result of liquid removal during salt-well pumping. The presence of a gas-filled cavern is plausible only in moist saltcake, where there is insufficient liquid to seal gas between solid particles. If the cavern were surrounded or capped by wet saturated saltcake, the interstitial liquid would drain into the cavern much as a salt well fills with liquid. That is, if salt-well pumping were able to remove the liquid and create the cavern, the material would need to be sufficiently porous for liquid to drain out. Therefore, we consider the retention of hydrogen in a cavern in a horizontal layer of moist but unsaturated saltcake with a steady influx of hydrogen from the bottom of the layer.

The presence of a cavern actually reduces the maximum concentration of hydrogen, because transport is more effective due to the lack of tortuosity in the cavern and perhaps also because of convective mixing. We can therefore obtain a conservative estimate of the concentration in a cavern by estimating the maximum steady-state hydrogen concentration in the absence of any caverns. (By concentration, we mean the volume fraction of hydrogen in the pore space.)

Now consider the hydrogen concentration profile (Brewster 1995). A uniform steady-state hydrogen generation rate per unit volume, G , is assumed in the lower, wet, gas-producing layer, whose depth is H_p . The assumption of steady-state diffusion with no generation within the upper layer of dry saltcake yields a linear concentration profile. We assume that sufficient mixing and ventilation is present at the surface to produce a negligible ($<0.05\%$, 500 ppm) hydrogen concentration.

The slope of the concentration profile is proportional to the flux (volumetric flow rate per unit surface area) from the producing layer ($G H_p$) and the tortuosity of the saltcake (x), and is inversely proportional to the porosity of the saltcake (e) and the diffusivity of hydrogen (D). We then find that the concentration profile is given by

$$C(z) = G H_p \frac{x z}{e D} \quad (4.4.1)$$

where z is the depth below the waste surface. The maximum hydrogen concentration in the saltcake is thus

$$C^* = G H_p \frac{x H_{sc}}{e D} \quad (4.4.2)$$

where H_{sc} is the total depth of the saltcake.

For a given total waste depth (wet layer plus dry saltcake) H_w , the maximum concentration, C^* , is attained when the producing layer and saltcake are equal depths. We then have

$$C^* = G H_w^2 \frac{x}{4 e D} \quad (4.4.3)$$

The maximum volumetric generation rate, G , has been estimated at about 1.5×10^{-4} SCM of hydrogen per day per m^3 of waste. (This is 70% of the SY-101 generation rate per total waste volume.) The maximum waste depth of saltcake tanks is assumed to be 8 m. The tortuosity of saltcake is not known; a conservative estimate is $x = 3$. Saltcake porosity is reasonably estimated to be $e = 0.3$. However, there will probably be some liquid remaining in dead-end pores or pores with small necks, and also some liquid bridges that effectively block certain pores with respect to diffusion. A conservative estimate of the effective porosity might then be $e = 0.2$. The diffusivity (D) will be assumed equal to the diffusivity of hydrogen in air, $0.6 \text{ cm}^2/\text{s}$ (CRC 1990) or about $5 \text{ m}^2/\text{d}$. We then have that the maximum volume fraction of hydrogen in the dry saltcake, which is an upper limit on the concentration in a cavern, is $C^* = 0.007 = 0.7\%$, less than 25% of the LFL.

The estimates above are very conservative. The concentration C^* is proportional to the square of the waste depth. Thus a decrease in total waste depth will have a big impact on reducing C^* . A greater or lesser fraction of saltcake versus gas generating material will reduce C^* . The concentration in the cavern will only approach the maximum concentration from the saltcake diffusion profile if

1. The cavern is at the bottom of the unsaturated saltcake layer. If it is higher, the concentration in the cavern will be no greater than $C^* H_f/H_{sc}$, where H_f is the depth of the cavern floor from the waste surface.
2. The cavern provides a negligible contribution to enabling transport toward the surface. This is a valid assumption only if the cavern is small. However, the concentration will always be greater than $C^* H_c/H_{sc}$, where H_c is the thickness of the cavern ceiling. The latter concentration will be approached if the cavern is well-mixed and wide enough.

We conclude that hypothetical gas releases due to collapse of caverns in the waste formed during salt-well pumping are not a concern.

4.4.5 Conclusions

Salt-well pumping has been accomplished in many tanks and is planned for many of the flammable gas SSTs. The rather meager monitoring data and other diagnostic information available during pumping is not entirely consistent with the current state of understanding of the process by which gas is released when liquid is removed.

Computational simulations and laboratory-scale experiments of salt-well pumping predict relatively high insoluble (hydrogen) gas release rates in the initial stages and very high soluble (ammonia) gas releases throughout the pumping campaign. With passive ventilation at 5 cfm, these combined releases could create head space gas mixtures that approach or exceed the LFL. But hydrogen concentrations of, at most, a few percent of the LFL have been measured during the salt-well pumping of the six tanks for which hydrogen or flammable gas monitoring data are available, and, although no ammonia monitoring data exist, there have been no ex-tank ammonia releases reported.

However, head-space gas samples show much higher hydrogen concentrations for flammable gas tanks such as A-101 (which is on the FGWL) than for the tanks that have been monitored during pumping. As shown in the table in Appendix A, samples from waste configuration type 1 typically have hydrogen concentrations from 500–800 ppm, while BY-103 and BY-106 are in the 20–100-ppm range. Thus the difference between the predicted high hydrogen levels and the low observed concentrations could be a result of the differences in the tank contents.

Additional analyses and experiments are planned that will help clarify our understanding of the effect of salt-well pumping on the waste. Also, the first few flammable gas tanks to undergo pumping in the near future will provide much more detailed monitoring data and are better characterized to begin with than has been the case previously.

Finally, though subsidence of the waste surface is known to occur following salt-well pumping, it is not clear how often it may be a result of collapse of a subsurface 'cavern.' If even a large cavern were to exist, however, it could not contain concentrated flammable gases, because the rate of dilution with the head-space atmosphere by diffusion greatly exceeds the gas-generation rate. Therefore, the postulated collapse of such a cavern presents no flammable gas hazard.

4.5 Gas Release During Local Disruption

A number of in-tank activities involve inserting objects such as thermocouple trees, liquid observation wells, and salt-well screens, to list a few, into the waste. These waste-intrusive activities are expected to initiate the release of some small fraction of the retained gas. Although it is difficult to prove that large releases will never occur, theory and observation do not support their probability. The vertical and horizontal limitations on the extent of connected gas bubbles discussed in Section 4.2 necessarily limit the amount of gas disturbed and potentially released by a local intrusion. Also, the limited number of field observations available during local disruptions reveal only inconsequential gas releases. These observations are summarized in Section 4.5.1

A series of laboratory experiments was conducted with clay simulants that behave in ways similar to sludge-like waste to quantify the fraction of retained gas that might be released as a result of intrusion. The conclusion is that even worst-case disruptions should not result in dome-space flammable gas concentrations in excess of the LFL. The experiment and results are detailed in Section 4.5.2, and overall conclusions on gas release by disruption are given in Section 4.5.3. General disruptions caused by earthquakes and liquid removal in salt-well pumping were described in Sections 4.3 and 4.4, respectively.

4.5.1 Summary of Field Observations

A complete summary of GRE evidence from the tanks' operational history is given in the rotary core sampling safety assessment (WHC 1996a). During 49 core sampling events, only one possible gas release was observed, that being in Tank A-103 between March 24 and 31, 1986, where the waste level dropped 2.4 inches over one week, bracketing the time lower segment samples were removed. All of the sampling intrusions were in FGWL tanks; 17 of these were SSTs.

No changes were evident in the temperature profiles during these events, which might have indicated waste motion potentially accompanying a large gas release. Three of 17 tanks with operating head-space gas monitors during these intrusions showed slight increases in flammable gas concentrations. These small gas releases were estimated to be less than 2 m^3 (70 ft^3), and the head space concentrations never exceeded 9% of the LFL.

During 38 liquid observation well installations in SSTs, only one, in SX-104 on May 24, 1984, showed a 2.1-inch level drop, but this occurred 1–8 days *before* LOW installation. However, there was no flammable gas monitoring during these installations. Typically, ammonia can be smelled at 20 ppm and causes discomfort at higher concentrations. No strong ammonia odor was reported during these activities, which is significant, because even small head-space ammonia concentrations ought to produce detectable odor in these passively ventilated tanks. However, most of these LOWs were installed more than 10 years ago, and reports of such occurrences (if they occurred) might not have survived.

Though not strictly representative of SSTs, the experience gained in deploying the VFI and ball rheometer in DSTs is instructive (Stewart et al. 1996). Both of these instruments plus a water lance were operated in two risers of each of the six tanks tested. The water lance dissolves a hole in the surface crust to allow the ball rheometer to pass through but does not disturb the settled solids layer. The ball moves up and down many times, thoroughly disturbing a region about 10 cm (4 in.) in diameter throughout most of the waste column. The VFI makes two or three traverses in each riser, each one disrupting a region about $100 \times 10 \text{ cm}$ ($40 \times 4 \text{ in.}$) throughout the nonconvective layer. The overall VFI/ball rheometer campaign thus produced over 50 major penetrations of the waste, all in the highest-priority DSTs on the FGWL.

Although some minor bubbling was observed on the liquid surface of SY-103 (the only tank in which a free surface formed during testing), a measurable gas release occurred only in AW-101. Hydrogen monitoring showed a peak of almost 2000 ppm following water lancing under riser 13A. This represents a release from the crust layer of about 2 m^3 (70 ft^3) of hydrogen or about 7 m^3 (250 ft^3) total gas release assuming 30% hydrogen. There were no further releases during ball rheometer operation or lancing through the crust in riser 1C. Following operation of the VFI in 13A, the hydrogen concentration rose to about 1500 ppm, and, shortly after the third traverse began in riser 1C, a larger release raised it to almost 5000 ppm. This last release was about 16 m^3 (600 ft^3), assuming 30% hydrogen.

The mixer pump installation and initial operation in SY-101 can be cited as an even more significant disruption. Mixing eventually disturbed most of the waste in the tank (Allemann et al. 1994). A slight head-space hydrogen elevation was observed during the water lance operation, but there were no significant gas releases until high-speed 'bumping' (five-minute runs at 1000 rpm twice daily) began July 26, 1993, when release of about 4 m^3 (150 ft^3) occurred. Over the next four months, until the end of November 1993 when most of the waste was mobilized, there were eight major pump-induced gas releases ranging from 8 to 16 m^3 (300 to 600 ft^3). One very large release of about 62 m^3 (2200 ft^3) took place August 27, 1993, and was probably SY-101's last natural buoyant displacement rather than a pump-induced release.

This evaluation shows that local intrusions in a DST, including core sampling, LOW installation, VFI operation, and even thorough mixing of the entire nonconvective layer, do not typically cause large gas releases. The largest observed in DSTs were less than 20 m³ (700 ft³). However, the existing observations do little to quantify what releases might be expected in SSTs, except that they are small. Accordingly, laboratory experiments were performed in an attempt to better understand the gas release potential.

4.5.2 Experimental Results

To quantify the range of likely behavior, gas release tests were conducted with clay simulants spanning a broad range of strengths. It is expected that the waste physical properties will affect the intrusion-triggered releases of gas, but it is difficult to determine (or estimate) the physical properties of actual waste. More specifically, it is expected that intrusion will more easily release bubbles from weak materials, while having only a minor effect in stronger materials. In addition to varying the simulant strength, the intensity of the waste intrusion was also varied from a slow penetration to vigorous shaking.

Figure 4.5.1 is a schematic of the experimental apparatus consisting of test vessel and a cylindrical rod for making intrusions into the simulant. The vessel was 21.4 cm in diameter, and the intrusion rod, which was sufficiently long to reach the bottom of the test vessel, had a diameter of 2.2 cm. The ratio of the rod diameter to the test vessel diameter is relatively small (1:10), indicating that these experiments correspond to the waste behavior near the intrusion device (~2 ft-diameter region around a 2.25-in.-diameter push mode sampler). Initially, it was planned to perform the experiments with a smaller-diameter intrusion rod, but preliminary testing with bubbly simulants showed that a smaller-diameter rod gave nearly undetectable gas releases. Because one of the objectives of these experiments was to determine how the simulant strength affects gas release, the larger, 2.2-cm intrusion rod was selected to provide measurable gas releases.

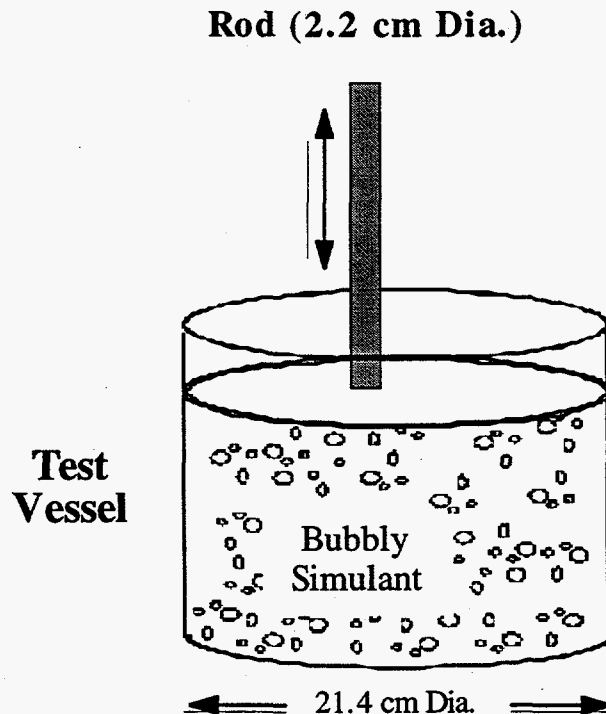


Figure 4.5.1. Schematic of Disruption Apparatus

For each experiment, the test vessel was filled with a bubbly clay simulant with a void fraction of about 0.2. In each experiment, the simulant was subjected to three disruptions of increasing intensity. A description of the disruptions is given below.

Slow Penetration: The intrusion rod was inserted from the top of the simulant to the bottom and then withdrawn. This slow intrusion, performed by hand, required about three seconds for the entire insertion and withdrawal. After removing the rod, the attached simulant was returned to the test vessel.

Energetic Penetration: The intrusion rod was inserted and withdrawn by hand ten times during about a seven-second period. After the final withdrawal, the attached simulant was returned to the test vessel.

Vigorous Shaking: For this disruption the test vessel rocked back and forth, allowing the vessel to hit the counter as it was rocked. The rocking was quick, with about two full back and forth motions completed per second; this shaking was continued for 15 seconds. For each experiment, essentially identical shaking was conducted.

The released gas was measured from changes in the surface level of the simulant. Before making each level measurement, the surface was smoothed with a spatula. While some gas bubbles were released by smoothing the surface, the smoothing released an undetectable amount of gas. Level measurements were made following each disruption in addition to the initial measurement. For each disruption, the measured levels were compared to the level prior to the first intrusion, and the fraction of the retained gas that was released was determined from these measurements. Accordingly, the reported gas released fraction is the cumulative gas release including the less energetic disruptions.

The simulants used in these experiments were mixtures of bentonite clay and water combined with a small amount of hydrogen peroxide (about 0.5 wt% of the solids layer). The hydrogen peroxide decomposed over a few hours to give oxygen bubbles. Table 4.5 gives the composition of the clay mixtures used in each experiment and the strength of each mixture in the absence of gas bubbles. The simulant strength ranged from 14 Pa, which poured easily, to 1040 Pa, which was stiff but easily spread with a spatula. For each experiment, a preliminary mixture of clay and water was prepared (accounting for the water to be added with the peroxide), then the peroxide was added and mixed quickly. The mixture was then immediately transferred to the test vessel, and the surface level was measured periodically to determine the fraction of trapped gas.

When the level increase indicated that the void fraction was 0.20, the first intrusion experiment (*Slow Penetration*) was started. In these measurements, the initial gas content of the clay mixture was not measured. Although the time between adding the peroxide and making the initial level measurement was short, typically a few minutes and always less than ten minutes, the initial void fraction was not negligible, and the void fraction was higher than 0.2. The initial gas content was due partly to the peroxide decomposition and also to the mixing process, which entrained gas bubbles. In the following section, the released gas volume is reported as the fraction of retained gas. Because the actual retained gas is higher than the assumed, the actual released gas fraction is lower than reported here.

Figure 4.5.2 shows the experimental results for the percentage of retained gas that was released during the three separate disturbance events. As expected, the results show that the amount of gas released decreased as the waste strength increased. For the *Slow Penetration* event, which was the primary measurement, a negligible amount of gas was released except for the weakest 14-Pa simulant. These results show that for a typical SST (assuming a waste strength greater than 100 Pa), a slow intrusion will release a negligible amount of gas.

Table 4.5. Clay Simulant Composition and Shear Strength for Each Disruption Experiment

Test	Bentonite Clay (wt%) ^(b)	Shear Strength Gas Free ^(a) (Pa)
1	11.3	14
2	12.5	31
3	13.8	67
4	15.0	147
5	16.3	323
6	17.5	656
7	18.8	1040

(a) The gas-free shear strengths of the different bentonite clay simulants were reported previously in a letter report by P.A. Gauglitz et al. entitled, *Gas Bubble Retention and Release from Simulated Single-Shell Tank Waste* (WSFG96.7) (April 1996); the values reported here are taken from the reported curve fit of a series of measurements.

(b) Weight fraction of bentonite clay as taken from the bag or the "as is wt%" reported by Gauglitz et al. (WSFG96.7; 1996).

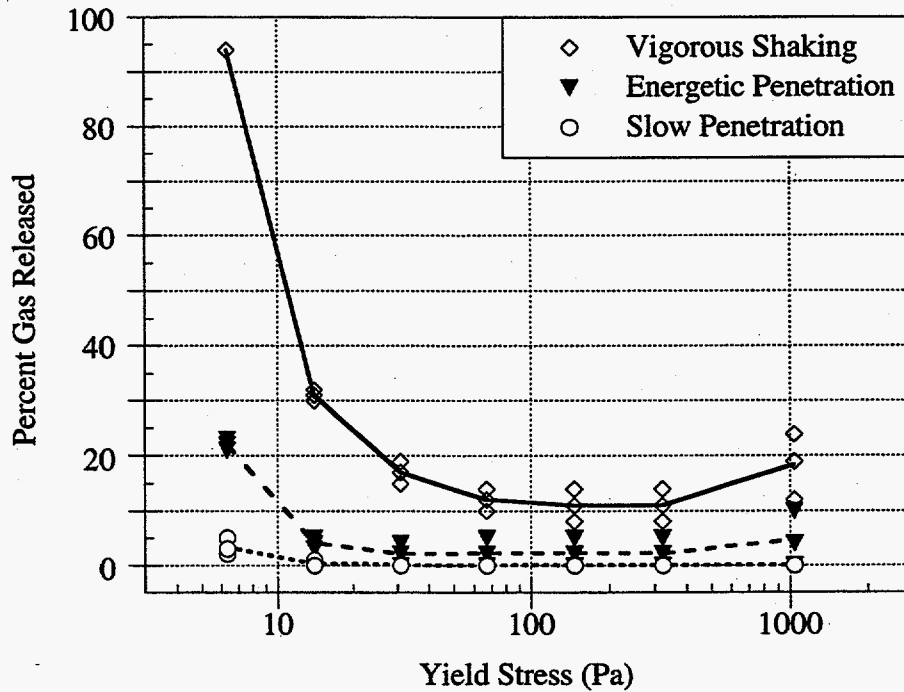


Figure 4.5.2. Percent of Gas Released as a Result of Disruption

The results in Figure 4.5.2 also show that increasing the energy of the disturbance increases the fraction of gas released, as one would expect. For example, the *Energetic Penetration* always released more gas than the *Slow Penetration* (within the experimental uncertainty of the measurements).

The gas released by *Vigorous Shaking* was always greater than the two less energetic disruptions, further confirming that the gas release depends on the intensity of the disruption. These shaking experiments were also conducted to mimic some aspects of how waste would respond to an earthquake. These results show that the gas release fraction decreases with increasing simulant strength. In addition, while we did not do quantitative experiments ranging from slow to energetic shaking, it was apparent that more intense shaking resulted in larger gas releases. These observations are entirely consistent with the analytical results presented in Section 4.3.

4.5.3 Analysis and Conclusions on Disruption

When gas release by penetration was proposed, there was a misconception that such an event created a local, 1 atm pressure sink deep in the waste that would 'suck in' surrounding gas and produce a large release. Actually, a local penetration cannot create a pressure sink unless the hardware is specifically designed to do so. The ambient hydrostatic head is transmitted through liquid waste flowing around the disturbance, or maintained by design in the case of hydrostatic fluid introduced in core sampling or the water jets on the end of a lance. If the waste liquid content is not sufficient to transmit hydrostatic pressure, it will not release gas, even to a 1 atm pressure sink. Also, the lateral extent of potentially connected gas regions is quite limited, so even a deliberate suction would be unable to access a large gas volume. Thus there is no clear mechanism for a local intrusion to release more gas than is contained in the waste actually disturbed. This is supported by field observation, analysis, and laboratory experiments.

Evaluation of past operational experience in SSTs and DSTs shows that local intrusions, even major ones, do not typically cause large gas releases. The largest observed in DSTs were less than 20 m³ (700 ft³), which could create a mixture at just 25% of the LFL in a nearly full tank if the gas released were 50% hydrogen. Existing observations do little to quantify what releases might be expected in SSTs, except that they are small.

Laboratory experiment results show that for typical SST conditions (waste strength greater than 100 Pa), a slow penetration will release a negligible amount of gas. Repeated, energetic penetration released less than 5% of the stored gas in this material. Even vigorous shaking, which might simulate a serious seismic event, produced gas releases under 20% for yield stresses over 100 Pa.

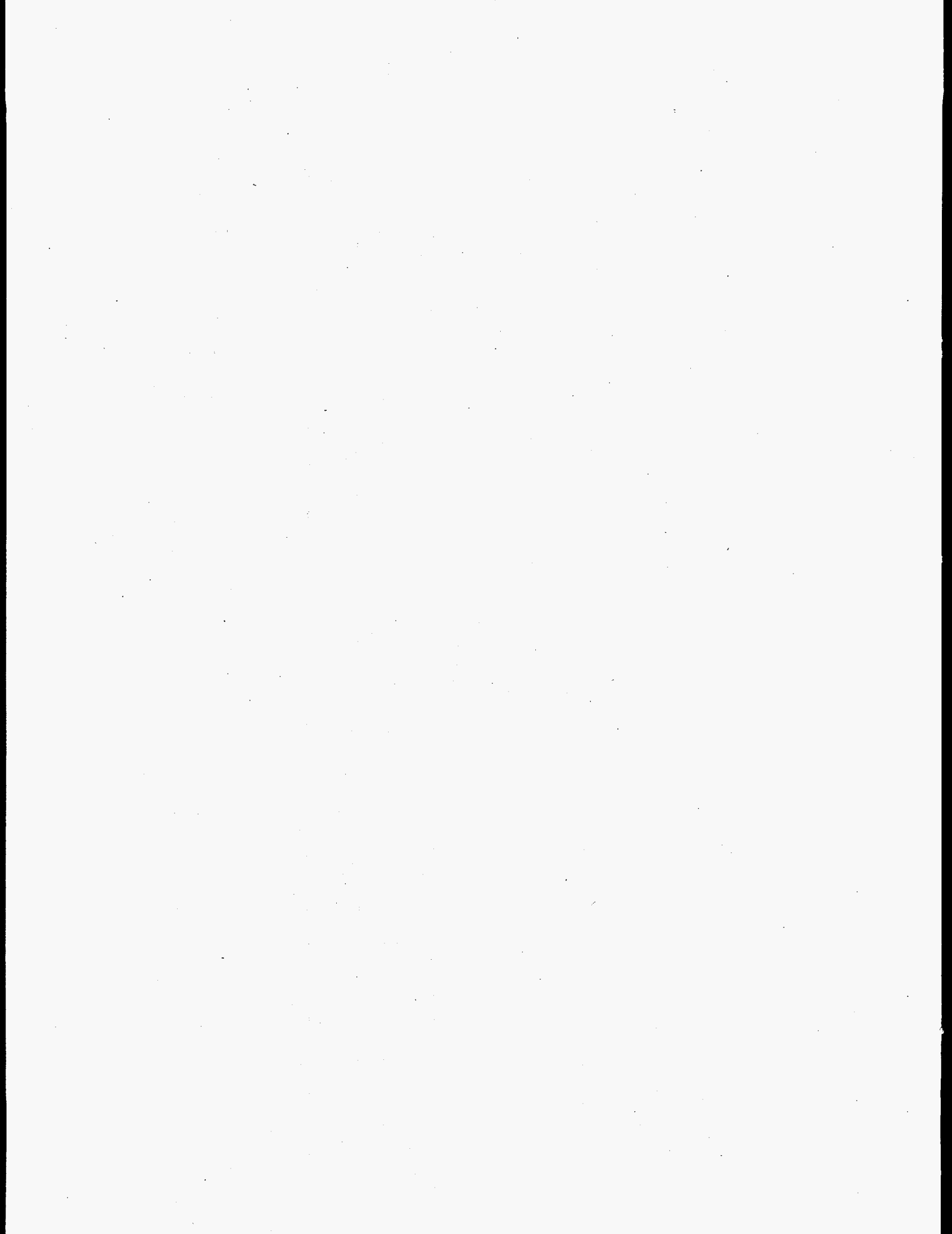
The hydro-dendritic bubble percolation mechanism might provide a bounding case for gas release from a local disruption event. The volume of a percolation cascade is probably greater than the volume of waste disturbed by any plausible local disruption. By the model proposed in Section 4.2, a large cascade might release on the order of 10% of the gas in a cylinder at most a few meters in diameter. At a 20% void fraction, this amounts to, at most, two or three cubic meters of gas.

This section is primarily concerned with mechanical disruption as by inserting a cylindrical object through the waste column. More general disruptions by earthquake and salt- well pumping are discussed in Sections 4.3 and 4.4, respectively. One other type of disruption is local dissolution due to water addition. This can occur by lancing, which differs little from a purely mechanical penetration, by water splashing on the waste surface during decontamination, or from other operations such as water jet cutting in the head space or sluicing in the waste.

At this time, we believe that gas release due to water addition can be treated the same way we recommend for mechanical penetration. Gas should only be released from the volume of waste actually disturbed hydraulically by a jet or chemically by dissolution. However, the dissolution process is very complex, and its relation to gas retention even more so. Therefore, the volume of waste subject to gas release due to dissolution may be difficult to calculate.

Waste disruption also is potentially accompanied by evaporation of dissolved ammonia if it brings free liquid to the surface. Ammonia was not a noticeable factor in any of the field observations mentioned in Section 4.5.1 above, and there is no reason to expect that local mechanical disruptions would create a large free liquid surface. There is some question about the affects of water addition, depending on the method. In any case, the maximum ammonia concentration in a tank's head space is achieved at equilibrium with the liquid. See Palmer et al. (1996) for a thorough discussion of ammonia release mechanisms.

In conclusion, evidence, analysis, and experiment all indicate that the most probable gas releases from SSTs due to intrusion, by whatever method, are proportional to the waste volume actually disrupted by the intrusion. This volume will be somewhat greater than the dimensions of the hardware creating the intrusion and may be difficult to calculate. We know no plausible mechanism for a local intrusion to release large fractions of the total stored gas volume.



5.0 Conclusions and Recommendations

The main objective of this report is to provide a sound technical foundation for estimates of undissolved gas release rates and volumes in SSTs considering all plausible mechanisms. Though actual models to predict release behavior are as yet incomplete and not fully validated, we believe all potential pathways for large gas releases have been defined. The current understanding of gas release in SSTs is described in Section 5.1, and recommendations to fill in the remaining gaps are given in Section 5.2.

5.1 Conclusions

The only mechanism demonstrably capable of producing large ($\sim 100 \text{ m}^3$), spontaneous gas releases is the buoyant displacement, which occurs only in tanks with a relatively deep layer of supernatant liquid. Only the DSTs currently satisfy this condition. All release mechanisms believed plausible in SSTs have been investigated, and none have the potential for large, spontaneous gas releases. Only small spontaneous gas releases of several cubic meters are likely by these mechanisms.

Beyond these small spontaneous releases, only severe earthquakes may have a potential to induce a large release in SSTs. However, sufficiently severe seismic events are rare; only those with estimated return frequencies of 1000 years are expected to release a large fraction of stored gas in SSTs, while a 100-year event might do so in DSTs. Ongoing studies will better quantify the potential for earthquake-induced gas releases.

Free gas can accumulate only in submerged solids (i.e., beneath the free liquid level); gas is not retained in unsubmerged solids because it escapes by diffusion. Note that a floating crust layer is mostly submerged. The configuration, limiting size, and maximum volume fraction of gas bubbles can now be predicted as a function of surface tension, particle size, yield stress, and waste depth (Gauglitz et al. 1996).

While most submerged waste is capable of holding gas fractions on the order of 30%, the size of individual bubbles (both round and dendritic) is quite limited. Pore-filling, litho-dendritic bubbles can exist only at depths greater than a few meters, and the balance of hydrostatic and capillary pressure limits their vertical extent to about 1 m. Particle displacing, hydrostatic or hydro-dendritic bubbles are limited to about 20 cm in height by the balance of hydrostatic pressure and waste yield stress. We estimate the horizontal extent of these bubbles to be no more than about three times their height. Very large ($\sim 1 \text{ m}$ in diameter) individual bubbles are not believed possible.

Because bubble size is so limited, local waste disruptions cannot suddenly trigger releases of large volumes of gas. Gas is released only from the volume of waste actually disturbed. A thorough study of 49 core sampling events and 38 liquid observation well insertions in SSTs (WHC 1996a), and over 50 waste penetrations involved with VFI and ball rheometer operation in DSTs (Stewart et al. 1996) revealed no bona-fide gas release in SSTs and only one instance of small release in a DST.

An example of a more general disruption is salt-well pumping, in which liquid removal is expected to release a relatively large volume of gas, but only slowly, as a series of small releases over many months. No large gas releases have been observed in the limited gas monitoring data available from recent pumping campaigns (Caley et al. 1996), although preliminary analysis

indicates relatively large ammonia releases are possible (Peurrung et al. 1996). In tanks with waste sufficiently permeable to allow most of the liquid to be removed by salt well pumping, the combination of decreasing the volume of wet solids available to store gas, reduction in hydrostatic head on the gas remaining, and the increase in tank head space is believed to effectively eliminate the flammable gas hazard.

Other proposed gas release mechanisms have been shown to be extremely unlikely or not hazardous. These are: penetration of a few very large bubbles; venting through a fracture, uncovering of a gas reservoir by dryout; collapse of a postulated 'cavern' created by subsidence following salt-well pumping; and a 'weak sludge' cascade release that has been observed in the laboratory under very specific conditions.

5.2 Recommendations

Ability to predict tank behavior is a possible criterion to decide when our understanding of gas release mechanisms is sufficient. By this measure, our understanding of the mechanisms capable of large rapid releases, which include buoyant displacement and earthquakes, is relatively advanced. However further study is required in the areas of salt-well pumping and small releases by dendritic bubble percolation. Additional experiments are desirable to complete the gas retention model.

The current understanding of gas retention mechanisms is based on laboratory experiments with simulants and real waste samples (Gauglitz et al. 1996) in relatively small apparatus that could not apply hydrostatic or lithostatic pressures typical of tank conditions. Gas generation rates were greatly accelerated compared with what could be expected in actual tanks. A large-scale, long-term experiment with a suitable simulant should be performed to remove these objections. Also, additional waste types need to be investigated, specifically coarse saltcake, to cover expected tank conditions.

The gas release processes during salt-well pumping need to be better understood. The limited field data from recent pumping campaigns are consistent neither with the theory nor from tank to tank. In the next planned salt-well pumping campaigns, a consistent, continuous set of data should be recorded; the data would include continuous gas monitoring of both insoluble (hydrogen) and soluble (ammonia) gases, continuous recording of the volume of liquid removed and the waste surface level (by FIC or Enraf), periodic recording of the ILL from neutron logs, and continuous in-tank video monitoring for subsidence. In situ measurements with the RGS before and after are needed to precisely measure the amount of gas release and the changes in gas distribution.

The relatively frequent small gas releases from SSTs now being observed in the head space gas monitoring data need to be analyzed and interpreted in the context of the currently understood gas retention and release mechanisms. This will allow the frequency, expected volume, and release rate to be estimated.

Finally, the understanding embodied in this report and improved models under development need to be incorporated into the flammable gas evaluation methodology. For example, except for earthquakes, gas release fractions are far less than the 25% assumed in the current methodology (Hodgson et al. 1996). Another area for improvement is the vertical distribution of stored gas and its effective pressure.

6.0 References

Agnew SF. 1995. *Hanford Defined Wastes: Chemical and Radionuclide Compositions*. LA-UR-94-2657 Rev. 2, Los Alamos National Laboratory, Los Alamos, New Mexico.

Agnew SF, P Baca, R Corbin, K Jurgensen, and B Young. 1995. *Tank Layer Model (TLM)*. LA-UR-94-4269 Rev 1, Los Alamos National Laboratory, Los Alamos, New Mexico.

Allemann RT, ZI Antoniak, JR Friley, CE Haines, LM Liljegren, and S Somasundaram. 1991. *Collection and Analysis of Existing Data for Waste Tank Mechanistic Analysis. Progress Report -- December 1990*. PNL-7658, Pacific Northwest Laboratory, Richland, Washington.

Allemann RT, ZI Antoniak, WD Chavala, LE Efferding, JG Fadeff, JR Friley, WB Gregory, JD Hudson, JJ Irwin, NW Kirch, TE Michener, FE Panisko, CW Stewart, and BM Wise. 1994. *Mitigation of Tank 241-SY-101 by Pump Mixing: Results of Testing Phases A and B*. PNL-9423, Pacific Northwest Laboratory, Richland, Washington.

Allemann RT, TM Burke, DA Reynolds and DE Simpson. 1993. *Assessment of Gas Accumulation and Retention - Tank 241-SY-101*. WHC-EP-0576, Westinghouse Hanford Company, Richland, Washington.

Anderson JD. 1990. *A History of the 200 Area Tank Farms*. WHC-MR0-0132, Westinghouse Hanford Company, Richland, Washington.

Avallone EA, ed. *Marks Standard Handbook for Mechanical Engineers*. McGraw-Hill, New York.

Babad H, GD Johnson, DA Reynolds, and DM Strachan. 1992. *Understanding of Cyclic Venting Phenomena in Hanford Site High-Level Waste Tanks: The Evaluation of Tank 241-SY-101*. WHC-SA-1364-FP, Westinghouse Hanford Company, Richland, Washington.

Beris, AN, JA Tsamopoulos, RC Armstrong, and RA Brown. 1985. "Creeping Motion of a Sphere through a Bingham Plastic." *J. Fluid Mechanics* 158, pp. 219-244.

Brevick CH. 1995. *Historical Tank Content Estimate (also called The Kaiser Reports)*. WHC-SD-WM-ER-351, Westinghouse Hanford Company, Richland, Washington.

Brevick CH, RL Newell, and JW Funk. 1996. *Historical Tank Content Estimate for the Northeast Quadrant of the Hanford 200 East Area*. WHC-SD-WM-ER-349 Rev. 1a, ICF Kaiser Hanford Company, Richland, Washington.

Brewster ME. June 1995. *Modeling Large Gas Release Events from 'Dry' Waste Tanks*. LA-UR-95-4038, presented at the 11th Annual Workshop on Mathematical Problems in Industry, University of New Mexico, Los Alamos, June 12-16, 1995.

Brewster ME, NB Gallagher, JD Hudson, and CW Stewart. 1995. *The Behavior, Quantity, and Location of Undissolved Gas in Tank 241-SY-101*. PNL-10861, Pacific Northwest Laboratory, Richland, Washington.

- Brewster ME, P Dellar, V Entov, B vd Fliert, A Fowler, B Grover, EJ Hinch, J Lister, F Ng, and T Shulze. 1996. "Gas Release from Sludge." *Proceedings of the 29th European Study Group with Industry*. Mathematical Institute, Oxford University, England.
- Brown TM, SJ Eberlein, and TJ Kunthara. 1995. *Tank Waste Characterization Basis*. WHC-SD-WM-TA-164 Rev. 1, Westinghouse Hanford Company, Richland, Washington.
- Caley SM, LA Mahoney, and PA Gauglitz. 1996. *Summary of Tank Information Relating Salt Well Pumping to Flammable Gas Safety Issues*. PNNL-11335, Pacific Northwest National Laboratory, Richland, Washington.
- Cannon NS and RC Knight. 1995. *Retained Gas Sampler System Acceptance Test Report*. WHC-SD-WM-ATR-137, Rev. 0, Westinghouse Hanford Company, Richland, Washington.
- Chhabra RP and PHT Uhlherr. 1986. "Static Equilibrium and Motion of Spheres in Viscoplastic Liquids." *Encyclopedia of Fluid Mech.* Vol. 21, NP Cheremisinoff (ed.), pp. 611-633.
- Chemical Rubber Company. 1990-1991. *CRC Handbook of Chemistry and Physics*, 71st edition, DR Lide, ed. CRC Press, Boca Raton, Florida.
- De Lorenzo DS, AT DiCenso, DB Hiller, KW Johnson, JH Rutherford, DJ Smith, and BC Simpson. 1994. *Tank Characterization Reference Guide*. WHC-SD-WM-TI-648 Rev. 0. Westinghouse Hanford Company, Richland, Washington.
- Dullien FAL. 1992. *Porous Media: Fluid Transport and Pore Structure*, 2nd Ed. Academic Press, San Diego.
- Gauglitz PA, LA Mahoney, DP Mendoza, and MC Miller. 1994. *Mechanisms of Bubble Retention*. PNL-10120, Pacific Northwest Laboratory, Richland, Washington.
- Gauglitz PA, SD Rassat, MR Powell, RR Shah, and LA Mahoney. 1995. *Gas Bubble Retention and Its Effects on Waste Properties: Retention Mechanisms, Viscosity, and Tensile and Shear Strengths*. PNL-10740, Pacific Northwest Laboratory, Richland, Washington.
- Gauglitz PA, SD Rassat, PR Bredt, JH Konynenbelt, SM Tingey, and DP Mendoza. 1996. *Mechanisms of Gas Bubble Retention and Release: Results for Hanford Waste Tanks 241-S-102 and 241-SY-103 and Single-Shell Tank Simulants*. PNNL-11298, Pacific Northwest National Laboratory, Richland, Washington.
- Herting DL, DB Bechtold, BE Hey, BD Keele, L Jensen, and TL Welsh. 1992. *Laboratory Characterization of Samples Taken in December 1991 (Window E) from Hanford Waste Tank 241-SY-101*. WHC-SD-WM-DTR-026, Westinghouse Hanford Company, Richland, Washington.
- Hodgson KM, RP Anantamula, SA Barker, KD Fowler, JD Hopkins, JA Lechelt, DA Reynolds, DC Hedengren, RE Stout, and RT Winward. 1996. *Evaluation of Hanford Tanks for Trapped Gas*. WHC-SD-WM-ER-526 Rev. 1, Westinghouse Hanford Company, Richland, Washington.
- Hopkins JD. 1995. *Methodology for Flammable Gas Evaluations*. WHC-SD-WM-TI-724 Rev. 0, Westinghouse Hanford Company, Richland, Washington.
- Johnson GD. 1996. *Evaluation of Recommendation for Addition of Tanks to the Flammable Gas Watch List*. WHC-SD-WM-ER-594 Rev 0, Westinghouse Hanford Company, Richland, Washington.

Li X and YC Yortsos. 1995. "Theory of Multiple Bubble Growth in Porous Media by Solute Diffusion." *Chem. Eng. Sci.*, 50(8):1247-1271.

McCabe WL and JC Smith. 1976. *Unit Operations of Chemical Engineering, 3rd Edition*. McGraw-Hill, New York.

Newmark NM and WJ Hall. *Development of Criteria for Seismic Review of Selected Nuclear Power Plants*. NUREG/CR-0098, U.S. Nuclear Regulatory Commission, Washington, D.C.

Palmer BJ, CM Anderson, G Chen, JM Cuta, TA Ferryman, and G Terrones. 1996. *Evaluation of the Potential for Significant Ammonia Releases from Hanford Waste Tanks*. PNNL-11237, Pacific Northwest National Laboratory, Richland, Washington.

Peurrung LM, SM Caley, EY Bian, and PA Gauglitz. 1996. *Gas Release During Salt-Well Pumping: Model Predictions and Comparisons to Laboratory Experiments*. PNNL-11310, Pacific Northwest National Laboratory, Richland, Washington.

Rassat SD and PA Gauglitz. 1995. *Bubble Retention in Synthetic Sludge: Testing of Alternative Gas Retention Apparatus*. PNL-10661, Pacific Northwest Laboratory, Richland, Washington.

Remund KM, CM Anderson, and BC Simpson. 1995. *Hanford Single-Shell Tank Grouping Study*. PNL-10749, Pacific Northwest National Laboratory, Richland, Washington.

SAP7. 1980. *Structural Analysis Program User's Manual*. SAP Users Group, University of Southern California Department of Civil Engineering, Los Angeles.

Schubert H, W Herrmann and H Rumpf. 1975. "Deformation Behaviour of Agglomerates under Tensile Stress." *Powder Tech.* 11: 121-131.

Shepard CL, CW Stewart, JM Alzheimer, G Terrones, G Chen, and NE Wilkins. 1995. *In Situ Determination of Rheological Properties and Void Fraction: Hanford Waste Tank 241-SY-103*. PNL-10865, Pacific Northwest Laboratory, Richland, Washington.

Stewart CW, CL Shepard, JM Alzheimer, and G Terrones. 1995 *In Situ Determination of Rheological Properties and Void Fraction in Hanford Waste Tank 241-SY-101*. PNL-10682, Pacific Northwest Laboratory, Richland, Washington.

Stewart CW, JM Alzheimer, ME Brewster, G Chen, RE Mendoza, HC Reid, CL Shepard, and G Terrones. 1996. *In Situ Rheology and Gas Volume in Hanford Double-Shell Waste Tanks*. PNNL-11296, Pacific Northwest National Laboratory, Richland, Washington.

WHC. 1995a. *TWRS SST Stabilization, Current Progress vs TPA*. WHC-EP-0182091, Westinghouse Hanford Company, Richland, Washington.

WHC. 1995b. *Tank Farms Operating Specification Document*. OSD-T-151-00030 B-12, Westinghouse Hanford Company, Richland, Washington.

WHC. 1996a. *A Safety Assessment of Push-Mode and Rotary-Mode Core Sampling in Flammable Gas Single Shell Tanks: Hanford Site, Richland, Washington*. WHC-SD-WM-SAD-035 Rev. 1, Appendix L, Westinghouse Hanford Company, Richland, Washington.

WHC. 1996b. *A Safety Assessment for Saltwell Jet Pumping Operations in Tank 241-A-101: Hanford Site, Richland, Washington*. WHC-SD-WM-SAD-036 Rev. 1, Westinghouse Hanford Company, Richland, Washington.

Wheeler MJ. *Tutorial on Random Vibration Analysis Using the ANSYS Program*. 1987. Swanson Analysis System Report DNT011, Pittsburgh, Pennsylvania.

Whitney PD. 1995. *Screening the Hanford Tanks for Trapped Gas*. PNL-10821, Pacific Northwest National Laboratory, Richland, Washington.

Whitney PD, PA Meyer, NE Wilkins, F Gao, and AG Wood. 1996. *Flammable Gas Data Evaluation Progress Report*. PNNL-11373, Pacific Northwest National Laboratory, Richland, Washington.

Wilkins NE, RE Bauer, and DM Ogden. 1996. *Results of Vapor Space Monitoring of Flammable Gas Watch List Tanks*. WHC-SD-WM-TI-797, Westinghouse Hanford Company, Richland, Washington.

Appendix A
SST Prioritization Data

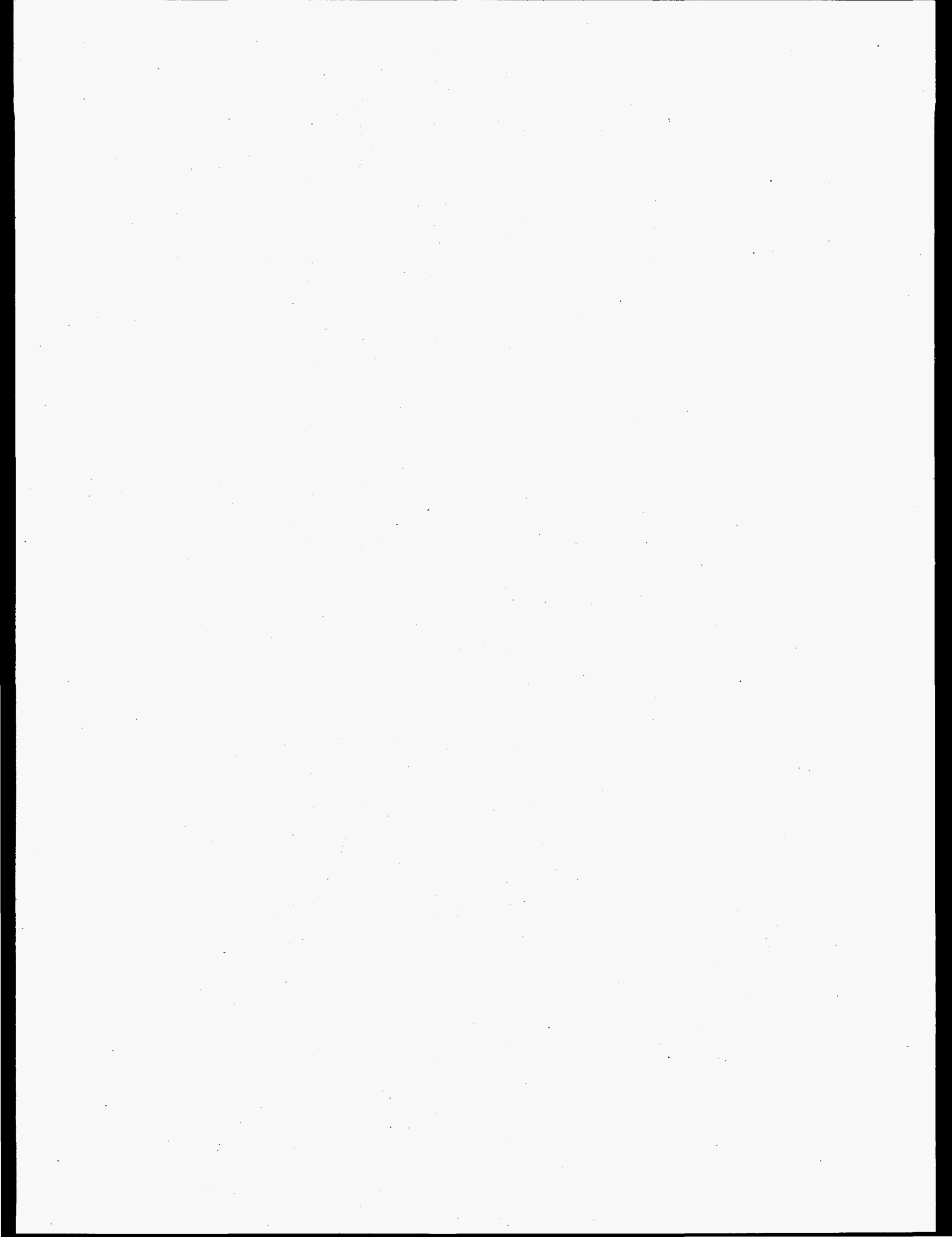


Table A.1. SST Prioritization Data

Tank	Cluster	WC	Watch List	Whitney	dL/dP	LR	Surf	Liq	H2	NH3	SL
S-102	13	1A	FG/ORG	FIC	-0.51	20	5.2	5.2	670	418	*
S-103	13	1A	fg	FIC	-0.34	12	2.7	2.6			*
SX-106	13	1A	FG/ORG	FIC/N	-0.23	64	5.1	5.1	<98	188	*
U-103	13	1A	FG/ORG	FIC/N	-0.27	10	4.2	4.5	557	761	*
U-105	13	1A	FG/ORG	FIC/MT	-0.23	13	3.8	4.1	<49	354	*
U-107	13	1A	FG/ORG	FIC/N	-0.18	18	3.7	3.7	505	474	*
U-108	13	1A	FG/org	FIC		6	4.2	4.5			*
U-109	13	1A	FG/org	FIC	-0.20	4	4.2	4.5			*
U-111	13	1A	ORG			15	3.0	3.3	250	682	*
A-101	22	1B	FG/ORG	FIC/MT	-0.15	-5	8.8	9.2	786	800	*
A-102	22	1B	org				0.4				
A-103	22	1B	fg	FIC	-0.19	0	3.4	3.5			
AX-101	22	1B	FG			-8	6.8	7.1	103	44	*
S-105	20	2A		FIC/N	-0.30	15	4.0	1.3	21	36	
S-106	20	2A	fg	FIC/E/N	-0.94	50	4.5	4.5			*
S-108	20	2A				-22	4.4	3.4			
S-109	20	2A		N		0	4.4	3.5			
S-111	20	2A	FG/ORG	FIC/E	-0.40	4	5.2	5.1	392	124	*
S-112	20	2A	FG			-12	5.0	3.0			*
SX-102	20	2A	FG	FIC	-0.35	-20	5.0	5.0			*
SX-103	20	2A	FG/ORG	FIC/MT	-0.57	-25	6.1	6.0	<23	80	*
SX-105	20	2A	FG	FIC		-35	6.2	6.2			*
U-106	20	2A	fg/ORG	FIC/N	-0.06	2	2.0	2.3	214	1013	
BX-111	15	2B					1.7	1.0			
BY-101	15	2B		N			3.7	1.9			
BY-102	15	2B	fg/org	MT			1.9	2.3			
BY-103	15	2B	fg/FC/org	MT		-5	3.8	3.6	22	30	
BY-106	15	2B	fg/FC/org			20	6.2	5.7	104	78	
BY-109	15	2B	fg	FIC	0.001		3.3	3.0			*
BY-111	15	2B	FC				4.2	2.1	<160	61	
BY-112	15	2B	FC				2.9	1.1	<94	71	
BY-104	21	3A	FC/org				3.3	2.2	312	255	*
BY-105	21	3A	fg/FC/org	N		-64	4.2	4.2	87	44	
BY-107	21	3A	FC/org				2.6	1.6	698	978	*
BY-110	21	3A	FC/org				2.5	1.9	<160	426	*
S-101	11	3B	fg	FIC	-0.15	-5	4.1	4.1			
S-110	11	3B					3.8	3.7			
SX-104	11	3B	FG	FIC	0.001	-25	5.6				*
BY-108	33	3C	FC/ORG				2.2		647	1140	*
C-102	6	4A	ORG			-5	3.8		165	192	*
C-105	6	4A		MT			1.1		24	3	
T-101	6	4A					0.8				
T-102	6	4A					0.2				
T-103	6	4A					0.1				
B-110	19	4B					2.2	2.5			
B-111	19	4B				-2	2.1	2.3			
T-105	19	4B					0.7				
T-110	19	4B	FG			5	3.7	4.1			*

Table A.1 (contd)

Tank	TCR	Core	Pump	Stab	LSF	Vol	Depth	SL(%)	SC(%)	SR(%)
S-102	446V	02/96			0.5	2086	5.1	1	37	62
S-103					0.25	878	2.1	4	52	45
SX-106	460V				0	1813	4.4	0	18	82
U-103		10/96			0.75	1729	4.2	7	66	27
U-105		03/96			0.5	1448	3.5	8	19	72
U-107	451V	04/96			0.75	1425	3.5	24	0	76
U-108		05/96			0.75	1687	4.1	7	52	41
U-109		01/96			0.75	1687	4.1	11	48	41
U-111					0	1250	3.0	8	33	59
A-101	505V	07/96			0	3621	8.8	0	57	42
A-102		1/88, 3/96	done	SN	0	141	0.3	8	51	41
A-103		01/88	done	AR	0	1391	3.4	1	99	0
AX-101					0	2842	6.9	2	68	30
S-105			done 76	JET		1726		0	100	0
S-106					0.25	1805	4.4	7	93	0
S-108			Jul-96		0	2295	5.6	1	99	0
S-109					0	2158	5.2	2	98	0
S-111		05/96				2227	5.4	24	76	0
S-112					0	1987	4.8	1	99	0
SX-102					0	2063	5.0	11	81	8
SX-103					0.25	2474	6.0	17	83	0
SX-105					0	2595	6.3	11	89	0
U-106	450V	05/96			0	802	1.9	12	88	0
BX-111			done	JET	0.75	802	1.9	15	85	0
BY-101			done 84	JET	0	1471	3.6	10	90	0
BY-102		07/96		JET	0.25	1296	3.1	9	91	0
BY-103	428V				0	1520	3.7	2	98	0
BY-106	420V	12/95			0.25	2440	5.9	15	85	0
BY-109					0	1607	3.9	9	91	0
BY-111	440V		done 84	JET	0	1744	4.2	6	94	0
BY-112	441V		done 84	JET	0	1106	2.7	6	94	0
BY-104	418V		done 84	JET	0	1543	3.7	37	63	0
BY-105	419V	IP	will resume		0.25	1919	4.7	33	67	0
BY-107	421V	06/96	done 84	JET	0	1011	2.5	44	56	0
BY-110	429V	08/95	done 84	JET	0	1512	3.7	48	52	0
S-101		04/96				1577	3.8	51	29	20
S-110		07/96			0.75	1482	3.6	29	71	0
SX-104						2333	5.7	28	72	0
BY-108	422V	8/95	done 84	JET	0	866	2.1	72	28	0
C-102	459V		done 95			1607	3.9	100	0	0
C-105	489, 443V					570	1.4	100	0	0
T-101			done	SN		384	0.9	100	0	0
T-102	PNL-10101		done	AR		72	0.2	100	0	0
T-103			done	AR		87	0.2	100	0	0
B-110	368	05/90	done 78	AR	0	931	2.3	100	0	0
B-111	PNL-10099	10/91	done 85	SN	0	897	2.2	100	0	0
T-105	369	5/93	done 78	AR	0	372	0.9	100	0	0
T-110					1	1429	3.5	100	0	0

Table A.1 (contd)

Tank	TOC	Nitrite	Alum	Rad	Density	Med T	Max T	pH	NS frac	gas frac
S-102	0.13%	0.52	2.10	894	1.82	106	122	>14	0.31	0.17
S-103	0.11%	0.42	1.64	317	1.79	87	130	13.6	0.36	0.18
SX-106	0.16%	0.65	2.61	717	1.87	102	125	13.2	0.26	0.08
U-103	0.07%	0.29	1.07	640	1.74	86	99	10.5	0.39	0.10
U-105	0.13%	0.57	2.25	443	1.82	84	101	>14	0.28	0.10
U-107	0.14%	0.61	2.96	476	1.84	76	89	11.4	0.27	0.07
U-108	0.10%	0.39	1.82	597	1.77	83	98	10	0.38	
U-109	0.09%	0.38	1.76	595	1.77	81	96	>14	0.37	0.08
U-111	0.12%	0.50	2.14	481	1.80	77	92	11.2	0.33	
A-101	0.22%	0.34	0.82	1254	1.59	155	180	>14	0.31	
A-102	0.57%	0.33	0.78	128	1.59	89	137	12	0.36	
A-103	0.02%	0.03	0.07	126	1.48	90	143	12.9	0.15	
AX-101	0.18%	0.25	0.60	1606	1.56	129	168	>14	0.27	
S-105										
S-106	0.04%	0.17	0.71	718	1.67	73	94	13.2	0.5	0.33
S-108	0.04%	0.12	0.41	979	1.68	78	94	13.6	0.49	
S-109	0.04%	0.14	0.51	779	1.67	66	83	13.2	0.49	
S-111	0.03%	0.11	1.02	926	1.66	80	97	>14	0.52	0.13
S-112	0.04%	0.12	0.42	969	1.68	77	92	12.2	0.49	
SX-102	0.05%	0.16	1.06	883	1.68	143	191	>14	0.49	0.11
SX-103	0.03%	0.10	1.10	1139	1.65	175	233	13.2	0.52	0.17
SX-105	0.03%	0.11	0.02	1352	1.67	169	230	13.8	0.51	
U-106	0.03%	0.11	0.33	292	1.68	76	92	13.9	0.45	
BX-111	0.05%	0.25	0.37	256	1.47	67	89	>14	0.68	
BY-101	0.05%	0.24	0.34	544	1.52	71	115	>14	0.65	
BY-102	0.05%	0.26	0.36	467	1.51	71	126	13.4	0.67	
BY-103	0.05%	0.27	0.50	557	1.50	75	137	13.5	0.69	
BY-106	0.13%	0.23	0.32	841	1.49	123	199	13.5	0.69	
BY-109	0.05%	0.25	0.35	596	1.51	66	138	13.4	0.65	
BY-111	0.05%	0.26	0.36	649	1.51	82	92		0.67	
BY-112	0.06%	0.25	0.36	404	1.50	82	90	>14	0.67	
BY-104	0.18%	0.17	0.24	473	1.49	122	237	>14	0.69	
BY-105	0.15%	0.18	0.26	602	1.5	103	180	13.3	0.67	
BY-107	0.24%	0.15	0.21	278	1.51	78	120	>14	0.64	
BY-110	0.26%	0.15	0.23	398	1.47	112	205	>14	0.69	
S-101	0.05%	0.25	3.14	923	1.66	124	90	13.4	0.54	0.06
S-110	0.03%	0.09	1.59	775	1.64	117	151	14	0.55	
SX-104	0.03%	0.09	1.53	1202	1.64	158	224	13	0.55	
BY-108	0.43%	0.07	0.10	198	1.47	84	154	>14	0.7	
C-102	0.00%	0.18	4.78	18	1.55	116	140	13.3	0.62	
C-105	0.00%	0.37	4.81	6	1.52	100	199	9.7	0.64	
T-101	0.03%	0.75	2.72	63	1.64	66	88	13.3	0.67	
T-102	0.00%	0.19	5.25	1	1.51	66	48	9.9	0.739	
T-103	0.01%	0.39	4.57	5	1.55	63	89	12.8	0.725	
B-110	0.00%	0.00	0.00	176	1.32	75	121	8.2	0.68	
B-111	0.00%	0.00	0.01	1266	1.32	81	98	10.2	0.69	
T-105	0.00%	0.04	0.23	7	1.29	74	93	12.7	0.74	
T-110	0.01%	0.00	0.00	0.2	1.31	62	91	9.1	0.74	

Table A.1 Legend

The origin of the information in Table A.1 is summarized below:

Cluster

Based on the study of Remund et al. (1995), who used the historical tank contents estimates (HTCE) to determine the concentrations of 16 analytes in all 149 SSTs. These analytes are

aluminum	iron	cesium-137	uranium
phosphate	chromium	nitrate	percent water
bismuth	sodium	strontium-90	plutonium
manganese	nitrite	fluoride	silicon

Notice that total organic carbon (TOC) is not used in the comparisons. A number of different metrics based on the differences in concentration for the 16 analytes were constructed and used to group the 149 tanks into separate clusters. All tanks in a given cluster were determined to be close to each other and relatively far from tanks not in the cluster, based on the metric. The metric for the grouping used in this spreadsheet normalized the differences by the mean concentration of each of the analytes in the tank.

Waste Configuration (WC)

The tanks are grouped according to the waste configuration type, determined from the historical tank contents estimates (HTCE). There are four basic waste configuration types included in this table, with at least two subcategories for each type.

Watch List Status (Watch List)

The status of the tanks under consideration was derived from WHC (1995):

FC: ferrocyanide
ORG: organic salt
FG: hydrogen/ flammable gas
HH: high heat

Appendix A tanks that are officially watch list tanks are capitalized.
Appendix B tanks that are effectively watch list tanks are in lower case.

Whitney Screening (Whitney)

If the screening calculation (Whitney 1995) for a level instrument (FIC, manual tape, Enraf, Neutron ILL) flagged the tank for a significant level response to barometric pressure variations, the abbreviations (FIC/MT/E/N) are entered in this column. The absence of an entry can mean the test was either inconclusive or negative.

Level Response to Barometric Pressure Variations (dL/dP)

The estimates for dL/dP were obtained from Hodgson et al. (1996) and were the Q-fit mean values used by Hodgson et al. to evaluate the waste tanks for trapped gas. Values based only on manual tape or the neutron monitor were discarded. Those dL/dP values whose standard deviation exceeded 100% of the mean are given in italics.

Level Rise (LR)

The level rise, in cm, was roughly estimated from the graphs of level measurements in Whitney (1995) and corresponds to the total level change after the last known transfer. Besides the uncertainty in the numerical value, there is some variability introduced by the choice of starting date from which to estimate the change in level. In some cases it was uncertain whether transfers such as saltwell pumping had occurred during this interval. Factors contributing to this value may be retained gas, accidental or intentional intrusions, and transfers. Welty (1988) was also consulted for level data prior to that in Whitney (1995) and for additional information about tank history.

Surface and Liquid (Surf, Liq)

The surface and liquid levels are reported in meters; these values were obtained from the figures in Whitney (1995). The value for the surface level was obtained from either Enraf, FIC, or MT measurements. When more than one type of measurement was available the preference was Enraf, followed by FIC data and then MT data. The liquid level was obtained from neutron ILL data, when available.

Headspace Gas Concentrations (H₂, NH₃)

Concentrations of H₂ and NH₃ from the TWINS database are reported if available as of 12/14/95; units are in ppm by volume.

Short List (*)

The tanks that are marked with an asterisk (*) in this column were included in the original short list summarized in Table 1.1 in the main body of the report. These tanks are considered to be of interest for more detailed modeling and analysis.

Tank Characterization reports (TCR)

If a TCR is known to be available, the document number is noted. If it is a headspace vapor and gas report, the suffix V is included. The full document number is WHC-SD-WM-ER-XXX.

Cores

The availability of core samples from the tanks is summarized. Information about cores already taken was obtained from D. McCain (personal communication, October 27, 1995 and from a review of the core extrusion reports written between 12/95 and 7/96.

Pumping History (pump)

Tanks for which salt-well pumping had been completed before about 1986 are noted in Welty (1988). Past pumping dates are recorded in that report and also in the Historical Contents reports.

Stabilization Status (Stab)

This summarizes stabilization status and method of stabilization: SN shows the supernatant liquid has been pumped, JET means it has been jet pumped, AR means it has been administratively classified as stabilized with no action taken. Tanks with no entry are considered not stabilized as of August 31, 1995. The status is taken from Hanlon (1995).

Liquid Surface Fraction (LSF)

The fraction of the surface that is liquid was estimated from the most recent photographs in historical tank contents estimates (Brevick 1995).

Waste Volume (Vol)

The values for the total waste volume in cubic meters were obtained from the tank layer model (Agnew et al. 1995).

Depth

The waste depth values in this column were obtained from the historical tank contents estimates (Brevick 1995). They should be compared with the direct measurements reported in the Surf column; they provide a check on the accuracy of the historical estimates.

Sludge, Saltcake, and Salt Slurry Fraction (SL, SC, SR)

The fractions of sludge, saltcake, and salt slurry were estimated from waste volumes calculated from the tank layering model (TLM) (Agnew et al. 1995). Graphical representations of the depths of these layers are also given at the end of the TLM document.

Total Organic Carbon (TOC)

The tank layering model, Agnew et al. (1995), was used to estimate the TOC content based on historical transfer information and tabulated in Brevick (1995). This value is in wt%.

Nitrite

Concentration of nitrite ion in moles/L is from the historical tank contents estimate (Brevick 1995).

Aluminum (Alum)

Concentration of aluminum in moles/L is from the historical tank contents estimate (Brevick 1995).

Radiation (Rad)

Total radiation in the tanks in kiloCuries. The radiation is assumed to come from only cesium and strontium. The total radiation of each of these components was obtained from the historical tank contents estimates (Brevick 1995).

Density

Values of the density were obtained from the historical tank contents estimates (Brevick 1995) and are reported in g/cm^3 .

Temperature (Median T, Max T)

The temperatures in degrees Fahrenheit were obtained from the documentation included in the historical tank contents estimates (Brevick 1995). These temperatures are based on a period of time usually spanning two to three years starting after 1990. Maximum and median temperatures were reported for this period.

pH

The pH was obtained from the level history diagrams included as part of the documentation in the historical tank contents estimates (Brevick 1995). The last measured pH value listed on the diagram is used in the spreadsheet. For most tanks, the pH has been measured recently, but some tanks have not been measured within the last decade. In some cases the last measurement was made before significant transfer activity, and the pH is not expected to accurately reflect current tank contents.

Non-Solid Fraction (NS frac)

These numbers were obtained from the historical tank contents estimates (Brevick 1995).

Gas Fraction (gas frac)

The gas fraction is calculated from the dL/dP , the densities, and the wetted waste depth as follows:

$$\alpha = \frac{dL}{dP} \frac{P}{h_w}$$

$$P = g(0.775\rho_b h_w + \rho_s \max(h_s - h_L, 0) + \rho_L \max(h_L - h_s, 0))$$

- where
- α = average gas fraction (void fraction)
 - P = the average pressure exerted on the gas
 - h_w = the wetted waste level (the minimum of the liquid and surface levels)
 - h_s = the surface (solid) level
 - h_L = the liquid level
 - ρ_b = the overall bulk density (liquid and solid together) from the historical tank contents estimates
 - ρ_L = the liquid density
 - ρ_s = the solid density.

The assumptions are that the average gas location is at 22.5% of the wetted waste height (Hodgson 1996) and that the gas exists as solids-displacing bubbles that support the weight of the solids above them as well as the liquid.

References

Agnew SF, P Baca, R Corbin, K Jurgensen, and B Young. 1995. *Tank Layer Model (TLM)*. LA-UR-94-4269 Rev 1, Los Alamos National Laboratory, Los Alamos, New Mexico.

Brevick CH. 1995. *Historical Tank Content Estimate* (also called *The Kaiser Reports*). WHC-SD-WM-ER-351, Westinghouse Hanford Company, Richland, Washington.

Hanlon BM. 1995. *Waste Tank Summary for Month Ending August 31, 1995*. WHC-EP-0182-89, Westinghouse Hanford Company, Richland, Washington.

Hodgson KM, RP Anantamula, SA Barker, KD Fowler, JD Hopkins, JA Lechelt, DA Reynolds, DC Hedengren, RE Stout, and RT Winward. 1996. *Evaluation of Hanford Tanks for Trapped Gas*. WHC-SD-WM-ER-526 Rev. 1, Westinghouse Hanford Company, Richland, Washington.

Remund KM, CM Anderson, and BC Simpson. 1995. *Hanford Single-Shell Tank Grouping Study*. PNL-10749, Pacific Northwest National Laboratory, Richland, Washington.

Welty RK. 1988. *Waste Storage Tank Status and Leak Detection Criteria*. WHC-SD-WM-TI-356, Westinghouse Hanford Company, Richland, Washington.

WHC. 1995. *Tank Farms Operating Specification Document*. OSD-T-151-00030 B-12, Westinghouse Hanford Company, Richland, Washington.

Whitney PD. 1995. *Screening the Hanford Tanks for Trapped Gas*. PNL-10821, Pacific Northwest National Laboratory, Richland, Washington

Appendix B

Core Descriptions

Appendix B

Core Descriptions

Table B.1. Core Descriptors






Legend	Type	Color	Moisture	Grain Size	Surface Trait
 Empty Segment	saltcake	white	dry	coarse	crumbly
 Saltcake	sludge	gray	damp	fine	subsegments
 Saltcake - Dark	salt slurry	brown	wet		putty-like
 Sludge		black	slushy		smooth
 Sludge and Saltcake		light (lt) dark (dk)			slushy

Table B.2. Tank 241-S-102, Core 125, Riser 11
(Logbook: WHC-N-1204, still photos)












Seg. No.	Sol. (cm)	Liq. (mL)	Height in Tank (m)	Sample Description
1	1	0	5.3	 saltcake, gray
2	15	0	4.8	 saltcake, brown and white, dry, coarse
3	30	0	4.3	 saltcake, gray-white, very dry, coarse, 3-cm subseg
4	38	0	3.9	 saltcake, light gray, dry, coarse, 5-cm subseg
5	36	0	3.4	 saltcake, light gray, dry, coarse, 5-cm subseg
6	33	0	2.9	 saltcake, gray
7	36	70	2.4	 saltcake, dk gray, wet, fine, slushy, gray, opaque liq.
8	28	0	1.9	 saltcake, gray, damp, fine, smooth to crumbly
9	48	0	1.5	 sludge, black, damp, fine, smooth, 7-cm pieces
10	43	0	1.0	 sludge, black, damp, fine, smooth, 5-cm pieces
11	25	3	0.5	 saltcake, gray, damp, fine, yellow, clear liquid

Table B.3. Tank 241-S-102, Core 130, Riser 14
(Logbook: WHC-N-1204, still photos)












Seg. No.	Sol. (cm)	Liq. (mL)	Height in Tank (m)		Sample Description
1	0	0	5.3		empty segment
2	20	0	4.8		saltcake, gray
3	25	0	4.3		saltcake, gray
4	25	0	3.9		saltcake, gray-white, fine, crumbly
5	30	30	3.4		saltcake (and sludge), gray; yellow-gray liquid
6	15	0	2.9		saltcake (and sludge), gray
6B	48	0			saltcake, lt gray, damp, fine, 4-cm subseg
7	10	0	2.4		saltcake, blue-gray, damp
8	15	0	1.9		saltcake, dark gray, damp
9	53	0	1.5		sludge, black, damp, fine, sandy/smooth
10	41	43	1.0		sludge, black, wet, fine, sandy/smooth, black liquid
11	23	0	0.5		sludge and saltcake, coarse, black

Table B.4. Tank 241-U-105, Core 131, Riser 20
(Logbook: WHC-N-1193, still photos)










Seg. No.	Sol. (cm)	Liq. (mL)	Height in Tank (m)		Sample Description
1	1	0	4.3		sludge, dark brown
2	15	0	3.9		saltcake, dark brown, coarse
3	15	0	3.4		saltcake, dark brown with white coarse crystals
4	28	0	2.9		saltcake, brown, damp, coarse, 4-cm subseg
5	18	0	2.4		saltcake, brown, damp, coarse, 2-5-cm subseg
6	18	0	1.9		sludge/saltcake, dark brown/gray, damp, coarse
7	41	0	1.5		sludge/saltcake, dark brown, damp, coarse
8	23	0	1.0		sludge/saltcake, dark brown, damp, coarse
9	25	0	0.5		sludge/saltcake, dk brown, damp, coarse, 4-cm subseg

Table B.5. Tank 241-U-105, Core 133, Riser 2
(Logbook: WHC-N-1193, still photos)










Seg. No.	Sol. (cm)	Liq. (mL)	Height in Tank (m)		Sample Description
1	0	10	4.3		no solids, clear, colorless liquid
2	3	0	3.9		sludge, dark brown, damp
3	6	0	3.4		sludge, dark brown, damp
4	17	0	2.9		saltcake, brown, wet, fine
5	1	0	2.4		saltcake, brown, coarse
6	13	0	1.9		saltcake, brown, coarse
7	0	0	1.5		empty
8	36	0	1.0		sludge and saltcake, dark brown, damp, fine
9	30	0	0.5		sludge and saltcake, dark brown, damp, fine

Table B.6. Tank 241-U-107, Core 129, Riser 9
(Logbook: WHC-N-1004)




Seg. No.	Sol. (cm)	Liq. (mL)	Height in Tank (m)		Sample Description
1	1	210	3.9		saltcake, lt yellow, coarse, yellow-green, clear liquid
2	8	225	3.4		saltcake, black/brown, coarse, brown, opaque liquid
3	38	0	2.9		saltcake, lt brown/gray, wet

Table B.7. Tank 241-U-107, Core 134, Riser 7
(Logbook: WHC-N-1004)








Seg. No.	Sol. (cm)	Liq. (mL)	Height in Tank (m)		Sample Description
1	0	0	3.9		empty
2	30	0	3.4		saltcake, gray-white, dry
3	17	0	2.9		saltcake, gray
4	44	0	2.4		upper - saltcake, dk gray; lower - sludge, black, damp
5	13	0	1.9		upper - sludge, black; lower - saltcake, gray
5A	3	0			saltcake, gray
5B	0	70			dark brown, opaque liquid

Table B.8. Tank 241-U-109, Core 123, Riser 2
(Logbook: WHC-N-1194, still photos)










Seg. No.	Sol. (cm)	Liq. (mL)	Height in Tank (m)		Sample Description
1	5	0	4.3		saltcake, gray, upper - dry, coarse; lower - wet, sandy
2	25	0	3.9		saltcake, gray, dry, fine, crumbly
3	25	0	3.4		saltcake, gray, dry, fine, crumbly
4	30	0	2.9		saltcake, bluish-gray, damp
5	10	0	2.4		saltcake, bluish-gray, damp
6	48	0	1.9		saltcake, gray, damp, putty-like
7	36	0	1.5		saltcake, bluish-gray, damp
8	41	0	1.0		saltcake, bluish-gray, damp
9	41	0	0.5		saltcake, bluish-gray, damp, lower - yellow

Table B.9. Tank 241-U-109, Core 124, Riser 19
(Logbook: WHC-N-1194)










Seg. No.	Sol. (cm)	Liq. (mL)	Height in Tank (m)		Sample Description
1	0	0	4.3		empty
2	5	0	3.9		saltcake, dark gray, damp, coarse
3	25	125	3.4		saltcake, gray, wet, slushy; black, opaque liquid
4	23	0	2.9		saltcake, bluish-gray, dry, coarse
5	46	0	2.4		saltcake, gray-white, damp, smooth
6	48	0	1.9		saltcake, gray, damp, fine, putty-like
7	44	0	1.5		saltcake, dark gray, damp, fine, putty-like
8	41	0	1.0		saltcake, dark gray, damp, fine, putty-like
9	30	0	0.5		saltcake, black/gray, damp, fine, putty-like, pitted

Table B.10. Tank 241-U-109, Core 128, Riser 7
(Logbook: WHC-N-1194)










Seg. No.	Sol. (cm)	Liq. (mL)	Height in Tank (m)		Sample Description
1	8	0	4.3		saltcake, medium gray, wet, crumbly
2	15	0	3.9		saltcake, medium gray
3	36	0	3.4		saltcake, medium gray, damp
4	36	0	2.9		saltcake, dark gray, wet
5	18	0	2.4		saltcake, dark gray
6	41	0	1.9		saltcake, dark gray, wet
7	46	0	1.5		saltcake, dark gray, damp
8	44	0	1.0		saltcake, dark gray
9	23	0	0.5		saltcake, dark gray

Table B.11. Tank 241-BY-104, Core 116
(Video: BY-FARM #2-C)









Seg. No.	Sol. (cm)	Liq. (mL)	Height in Tank (m)		Sample Description
1			3.9		empty
2	15	0	3.4		saltcake, brown, dry, crumbly, 5-cm subseg
3	25	0	2.9		saltcake, lt brown, dry, coarse, crumbly
4	35	0	2.4		saltcake, brown, wet to dry, coarse, crumbly, 2-7-cm subseg
5	48	0	1.9		saltcake, brown, wet, crumbly, 5-cm subseg
6	48	0	1.5		saltcake, brown, wet, fine, putty/slush, 3-cm subseg
7	48	0	1.0		sludge/saltcake, brown, damp to wet, fine to coarse
8	25	0	0.5		sludge, red-brown, wet, fine, smooth 15-cm piece up

Table B.12. Tank 241-BY-104, Core 117
(Video: BY-FARM #2-C)






Seg. No.	Sol. (cm)	Liq. (mL)	Height in Tank (m)		Sample Description
1	2	90	3.9		saltcake, lt brown to white, wet, crumbly; brn, opaq liq
2	20	50	3.4		saltcake, dk brown, wet, putty/slushy; brn, opaq liquid
3	30	0	2.9		saltcake, dk brown, wet, crumbly, 2-cm subseg
4	25	0	2.4		saltcake, brown, damp, crumbly, 2-cm subseg
5	12	0	1.9		saltcake, dk brown, damp, pasty, 2-cm subseg

Table B.13. Tank 241-BY-105, Core 108, Riser 12A
(Video: BY-FARM #2-C, 0:19:07)




Seg. No.	Sol. (cm)	Liq. (mL)	Height in Tank (m)		Sample Description
1R	25	0	4.8		saltcake, lt brown, wet, coarse, crumbly, 2-cm subseg
2R	10	0	4.3		saltcake, brown, wet, coarse, slushy
3	10	0	3.9		saltcake, brown, wet, coarse, slushy

Table B.14. Tank 241-BY-105, Core 133, Riser 2







Seg. No.	Sol. (cm)	Liq. (mL)	Height in Tank (m)		Sample Description
1	0	10	4.8		no solids; clear, colorless liquid
2	3	0	4.3		resembled a sludge, dark brown
3	6	0	3.9		resembled a sludge, brown, damp
4	17	0	3.4		resembled a saltcake, brown
5	1	0	2.9		resembled a saltcake, grayish-brown
6	13	0	2.4		resembled a saltcake, dk brown

Table B.15. Tank 241-BY-106, Core 64, Riser 10B
(Video: A-104 11/8/94)






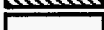






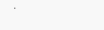
Seg. No.	Sol. (cm)	Liq. (mL)	Height in Tank (m)		Sample Description
1	2	0	6.3		sludge, lt yellow-gray, wet, pasty
2	4	0	5.8		saltcake, lt gray, wet, slushy, 2-cm subseg
3	2	95	5.3		saltcake, lt gray, wet, soupy, 2-cm subseg; gray liquid
4	30	0	4.8		saltcake, lt gray, wet, coarse, slushy
5	2	0	4.3		saltcake, lt gray, wet, slushy
6	1	20	3.9		saltcake, lt gray, wet, slushy; gray liquid
7			3.4		empty
8	30	0	2.9		saltcake, lt gray, wet, slushy
9	?	0	2.4		saltcake, lt gray, damp, coarse, slushy
10	15	200	1.9		saltcake, lt gray, wet, slushy; gray liquid
11	8	0	1.5		saltcake, lt gray, dry, coarse, subseg hard
12	10	0	1.0		saltcake, gray, wet, slushy
13	2	0	0.5		saltcake, gray, dry, coarse, crumbly

Table B.16. Tank 241-BY-106, Core 65
(Video: A-104 11/8/94)

Seg. No.	Sol. (cm)	Liq. (mL)	Height in Tank (m)	Sample Description
1	1	220	6.3	██████████ saltcake, white, wet, coarse, slushy; clear, thick liq.
2	2	>240	5.8	██████████ saltcake, white, wet, coarse, slushy; clear, thick liq.
3	2	>240	5.3	██████████ saltcake, white, wet, coarse, slushy; clear, thick liq.
4	4	>200	4.8	██████████ saltcake, white, wet, coarse, slushy; clear, thick liq.
5	3	>240	4.3	██████████ saltcake, white, wet, coarse, slushy; cloudy, thick liq.
6	1	>240	3.9	██████████ saltcake, white, wet, coarse, slushy; cloudy, thick liq.
7	2	>240	3.4	██████████ saltcake, white, wet, coarse, slushy; cloudy, thick liq.
8	3	>240	2.9	██████████ saltcake, white, wet, coarse, slushy; cloudy, thick liq.
9	2	0	2.4	██████████ saltcake, lt gray, wet
10	4	?	1.9	██████████ saltcake, white, wet, coarse, slushy; cloudy, thick liq.
11	0.5	40	1.5	██████████ saltcake, white, wet, coarse, slushy; cloudy, thick liq.
12	0	20	1.0	██████████ cloudy, thick liquid
13	13	0	0.5	██████████ saltcake, dk brown to white, wet, 2-4-cm subseg

Table B.17. Tank 241-BY-106, Core 121, Riser 5
(Tape: BY-FARM #2-C, logbook: WHC-N-996)

Seg. No.	Sol. (cm)	Liq. (mL)	Height in Tank (m)	Sample Description
1	3	0	6.3	██████████ saltcake, off-white, dry
2	11	0	5.8	██████████ saltcake, off-white, damp
3	32	0	5.3	██████████ saltcake, lt gray, damp, coarse, subseg
4	36	0	4.8	██████████ saltcake, lt gray, damp, coarse, subseg/putty-like
5	23	0	4.3	██████████ saltcake, lt gray, damp, coarse, subseg/putty-like
6	28	0	3.9	██████████ saltcake, lt gray, damp, coarse, subseg/putty-like
7	23	0	3.4	██████████ saltcake, lt gray, damp, coarse, 5-cm subseg/putty-like
8	41	0	2.9	██████████ saltcake, gray, damp
9	3	0	2.4	██████████ saltcake, dk gray, damp
10	18	0	1.9	██████████ saltcake, dk gray, damp
10B	18	190	1.5	██████████ saltcake, gray-green, wet; lt green, opaque liquid

Table B.18. Tank 241-BY-108, Core 98, Riser 12A
(Video: BY-FARM #2)

Seg. No.	Sol. (cm)	Liq. (mL)	Height in Tank (m)	Sample Description
1	12	0	2.9	██████████ saltcake, lt yellow-gray, wet, coarse, slushy
2	30	?	2.4	██████████ saltcake, lt brown, wet, coarse, slushy; yellow liquid
3	30	0	1.9	██████████ saltcake, brown, wet, coarse, slushy
4	48	0	1.5	██████████ sludge, brown, damp, fine, pasty/smooth/subseg

Table B.19. Tank 241-BY-108, Core 101, Riser 7
(Video: BY-FARM #2A, 0:29:26)







Seg. No.	Sol. (cm)	Liq. (mL)	Height in Tank (m)		Sample Description
1	0	0	2.9		empty
2	4	0	2.4		saltcake, lt brown, dry, coarse, crumbly
3	4	0	1.9		saltcake, lt brown, dry, coarse, crumbly
4	0.5	0	1.5		saltcake, dk brown, damp, coarse, crumbly
5	10	0	1.0		saltcake, dk brown, dry, coarse, 2-cm subsegments
6	1	0	0.5		saltcake, dk brown, wet, coarse, crumbly

Table B.20. Tank 241-BY-108, Core 102, Riser 7
(Video: BY-110 #2B, 0:19:37)







Seg. No.	Sol. (cm)	Liq. (mL)	Height in Tank (m)		
1	10	0	2.9		saltcake, lt yellow, dry, 2-cm subsegments
2	48	0	2.4		saltcake, brown, wet, 2-4-cm subsegments
3	43	0	1.9		saltcake, brown, wet, 2-cm subsegments
4	38	0	1.5		sludge/saltcake, brown, wet, coarse; slushy/sandy
5	41	0	1.0		upper 1/4 - saltcake, dk brown, wet, coarse
					lower 3/4 - sludge, dk brown, damp, sandy, smooth

Table B.21. Tank 241-BY-110, Core 92, Riser 12B
(Video: BY-FARM #2, 0:59:07)








Seg. No.	Sol. (cm)	Liq. (mL)	Height in Tank (m)		Sample Description
1	0	0	4.3		empty
2	0	0	3.9		empty
3	0	0	3.4		empty
4	5	0	2.9		saltcake, dk brown, dry, coarse, subsegmented
5	12	0	2.4		saltcake, dk brown, dry, coarse, subsegmented
6	15	0	1.9		saltcake, lt yellow, wet, coarse, crumbly
7	?	20?	1.5		saltcake, green-yellow, coarse, slushy-soupy

Table B.22. Tank 241-BY-110 Core 101, Riser 7
 (Video: BY-FARM #2A, 0:29:26; BY-110 #2B, 0:19:37)

Seg. No.	Sol. (cm)	Liq. (mL)	Height in Tank (m)	Sample Description
1	0	0	4.3	empty
2	4	0	3.9	saltcake, lt brown, dry, coarse, crumbly
3	4	0	3.4	saltcake, lt brown, dry, coarse, crumbly
4	0.5	0	2.9	saltcake, dk brown, damp, coarse, crumbly
5	10	0	2.4	saltcake, dk brown, dry, coarse, 2-cm subseg
6	1	0	1.9	saltcake, dk brown, wet, coarse, crumbly
7	48	0	1.5	saltcake, dk brown, wet, coarse, crumbly, 2-cm subseg
8	43	0	1.0	saltcake, dk brown, wet, coarse, crumbly, 4-cm subseg
9	48	0	0.5	sludge, dk brown, damp, fine, smooth

Table B.23. Tank 241-BY-110 Core 103, Riser 7
 (Video: BY-110 #2B, 00:00)

Seg. No.	Sol. (cm)	Liq. (mL)	Height in Tank (m)	Sample Description
1	25	0	4.3	saltcake, lt brown to white, dry, coarse, crumbly
2	25	0	3.9	saltcake, lt brown, dry, coarse, crumbly
3	15	0	3.4	saltcake, lt brown, dry, coarse, crumbly, 2-cm subseg
4	41	0	2.9	saltcake, lt brown, dry, coarse, crumbly, 2-cm subseg
5	25	0	2.4	saltcake, brown, dry, coarse, crumbly, 2-cm subseg
6	41	0	1.9	saltcake, brown, wet, crumbly, 2-cm subseg; brn liq.
7	23	0	1.5	saltcake, dk brown, wet, coarse, crumbly, 2-cm subseg
8	38	0	1.0	saltcake, dk brown, wet, coarse, crumbly, 2-cm subseg
9	43	0	0.5	sludge/saltcake, dk brown, damp, fine, smooth; lower 20 cm is sludge

Table B.24. Tank 241-BY-110 Core 107, Riser 7
 (Video: BY-110 #2B, 0:51:03)

Seg. No.	Sol. (cm)	Liq. (mL)	Height in Tank (m)	Sample Description
1	3	0	4.3	saltcake, white, dry, coarse, crumbly
2	18	0	3.9	saltcake, lt brown, dry, coarse, crumbly, 2-cm subseg
3	18	0	3.4	saltcake, brown, dry, coarse, crumbly, 2-cm subseg
4	23	0	2.9	saltcake, dk brown, dry, coarse, crumbly, 2-cm subseg
5	23	0	2.4	saltcake, dk brown, damp, coarse, crumbly, 2-cm subseg
6	35	0	1.9	saltcake, dk brown, wet, coarse, crumbly, 2-cm subseg
7	30	0	1.5	saltcake, dk brown, wet, coarse, slushy, 2-cm subseg
8	25	0	1.0	saltcake, dk brown, wet, coarse, slushy, 2-cm subseg
9	48	0	0.5	sludge, dk brown, damp, fine, smooth

**Table B.25. Tank 241-BY-110 Core 113, Riser 4
(Video: BY-FARM #2A, 54:00)**









Seg. No.	Sol. (cm)	Liq. (mL)	Height in Tank (m)		Sample Description
1	10	0	4.3		saltcake, lt yellow to white, dry, coarse, crumbly
2	5	0	3.9		saltcake, lt brown, dry, coarse, crumbly
3	13	0	3.4		saltcake, dk brown, dry, coarse, crumbly, 2-cm subseg
4	7	0	2.9		saltcake, dk brown, dry, coarse, crumbly
5	13	0	2.4		saltcake, dk brown, wet, coarse, slushy/sandy
6	36	0	1.9		saltcake, dk brown, wet, coarse, slushy/sandy
7	40	0	1.5		saltcake, red-brown, wet, coarse, 5-cm subseg
8	44	0	1.0		sludge, brown, damp, fine, smooth; lower-10 cm is saltcake

Table B.26. Surface Descriptions of Waste Configuration 1 Tanks

Tank	Surface Description
S-102	Yellowish-gray, floating, saltcake crust covering about 75% of surface on dark liquid. Photo date: 3/18/88. ^(a,b) General appearance is much like Figure 12.
S-103	Light yellow, cracked, saltcake surface with dark liquid covering about 50%. Photo date: 6/1/89. ^(a,b) See Figure 12.
SX-106	Yellowish-gray, (appears to be a floating crust), dry, saltcake on liquid. Photo date: 6/1/89. ^(a,b) See Figure 12.
U-103	Yellowish-gray, crust(?) appears to be floating in places and in others to be islands in dark liquid. Photo date: 9/13/88. ^(a) See Figure 12.
U-105	Yellow and gray crust apparently floating on dark liquid. About 50% surface coverage. Photo date: 7/7/88. ^(a) See Figure 12.
U-107	Dark liquid surface with small "lily pad"-looking areas of crust forming. Photo date: 7/7/88. ^(a) See Figure 12.
U-108	Yellowish crust apparently floating on dark liquid. About 50% surface coverage. Photo date: 7/7/88. ^(a) See Figure 12.
U-109	Yellowish crust apparently floating on dark liquid. Crust covers about 25% of surface. Photo date: 7/7/88. ^(a) See Figure 12.
U-111	Gray to off-white "pebbly" solids with dark liquid covering about 25%(?) of surface. Photo date: 6/23/88. ^(a)
A-101	Pale yellow to gray, dry, saltcake surface. ^(b) See Figure 13.
A-102	Photo ^(b) from 1/27/89 is out of date. Tank has been salt-well pumped. See Figure 13.
A-103	Gray, dry, saltcake surface about 25% covered by dark liquid. ^(c) See Figure 13.
AX-101	Gray and pale yellow, very dry, saltcake surface. Photo date is 8/18/87. ^(b) See Figure 13.
^(a) WHC-SD-WM-ER-352.	
^(b) http://twins.pnl.gov:8001/photo.html .	
^(c) VIDON in-tank photo library, 2750E/D164/200E.	

Table B.27. Surface Descriptions of Waste Configuration 2 Tanks

Tank	Surface Description
S-106	Yellowish-gray, dry, saltcake surface. Surface appears to vary by as much as 1 meter, with waste built up at the tank walls. ^(a,b,c,d) Photo date: 3/17/89.
S-108	Yellowish-gray, dry, saltcake surface. ^(a,b,c) Variable surface height.
S-109	Yellowish-gray, dry, saltcake surface. ^(a,b,c) Variable surface height. Small patches of wet areas of dark purple color. Photo date: 8/24/84.
S-111	Yellow and gray, dry, saltcake with large pools of dark liquid. ^(a,b,c) Appearance similar to Figure XX (S-102). Photo date: 8/10/89.
S-112	Yellow and gray, dry, saltcake. Variable surface height. ^(a,b,c) Photo date: 3/24/87.
SX-102	Yellow, brown, and gray, dry, saltcake. Variable surface height. ^(a,c) Photo date: 1/7/88.
SX-103	Yellow, brown, and gray, damp, saltcake with pools of yellow-brown liquid. ^(a,b,c) Photo date: 12/17/87.
SX-105	Yellow and gray, dry, saltcake with fairly smooth surface. Photo date: 6/15/88 (WHC-SD-WM-ER-352).
U-106	Entire surface appears to be liquid over saltcake. ^(c) Photo date: 7/7/88.
BX-111	Black, yellow, blue, and gray surface partially covered by a yellowish-green liquid. ^(c) Photo date: 5/19/94.
BY-101	Yellow and gray, dry, saltcake. ^(c) Photo date: 9/19/89.
BY-102	Pale yellow and gray, dry, saltcake with a central pool of dark liquid. ^(b,c) Photo date: 9/11/87.
BY-103	Yellow and gray, dry, saltcake with dried-up gray pools. ^(b,c) Photo date: 9/7/89.
BY-106	Yellow and white, dry, "foamy" surface with small, liquid pools. ^(c) Photo date: 11/4/82.
BY-109	Photo ^(c) from 10/15/86 is out of date.
BY-111	Light yellow/gray, dry, uneven height, saltcake surface. ^(c) Photo date: 10/31/86.
BY-112	Light Yellow/gray, dry, uneven height, saltcake surface. ^(c) Photo date: 4/14/88.
^(a) WHC-SD-WM-ER-352. ^(b) http://twins.pnl.gov:8001/photo.html . ^(c) VIDON in-tank photo library, 2750E/D164/200E. ^(d) Video dated 9/12/94 (WP # 2W-94-00930).	

Table B.28. Surface Descriptions of Waste Configuration 3 Tanks

Tank	Surface Description
BY-104	Yellow/gray, dry, saltcake of varying surface elevation. Surface appears to vary by about 1 m. Waste is caked to the tank walls. Small pools clear liquid. Video date: 8/29/95. ^(d) 4/27/83 photo ^(b,c) shows similar surface.
BY-105	Very similar to BY-104; waste caked to tank walls, etc. Video ^(d) date 11/1/95. Photo ^(b,c) from 12/2/88 shows similar surface.
BY-107	Very similar to BY-104; waste caked to tank walls, etc. Photo ^(a,b,c) date: 10/15/86.
BY-110	Grayish to yellow-white damp, saltcake with dry, cracked pieces 0.1-1 m in size. Video ^(d) date: 7/11/95. Surface looks about the same as it did in an in-tank surface photo dated 1/1/40. ^(b,c)
S-101	Yellow-gray, dry, uneven height, saltcake. ^(c)
S-110	Yellow-gray, dry, uneven height, saltcake. Photo ^(b,c) date: 3/12/87.
SX-104	Yellow-gray, dry, uneven height, saltcake. Photo ^(b,c) date: 9/8/88.
BY-108	Yellow-gray, dry, uneven height, saltcake. Photo ^(b,c) date: 10/15/86.
^(a) WHC-SD-WM-ER-352. ^(b) http://twins.pnl.gov:8001/photo.html . ^(c) VIDON in-tank photo library, 2750E/D164/200E. ^(d) In-tank video from Kent Hodgson, WHC, 7/1995-2/1996.	

Table B.29. Surface Descriptions of Waste Configuration 4 Tanks

Tank	Surface Description
C-102	Black/brown, damp, mud-like surface. Photo ^(ca) date 5/18/76.
C-105	Dark brown, damp, mud-like surface with drier, yellow patches. Photo ^(a,c) date: 8/5/94.
T-101	Dark brown, damp, cracked, mud-like surface. Photo ^(a,c) date: 4/7/93.
T-102	Dark brown, damp, cracked, mud-like surface with yellow-brown liquid covering large portion of surface. Photo ^(a) date: 6/28/89.
T-103	Very similar to T-102. Photo ^(a,b) date: 7/3/84
B-110	Dark brown, damp, cracked, mud-like surface. Photo ^(a,b) date: 3/17/88.
B-111	Dark brown, damp, cracked, mud-like surface. Photo ^(a) date: 6/26/85.
T-105	Dark brown, damp, lumpy, mud-like surface. Photo ^(a,b) date: 5/14/87.
T-110	Dark brown, damp, cracked, mud-like surface with central clear yellow liquid pool. Photo ^(a,b) date: 6/26/85.
<p>^(a) VIDON in-tank photo library, 2750E/D164/200E. ^(b) http://twins.pnl.gov:8001/photo.html. ^(c) WHC-SD-WM-ER-352.</p>	



Figure B.1. Saltcake, Light Brown to White, Dry, Coarse, Crumbly
(BY110, C103, Segment 1; 8/95)



Figure B.2. Saltcake, Light Brown, Dry, Coarse, Crumbly
(BY-110, C103, Segment 2; 8/95)



Figure B.3. Saltcake, Brown, Dry, Coarse, Crumbly
(BY-110, C103, Segment 5; 8/95)



Figure B.4. Saltcake, Brown, Damp, Coarse, 2-5cm Subsegments
(U-105, C131, Segment 5; 2/96)



Figure B.5. Saltcake, Brown, Wet to Dry, Coarse, Crumbly, 2-7cm Subsegments
(BY-104, C116, Segment 4; 11/95)



Figure B.6. Sludge, Brown, Damp, Fine, Smooth, 15cm Subsegment
(BY-104, C116, Segment 8; 11/95)



Figure B.7. Sludge, Brown, Damp, Fine, Pasty/Smooth/Clay-like
(BY-108, C98, Segment 4; 8/95)



Figure B.8. Saltcake, Dark Gray, Damp, Fine, Putty-like
(U-109, C124, Segment 6; 1/96)



Figure B.9. Saltcake, Light Gray, Dry, Coarse, 5cm Subsegments
(S-102, C125, Segment 5; 1/96)



Figure B.10. Saltcake, Dark Gray, Wet, Fine, Slushy
(S-102, C125, Segment 5; 1/96)



Figure B.11. Sludge, Black, Wet, Fine, Sandy/Smooth
(S-102, C130, Segment 10; 1/96)

Distribution

<u>No. of Copies</u>		<u>No. of Copies</u>	
Offsite			
2	DOE Office of Scientific and Technical Information		D. Pepson U.S. Department of Energy Trevion II Building, EM-35 Washington, D.C. 20585-0002
	D. Campbell 102 Windham Road Oak Ridge, TN 37830		Scott E. Slezak 806 Hermosa NE Albuquerque, NM 87110
	Charles W. Forsberg Oak Ridge National Laboratory P.O. Box 2008, MS-6495 Oak Ridge, TN 37831-6495 Argonne National Laboratory		Dana A. Powers Sandia National Laboratory Nuclear Facilities Safety Department MS-0744 Albuquerque, NM 87185-0744
2	S. J. Eberlein Westinghouse Savannah River Co. Savannah River Site, 271-121 H Aiken, SC 29802		J. Tseng U.S. Department of Energy Trevion II Building, EM-35 Washington, D.C. 20585-0002
	Billy C. Hudson P.O. Box 271 Lindsborg, KS 67456		
	M. S. Kazimi Massachusetts Institute of Technology Department of Nuclear Engineering 77 Massachusetts Avenue Cambridge, MA 02139		
	J. Louis Kovach P.O. Box 29151 70000 Huntley Road Columbus, OH 43229		
	Thomas S. Kress 102-B Newridge Road Oak Ridge, TN 37830		
	Thomas E. Larson 2711 Walnut St. Los Alamos, NM 87545		
3	Los Alamos National Laboratory P.O. Box 1663 Los Alamos, NM 87545 Attn: W. L. Kubic K557 K. Pasamehmetoglu K555 C. Unal K575		
		Onsite	
		14	DOE Richland Operations Office
			M. H. Campbell S7-73 J. M. Gray (10) S7-54 C. A. Groendyke S7-54 J. C. Peschong S7-53 G. W. Rosenwald S7-54
		38	Hanford Contractors
			S. A. Barker R2-11 W. B. Barton R2-11 R. E. Bauer S7-14 R. J. Cash S7-14 G. L. Dunford A2-34 R. F. Eggers R2-12 D. L. Herting T6-09 K. M. Hodgson H0-34 J. R. Jewett T6-09 G. D. Johnson (15) S7-14 N. W. Kirch R2-11 J. R. Kristofzki R2-12 J. A. Lechelt R2-11 J. W. Lentsch S7-14 R. M. Marusich A3-34

No. of
Copies

No. of
Copies

	D. M. Ogden	HO-34	J. W. Brothers	K5-22
	D. A. Reynolds	R2-11	P. A. Gauglitz	P7-41
	G. R. Sawtelle	A3-37	L. A. Mahoney	K7-15
	E. R. Siciliano	HO-31	P. A. Meyer	K7-15
	L. A. Stauffer	R2-11	B. J. Palmer	K7-15
	L. M. Stock	S7-14	L. R. Pederson	K2-44
	R. J. Van Vleet	A3-34	L. M. Peurrung	P7-41
	J. R. White	H5-09	M. R. Powell	P7-19
	N. E. Wilkins	R2-11	S. D. Rassat	P7-41
			K. P. Recknagle	K7-15
			D. R. Rector	K7-15
41	Pacific Northwest Laboratory		H. C. Reid	K7-15
	Z. I. Antoniak	K7-15	A. Shekarriz	K7-15
	J. M. Bates	K7-15	C. W. Stewart (15)	K7-15
	S. Q. Bennett	K7-90	G. Terrones	K7-15
	P. R. Bredt	P7-25	J. M. Tingey	P7-25
	M. E. Brewster	K7-15	P. D. Whitney	K5-12
			Information Release (5)	K6-06